DYNAMICS, SIMULATION AND CONTROL OF WATERJET PROPULSION FOR S.E.S.

Romeo Holgado Bruce

DYNAMICS, SIMULATION AND CONTROL OF WATERJET PROPULSION FOR S.E.S.

by

ROMEO HOLGADO BRUCE

LIEUTENANT, PHILIPPINE NAVY

B.S., Philippine Military Academy

(1966)

Submitted in Partial Fulfillment of the

Requirements for the Degree of

Ocean Engineer

and the Degree of

Master of Science in Mechanical Engineering

at the

MASSACHUSETTS INSTITUTE OF TECHNOLOGY

May, 1974

ABSTRACT

Dynamics, Simulation and Control of Waterjet Propulsion for S.E.S.

Romeo H. Bruce

Submitted to the Department of Ocean Engineering and the Department of Mechanical Engineering on May 10, 1974 in partial fulfillment of the requirements for the degree of Master of Science in Mechanical Engineering and Engineer's degree in Ocean Engineering.

A mathematical model of the waterjet propulsion plant for surface effect ships consisting of gas turbine, reduction gear, axial pump, variable flushed inlet, diffuser and fixed nozzle was developed. Control algorithms were also developed for the variable geometry flushed inlet and for the pump RPM, and were tested by digital simulation of the mathematical model. Pump cavitation was included in the model and simulation.

The control scheme for the variable flushed inlet involves the maintainance of a diffusion flow pattern about the flushed inlet. The control scheme for the pump involves the maintainance of pump RPM as dictated by the throttle RPM setting. In both control schemes, the rate and hard limits, on the hydraulic actuator for the flushed inlet and on the fuel flow rate of the gas turbine, were considered. Results of real time tests of the developed algorithm are presented.

Thesis Supervisor: Richard S. Sidell
Title: Assistant Professor of Mechanical Engineering

Thesis Advisor: A. Douglas Carmichael
Title: Professor of Power Engineering

Thesis Reader: Chryssostomos Chryssostomidis
Title: Assistant Professor of Naval Architecture

TABLE OF CONTENTS

INTRODUCTION

The inherent geometrical flexibility of Waterjet Propulsion system commands a significant interest for its use in Surface Effect Ship (S.E.S.). In particular where the power level of the propulsion train is high, waterjet system, despite its relatively lower propulsive efficiency compared to the controllable reversible pitch supercavitating propellers (Fig. 1) is considered to be a more reliable system to fit the sidewall configuration of the S.E.S. A great risk is involved when propeller shafts at power levels of 20,000 H.P. and above are turned around corners to drive propellers.

Thus the current U.S.A. effort for the projected 2,000 ton S.E.S. having a cruise speed of approximately 80 knots focuses attention to the waterjet system as the best choice for propulsion. As a result of the experience of the 100 ton waterjet driven S.E.S., it was recognized that a variable inlet geometry was needed to maintain high pressure recovery at all speed levels, particularly at hump speed and at cruise (Fig. 2). Fig. 3 shows the typical speed resistance of the S.E.S. One of the design requirements is that

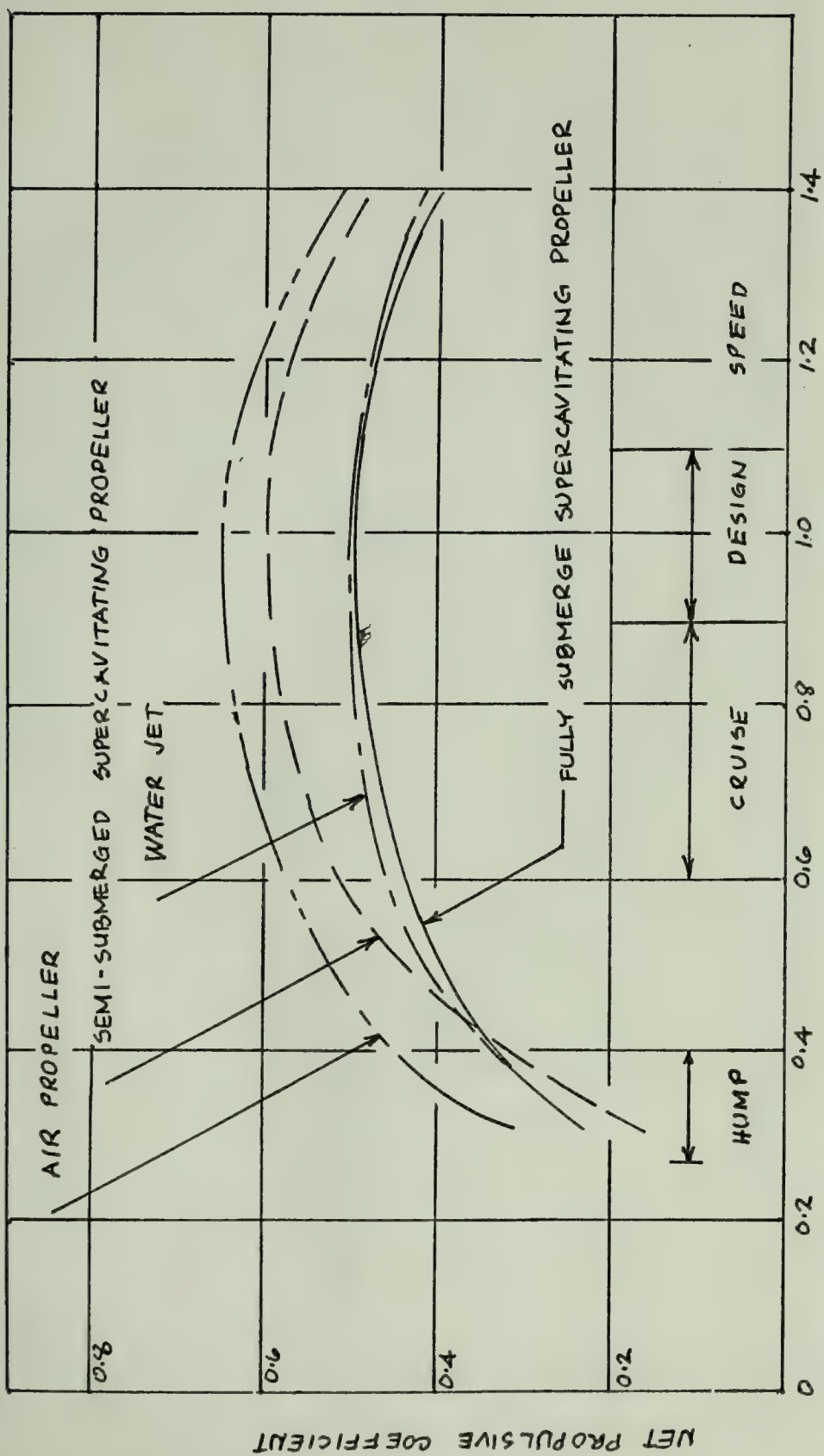

FIGURE 1 TYPICAL NET PROPULSIVE COEFFICIENT VS S.E.S. SPEED

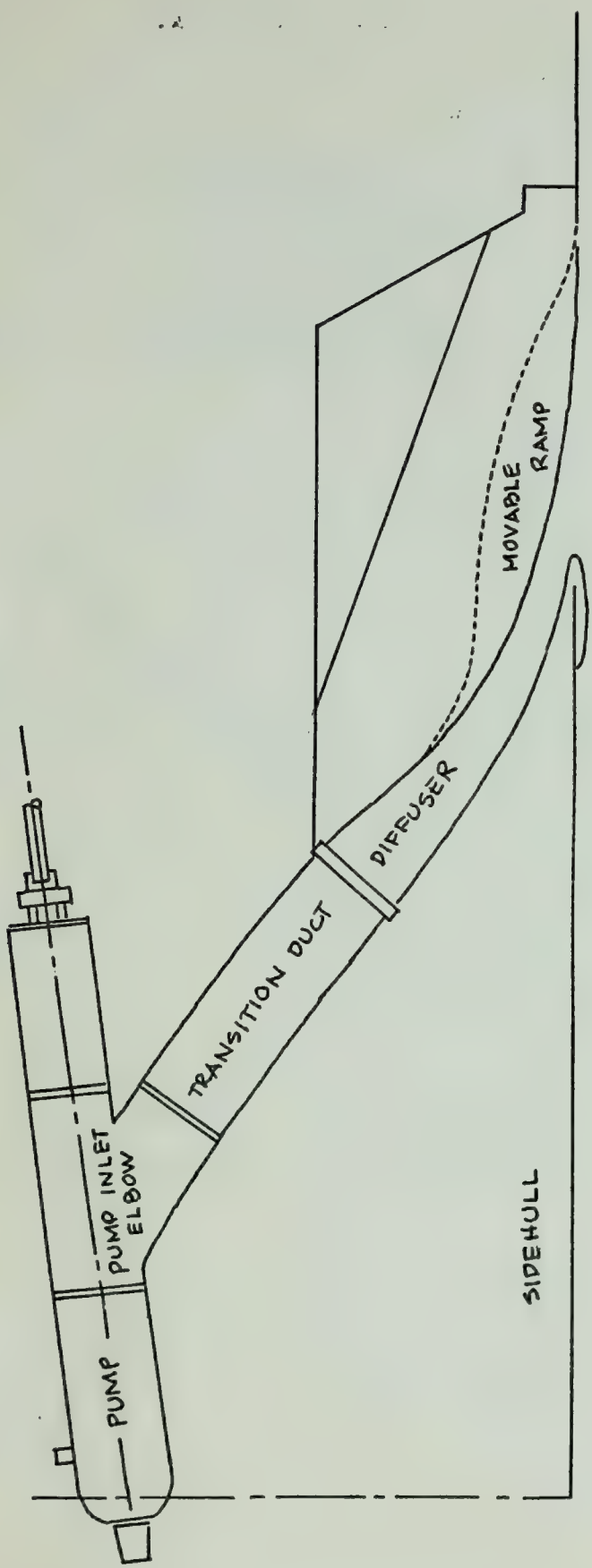

FIGURE 2 SCHEMATIC VIEW OF WATERJET SYSTEM FLUSHED INLET

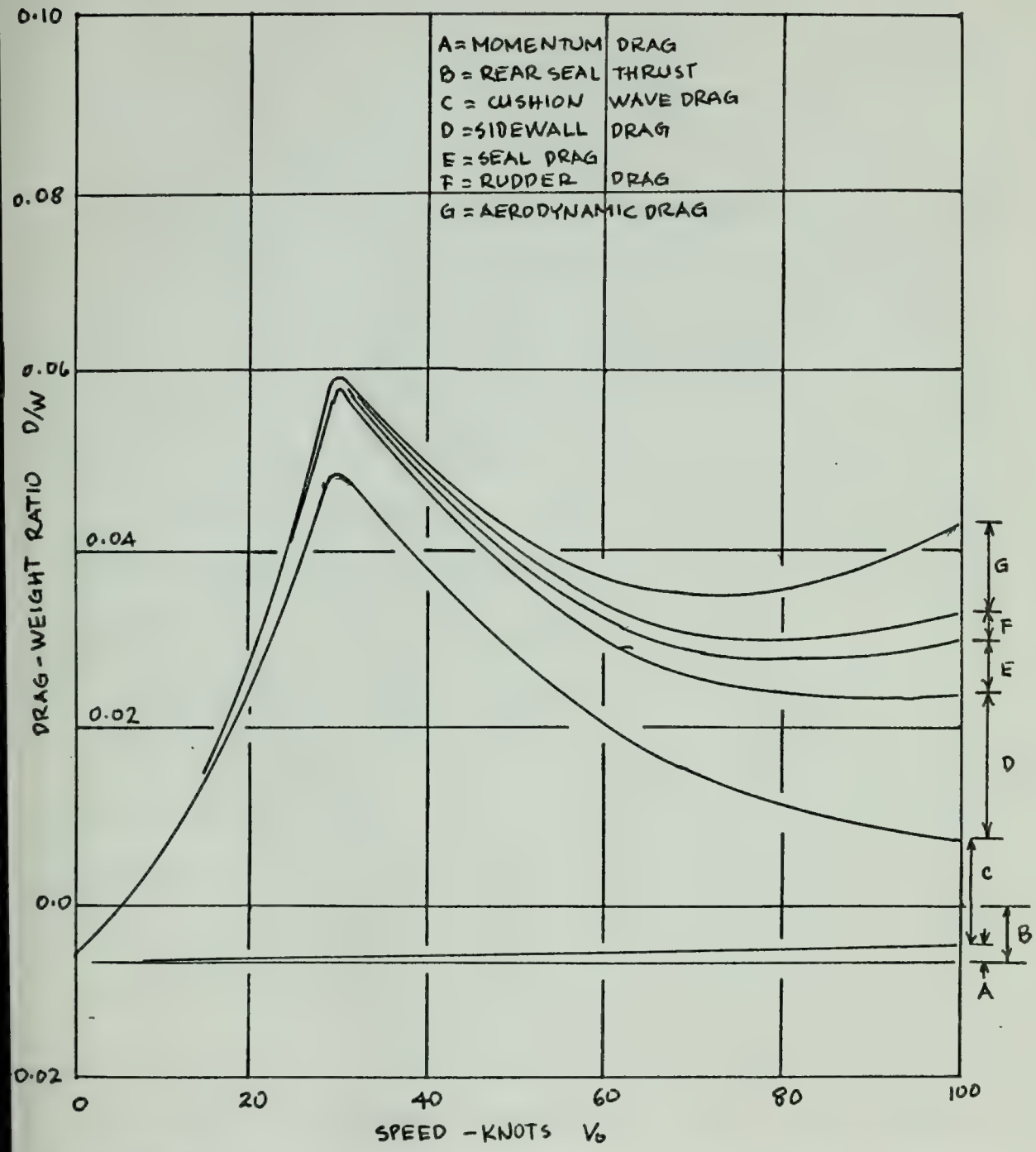

FIGURE 3 DRAG BUILD UP FOR SES WITH $L_c/B = 2$, $P_c/L_c = 1.5$
$C_{QA} = 0.1$

at hump speed the waterjet system must be able to deliver a maximum thrust of at least 20% greater than hump total resistance for an acceptable acceleration performance. This implies that the water flow rate for the system at cruise speed and hump speed will be approximately the same. Since the ratio of cruise speed to hump speed is approximately 3, the flush inlet area must have to be adjusted accordingly so that a diffusion flow pattern will be maintained always from the region in front of the flush inlet to the pump inlet (Fig. 4). If not, then pressure recovery will be seriously degraded and the pump may cavitate due to insufficient suction head pressure.

At present, work is being conducted at M.I.T. to optimize the design of components of the waterjet system for the S.E.S. so maximum payload can be obtained for a given displacement range, cruise speed and hump speed.

The purpose of this paper then is to model and simulate the dynamic performance of these conponents and to identify and bring out problems that may arise in the overall control of the system and possible criteria for the selection of the components. The case study presented herein is that of a 2109 ton S.E.S. whose waterjet system consists of six LM2500 gas turbines, reduction gears, axial water pumps,

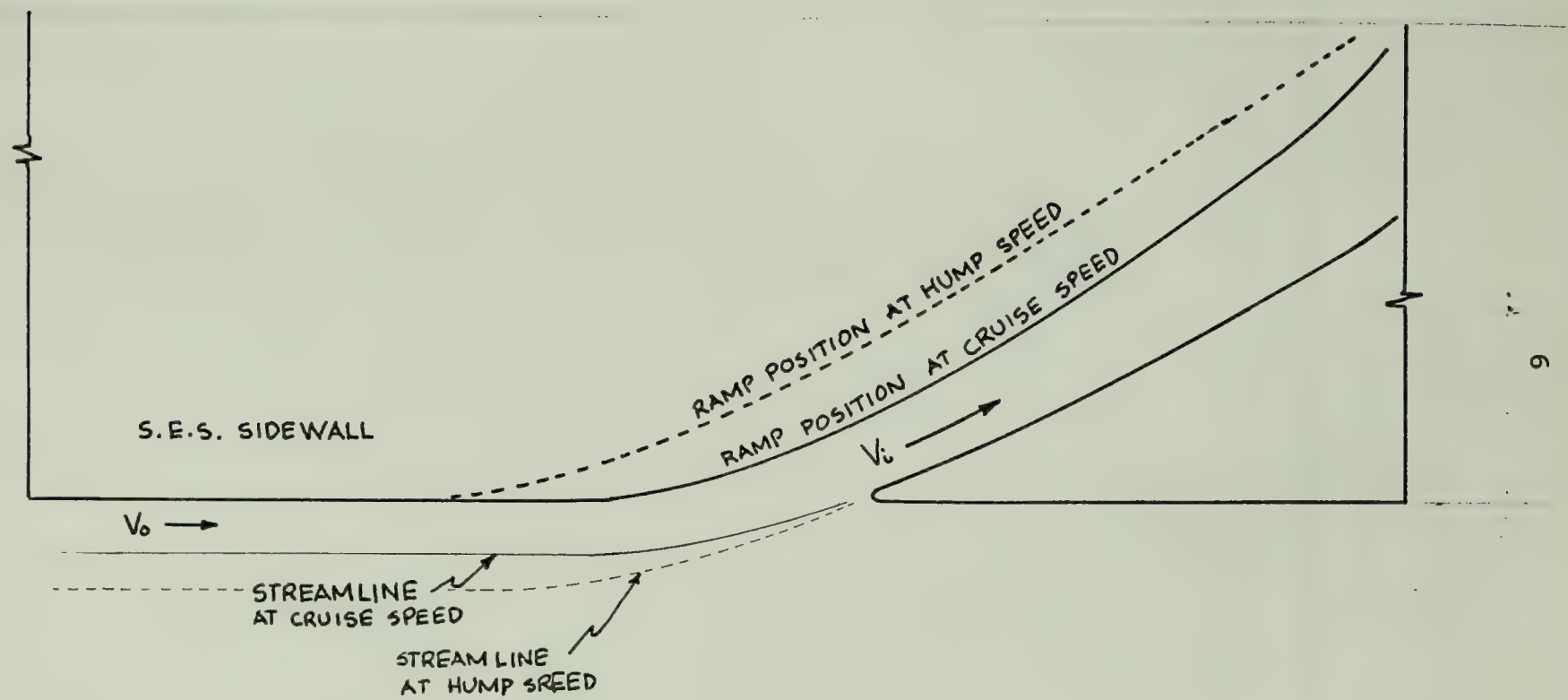

FIGURE 4 DIFFUSION FLOW PATTERN AT INLET AT HUMP AND CRUISE SPEEDS ($V_i/V_o < 1$)

variable inlet geometry flushed inlet and fixed geometry nozzle. The simulation program has been set up in such a way that thrust reverser characteristics can also be added to analyze the backing performance of the craft.

CHAPTER I

WATERJET PROPULSION COMPONENT MATCHING

I-1 GENERAL:

In order for the waterjet system to function efficiently, pump design point must match accordingly to the thrust requirements both at hump and at cruise speeds. This includes the determination of the following: design range of variable inlet, area design pump RPM, design pump flow rate, design nozzle area. Using the momentum equation the thrust delivered by the system is:

$$T_d = \frac{\rho Q}{g} (V_j \cos\alpha - V_o) \qquad (1\text{-}1)$$

where: T_d = thrust develop (lbf)

ρ = water density (lbm/ft^3)

Q = water flow rate (ft/sec)

g = gravity (32.2 ft/sec)

V_j = waterjet velocity (ft/sec)

V_o = S.E.S. velocity (ft/sec)

α = depression angle of the nozzle

For most design $\cos\alpha$ is approximately equal to unity thus can be neglected in the preliminary calculation. The

thrust develop then is:

$$T_d = \frac{\rho Q V_o}{g}\left[\frac{V_j}{V_o} - 1\right] \qquad (1\text{-}2)$$

The thrust required at hump speed is:

$$T_{RH} = 1.2\ (R_{SH} + R_{IH}) \qquad (1\text{-}3a)$$

where: T_{RH} = thrust required at hump speed (lbf)

R_{SH} = bare hull resistance at hump speed (lbf)

R_{IH} = inlet appendage drag at hump speed (lbf)

The factor 1.2 is the required minimum acceleration margin.

The thrust required at cruise speed is:

$$T_{RC} = R_{SC} + R_{IC} \qquad (1\text{-}3b)$$

where: T_{RC} = thrust required at cruise speed (lbf)

R_{SC} = bare hull resistance at cruise speed (lbf)

R_{IC} = inlet appendage drag at cruise speed (lbf)

The inlet appendage drag for equations (1-3) is:

$$R_{IH} = C_{DH}\ \frac{\rho g}{2}\ V_{OH} Q_H \qquad (1\text{-}4a)$$

$$R_{IC} = C_{DC} \frac{\rho g}{2} V_{OC} Q_C \qquad (1\text{-}4b)$$

where: C_{DH} and C_{DC} = inlet drag coefficients at hump and cruise speeds respectively

V_{OH} and V_{OC} = S.E.S. velocity at hump and cruise speeds respectively

Q_H and Q_C = water flow rate at hump and cruise speeds respectively

Equating thrust delivered and thrust required and substituting equations (1-4) to equations (1-3) results in:

$$Q_H = \frac{1.2\ R_{SH}}{\frac{\rho}{g} V_{OH} \left[\frac{V_{jH}}{V_{OH}} - (1+0.6C_{DH}) \right]} \qquad (1\text{-}5a)$$

$$Q_C = \frac{R_{SC}}{\frac{\rho}{g} V_{OC} \left[\frac{V_{jC}}{V_{OC}} - (1+0.5C_{DC}) \right]} \qquad (1\text{-}5b)$$

The pump head required at hump and cruise speeds from Bernoulli equation are respectively:

$$H_{PH} = \frac{V_{OH}^2}{2g} \left[\left(\frac{V_{jH}}{V_{OH}} \right)^2 + \frac{2gH_{WL}}{V_{OH}^2} - \eta_{oa} \right] \qquad (1\text{-}6a)$$

$$H_{PC} = \frac{V_{OC}^2}{2g} \left[\left(\frac{V_{jC}}{V_{OC}} \right)^2 + \frac{2gH_{WL}}{V_{OH}} - \eta_{oa} \right] \qquad (1\text{-}6b)$$

where: η_{oa} = overall efficiency of inlet and diffuser

H_{WL} = height of the nozzle above the waterline (ft)

The effective horsepower required ($EHP = \rho H_p Q$) for hump and cruise speeds from equations (1-5) and (1-6) are:

$$EHP_H = \frac{1.2 R_H V_{OH}}{(2)(550)} \frac{\left[\left(\frac{V_{jH}}{V_{OH}}\right)^2 + \frac{2gH_{WL}}{V_{OH}^2} - \eta_{oa}\right]}{\left[\frac{V_{jH}}{V_{OH}} - (1+0.6\ C_D)\right]} \qquad (1\text{-}7a)$$

$$EHP_C = \frac{R_C V_{OC}}{(2)(550)} \frac{\left[\left(\frac{V_{jC}}{V_{OC}}\right)^2 + \frac{2gH_{WL}}{V_{OC}^2} - \eta_{oa}\right]}{\left[\frac{V_{jC}}{V_{OC}} - (1+0.5\ C_D)\right]} \qquad (1\text{-}7b)$$

Note that equations (1-5), (1-6), and (1-7) are all expressed as a function of jet velocity ratio (V_j/V_O). In the case of a fixed inlet area the jet velocity ratio and flow rate at hump and cruise speeds can be related to the nozzle jet area (A_j) by:

$$A_j = \frac{Q_H}{V_{jH}} = \frac{Q_C}{V_{jC}} \qquad (1\text{-}8)$$

Fig. 5 shows a typical propulsive efficiency (RV_O/EHP) versus jet velocity ratio (V_j/V_O) for different values of loss coefficient K_D where total head loss

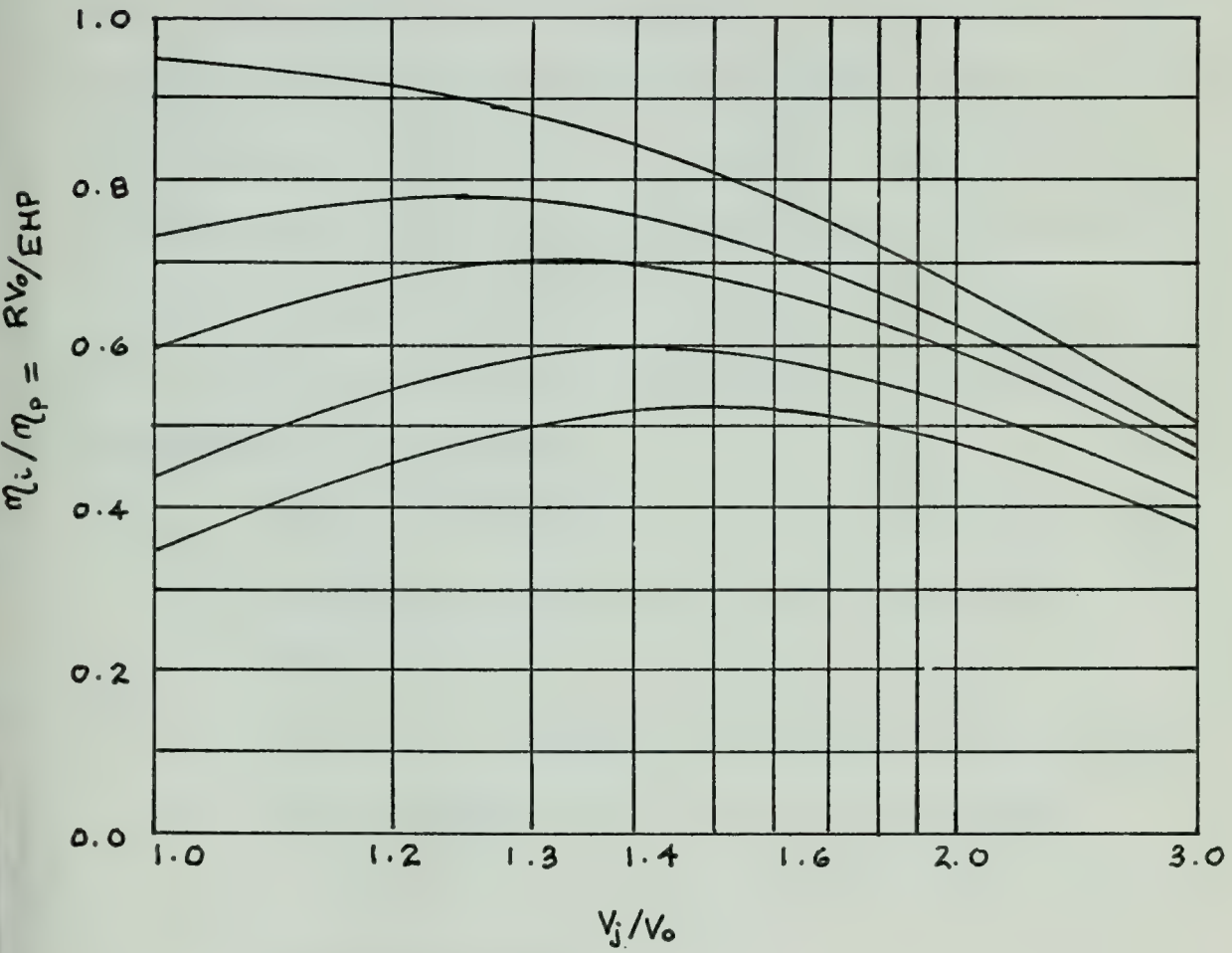

FIGURE 5 PROPULSIVE EFFICIENCY VERSUS JET VELOCITY RATIO FOR VALUES OF LOSS COEFFICIENT

$H_L = K_D V_j^2/2g$. Maximum efficiency is observed to occur for most practical designs between V_j/V_O of 1.5 to 2.0. Likewise equation (1-7b) can be differentiated with respect to (V_j/V_O) to obtain minimum EHP. However, the result may not be compatible to the requirement of equations (1-5a), (1-6a) and (1-7a) because of the fixed nozzle area constraint unless the total hump resistance $(R_{SH} + R_{IH})$ is lower than some critical value. For the case where the total hump speed resistance is greater than this critical value the approach in finding the optimum cross sectional area of the nozzle and jet velocity ratios at hump and cruise speeds is as follows:

a. Choose some multiple integral number of existing prime movers with a given shaft horsepower (SHP) rating.

b. Multiply the maximum intermittent SHP available by the reduction gear efficiency and pump efficiency to obtain the maximum intermittent total EHP available.

c. Substitute in equation (1-7a) and solve the quadratic equation for (V_{jH}/V_{OH}). The two values of (V_{jH}/V_{OH}) represent the maximum and minimum values of (V_{jH}/V_{OH}) for which equation (1-7a) will be satisfied.

d. Solve for A_j using equations (1-5a) and (1-8) using values of V_{jH}/V_{OH} within the range obtained in step c.

e. Solve for V_{jC}/V_{OC} and check equation (1-7b) if the total sustained EHP is within acceptable limits.

f. Iterate steps a to e until optimum number of engines, A_j, propulsive efficiency is obtained.

For the case where the total hump speed resistance is less than the critical value as dictated by equations (1-7a), (1-7b) and (1-8) the procedure becomes easier since $\frac{\partial (EHP_C)}{\partial (V_{jC}/V_{OC})}$ need only to be set to zero to solve for optimum (V_{jC}/V_{OC}) and the rest follows.

I-2 PRELIMINARY PUMP DESIGN:

The procedure stated herein applies primarily to determine the rated pump RPM, pump diameter, annulus area and other related pump characteristics based on designed flow coefficient (ϕ) and head coefficient (ψ), designed flow rate (Q) and designed pump head (H_p). By definition:

$$\phi = \frac{C_x}{U} = \frac{\frac{Q}{A_n}}{\frac{N \pi D}{60}} \qquad (1\text{-}9)$$

$$\psi = \frac{gH_p}{U^2} = \frac{gH_p}{\left(\frac{N\pi D}{60}\right)^2} \qquad (1\text{-}10)$$

where: C_x = water axial velocity (ft/sec)

U = blade tip velocity (ft/sec)

Q = water flow rate (ft/sec)

A_n = pump annulus area (ft^2)

N = pump RPM

D = pump tip diameter (ft)

The axial pump annulus area (a) is:

$$A_n = \frac{\pi D^2}{4}\left(1 - (d/D)^2\right) \qquad (1\text{-}11)$$

Where: d = pump hub diameter (ft).

The design flow rate from equations (1-5) and the design pump head from equation (1-6) can be substituted in equations (1-9), (1-10) and (1-11) to solve for A_n, N, D for a given value of hub to tip diameter ratio.

I-3 REDUCTION GEAR RATIO:

The purpose of the reduction gear is to match the point of best efficiency of the pump to the point of best efficiency of the prime mover. Engine performance maps are usually expressed as plots of break horse power versus RPM

for various levels of specific fuel consumption (Fig. 6 and Fig. 7). Performance maps are also expressed as plots of torque versus RPM for various levels of fuel consumption (Fig. 8 and Fig. 9). In either case the point of best efficiency corresponding to power level required in equations (1-7) plus additional power for frictional losses and pump efficiency can easily be pinpointed. Thus the reduction gear ratio is determined as the ratio of the prime mover RPM at this point of best efficiency and the designed pump RPM (N).

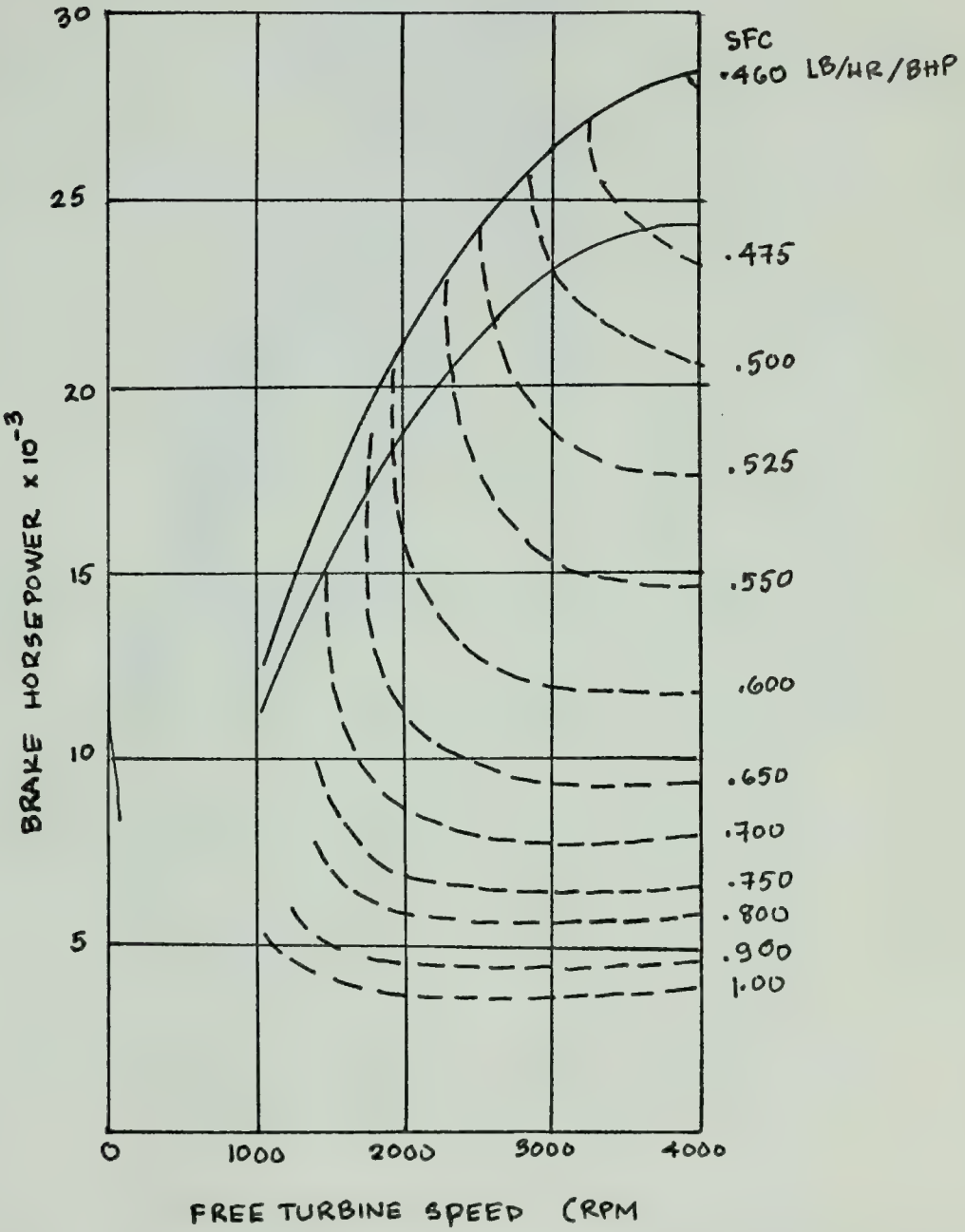

FIGURE 6 FT4A2 FREE TURBINE SPEED VS BHP

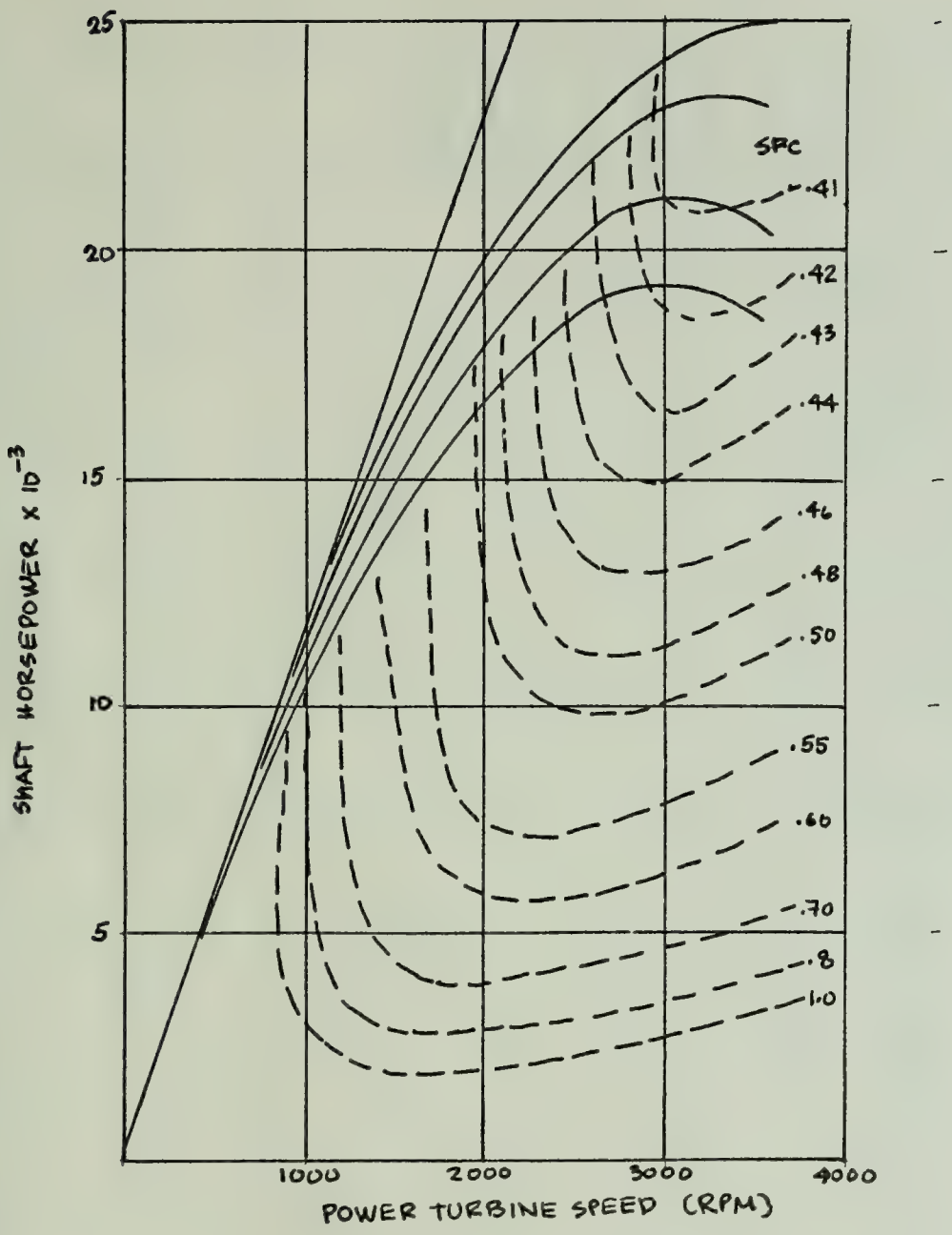

FIGURE 7 LM2500-A SHAFT HORSEPOWER VS TURBINE SPEED

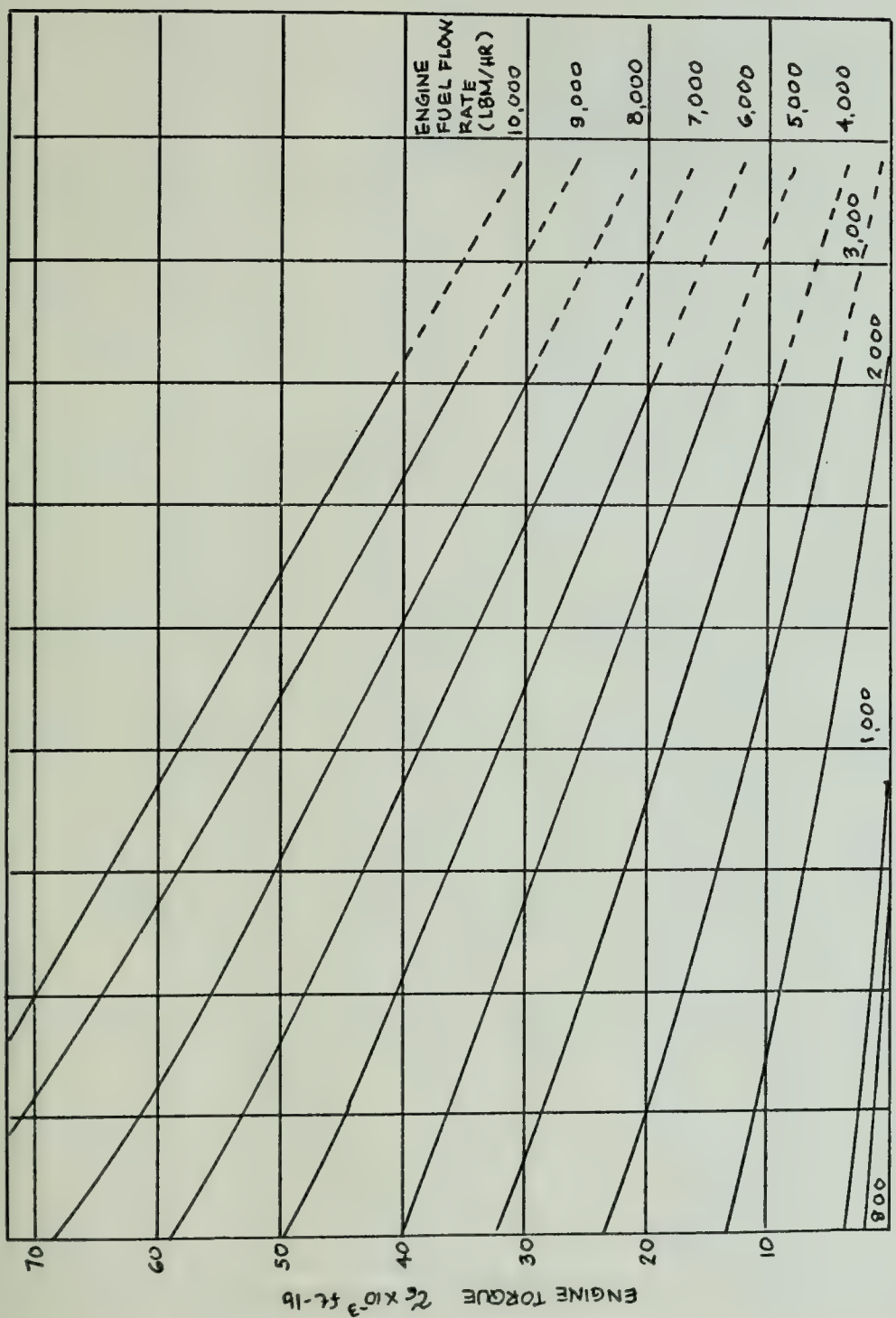

FIGURE 8 LM 2500 PERFORMANCE MAP

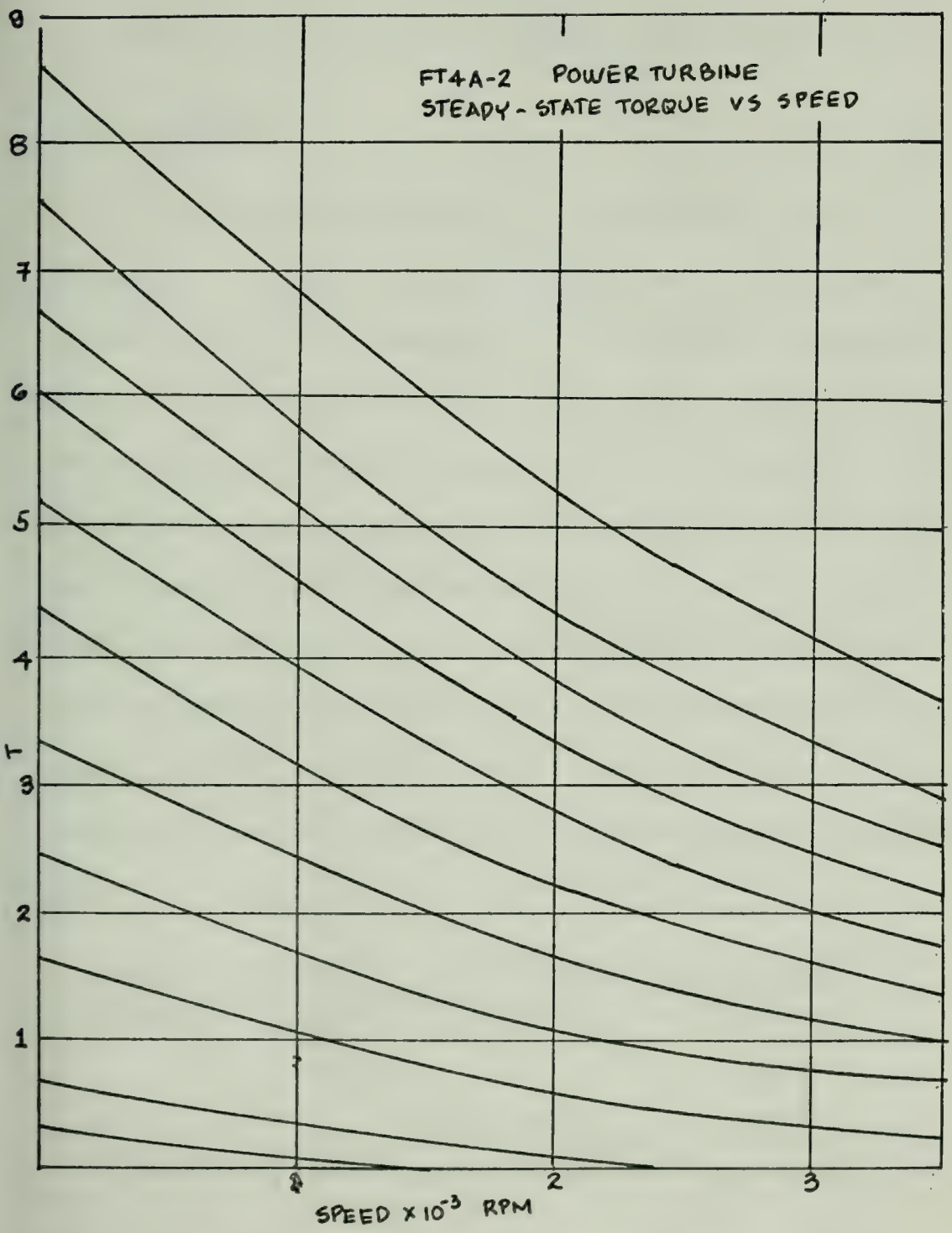

FIGURE 9 FT4A2 POWER TUBBINE TORQUE VS SPEED

CHAPTER II

MODELING OF S.E.S. AND WATERJET PROPULSION PLANT

II-1 GENERAL:

In order to simulate the interaction of the components of the waterjet propulsion plant with the motion of the S.E.S., it is necessary to obtain the mathematical model of such an installation. The model would then allow the development of the appropriate control algorithm without actually employing the hardware involved. To obtain such a model a thermodynamic approach was chosen. Fig. 10 shows the power flow block diagram of the waterjet propulsion train. At this point it is recommended for the reader to take a look on ref. (1) and ref. (2) for the bond graft technique which will be used frequently in this paper.

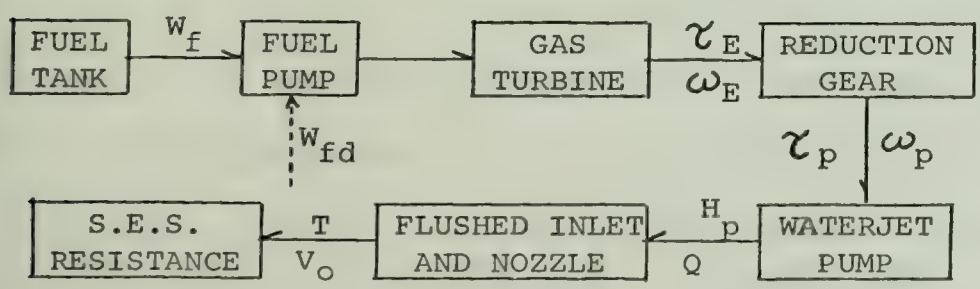

Figure 10. Block diagram of waterjet propulsion train

where: W_{fd} = fuel flow rate demand (lbs/hr)

W_f = actual fuel flow rate (lbs/hr)

τ_E = power turbine torque (ftlb)

ω = power turbine speed (RPM)

τ_p = pump torque (ftlbs)

ω_p = pump speed (RPM)

H_p = pump total head (ft)

T = thrust (lbs)

V_o = S.E.S. velocity (ft/sec)

The above diagram is interesting from the point of view of thermodynamic accounting of energies involved. The light broken arrows represent signal power level and the darkened arrows represent high power level transmission. The product of the variables affixed to the arrows multiplied by some constant represents power. For simplicity, the energy storage and energy dissipator elements associated with each component and power transmission are not included in the detailed modeling of each component which follows. Notice that all the energy associated with the fuel will in the end be dissipated into the environment primarily due to the S.E.S. resistance and secondarily but not avoidably due to the "resistances" inherent with the inefficiency of each component and inefficiency of power transmission. Thus

from the thermodynamic point of view, for the model to be valid in the steady state the power input for each component must be greater than the power output in either direction. Likewise the first law and second law of thermodynamics must be satisfied during the transient conditions.

II-2 FUEL:

The purpose of fuel is to provide energy primarily in the form of heat to the driving engine which is a gas turbine in this case study. The energy associated with the fuel can be expressed as heating value per unit weight (h). Fuel reaction with air mainly is as follows:

$$2\ C_6H_{18} + 21\ O_2 \xrightarrow{T_{FP}} 12\ CO + 18\ H_2O + 6\ O_2 + Q_1 \longrightarrow$$

$$12\ CO_2 + 18\ H_2O + Q_1 + Q_2 \qquad (2\text{-}1)$$

where: T_{FP} = flush point temperature

Q_1, Q_2 = heat evolve in the combustion process respectively

The degree on which the above combustion process proceeds to the right is dependent on combustion temperature, fuel-air ratio and time on which the process is allowed to proceed in the combustion chamber of the gas turbine.

Thus the total heat evolved per unit fuel weight as function of time (h(t)) can be assumed in block diagram to be:

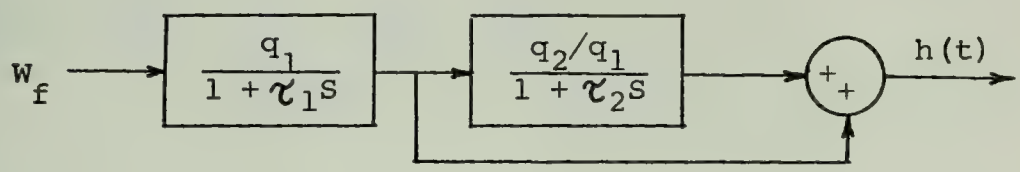

where: q_1, q_2 = heating values per unit weight of fuel from equation (2-1)

$h(t)$ = total heating value of fuel per weight

W_f = fuel flow rate

τ_1, τ_2 = the exponential time constants of the above combustion process.

τ_1 and τ_2 are very small terms but significant when convection time from fuel spray area of the combustion chamber to the turbine inlet is considered (Fig. 16).

II-3 FUEL PUMP:

The purpose of the fuel pump is to drive the fuel from the fuel tank into the combustion chamber of the gas turbine which is at a higher pressure. For the case of a positive displacement fuel pump (Fig. 9) represents the power flow diagram.

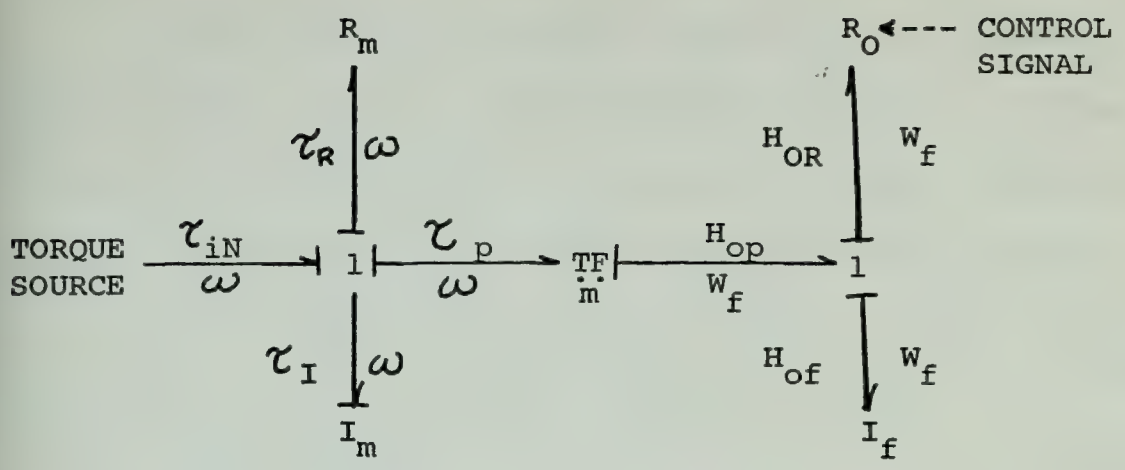

Figure 11. Pump power flow diagram

where: τ_{iN} = input torque into the pump

ω = pump speed

R_m = pump mechanical frictional resistance

H_{op} = total lead developed by pump

W_f = weight fuel flow rate

R_f = fluid resistance associated with fuel value and fuel pipings

τ_p = pump torque

I_f = fuel inertance associated in the fuel pipings

m = modulo relating τ_p to H_{op} or modulo relating ω to W_f

TF = ideal transformer of mechanical power to fluid power

1-junction = point of same ω or the same W_f.

Since I_f and I_m are not independent for positive displacement pumps, I_m can be referred to the fluid side (or I_f can be referred to the mechanical side). Similarly R_m can be referred to the fluid side. For the case where:

$$\text{(a)} \quad mW_f = \quad \text{or } H_{op} = m\tau_p \tag{2-2a}$$

$$\text{(b)} \quad R_m = b\omega \tag{2-2b}$$

$$\text{(c)} \quad R_f = c_1 W_f^2 + \frac{W_f}{2gC_2 (\rho A_o)^2} \tag{2-2c}$$

then

$$(m^2 I_m + \frac{I_f}{\rho}) \frac{dW_f}{dt} = (m\tau_{iN} - m^2 b W_f - W_f |W_f| (C_1 + \frac{1}{2gC_2(\rho A_o)^2})) \tag{2-3}$$

where: b = mechanical frictional resistance coefficient

c_1 = fluid frictional resistance coefficient in pipings

A_o = orifice area of the fuel valve

C_2 = orifice coefficient of the valve

II-4 GAS TURBINE:

Fig. 12 shows a schematic diagram of a typical aircraft gas turbine derivative. It is composed of two major units - the gas generator and the power turbine. The gas generator is a twin spool engine, consisting of low pressure

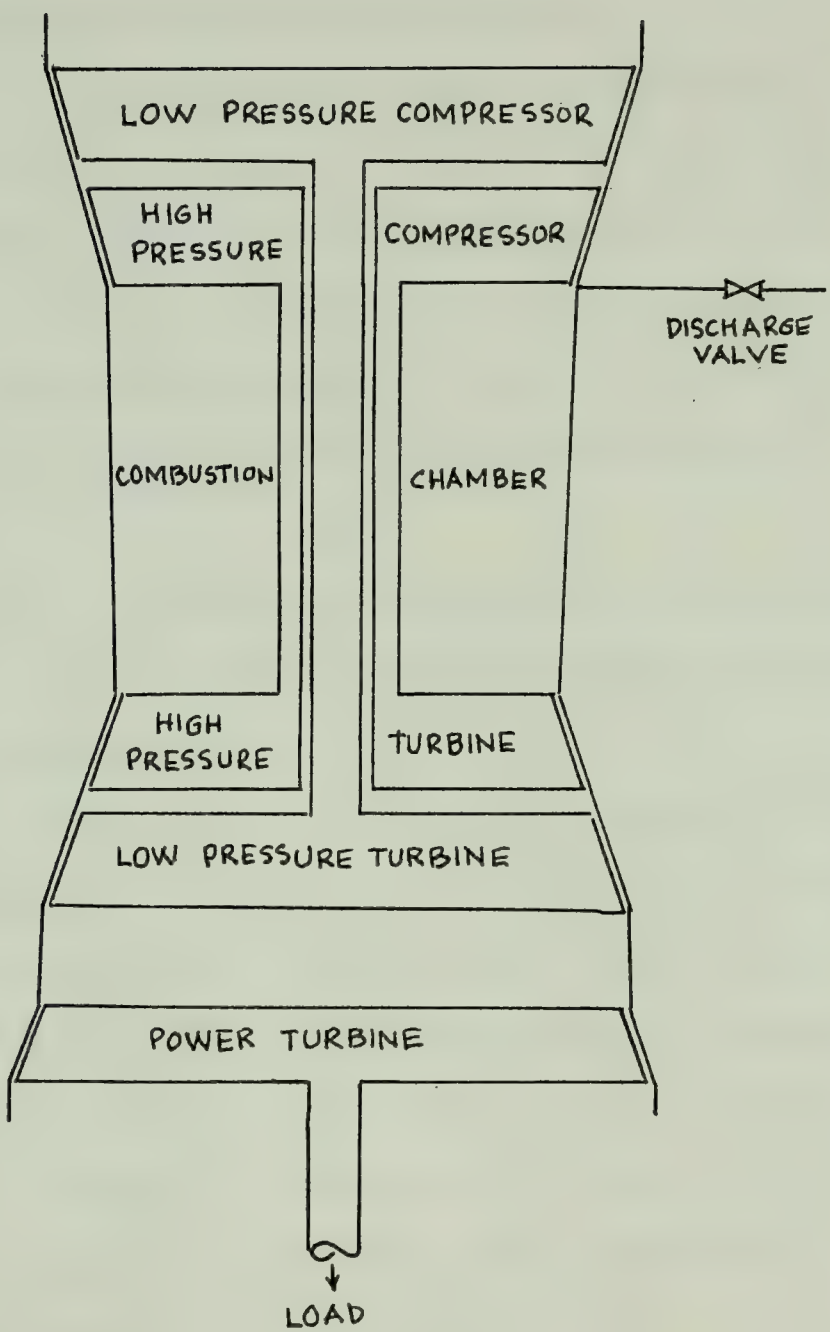

FIGURE 12 SCHEMATIC DIAGRAM OF FT-4 GAS TURBINE

compressor (L.P.C.), high pressure compressor (H.P.C.), combustion section, high pressure turbine (L.H.T.) and low pressure turbine. The power turbine (P.T.) is adapted to the gas generator by an annular diffusing transition duct. Thus the operating speed of the power turbine is independent of the gas generator speeds. The engine also comes with a fuel control package to ensure that starting and operating schedules of the gas turbines are met automatically without the gas generator going into surge and without subjecting the turbine inlet to excessive gas temperature.

In order to coordinate the gas turbine package to the waterjet propulsion system, a mathematical model is developed as a part of this paper.

For a satisfactory model, it can be assumed that the main accumulator of energy occurs in the gas pipe volumes and in the rotating parts. Although some heat energy is stored in the metal parts, its accumulation and discharge is carried out sufficiently slower. Thus during sharp load changes the transient is mainly from the dynamic interaction of rotors, volume and power turbine speed regulators.

When a sharp load torque decrease occurs, the power turbine speed regulator initial action is to decrease quickly

the fuel flow to low value open up discharge value to release air intensively from gas turbine limit to evacuate the large quantity of stored energy. After which the discharge valve is closed and fuel flow is increased to the desired RPM.

When an increase load is desired on the power turbine, it is necessary to increase the gas generator speed and therefore the stored energy therein. However in this transient process the compressor speed lags behind the pressure and temperature increase due to fuel flow increase. Thus not only for the protection of turbine against excessive temperature but also preventing compressor insurge, the rate of fuel flow increase is strictly limited in accordance with air flow increase. Surge is also excluded at low speeds by discharging air at the first group of stages or from compressor delivery valve.

In order to see the basic principle underlying surge, consider a multistage axial compressor having the same flow coefficient $\phi = C_x/U$ and air axial velocity C_x for all stages, at design point. At very low speed C_x has to increase greatly through the compressor since the outlet air density is now approximately equal to inlet air density. This means that the first stages are operating at a very high incidence

angle or positive stall value while the last stages will be at negative incidence angle or negative stall value or turbining value. Now, with sudden increase of fuel flow the compressor outlet pressure will also increase very quickly. Thus C_x also decreases shifting the positive stall region toward the last stages. Since the first stages are not contributing any pressure increase, back air flow rapidly occurs as soon as stall hits the last stage with an accompanying explosive sound.

With the above qualitative background, Fig. 13 is shown as the bond graph model of the gas turbine unit. Three variables are needed to describe power flow of compressible gas: mass flow rate (m_a), total pressure (P_o), total temperature (T_o). The subscripts are evident from Fig. 12. The rest of the notations are:

τ = torque

ω = angular speed

W_f = fuel weight flow rate

R = frictional resistance for shafts or orifices

I = polar moment of inertia

H_o = total head of fuel

V = effective air volume capacitance

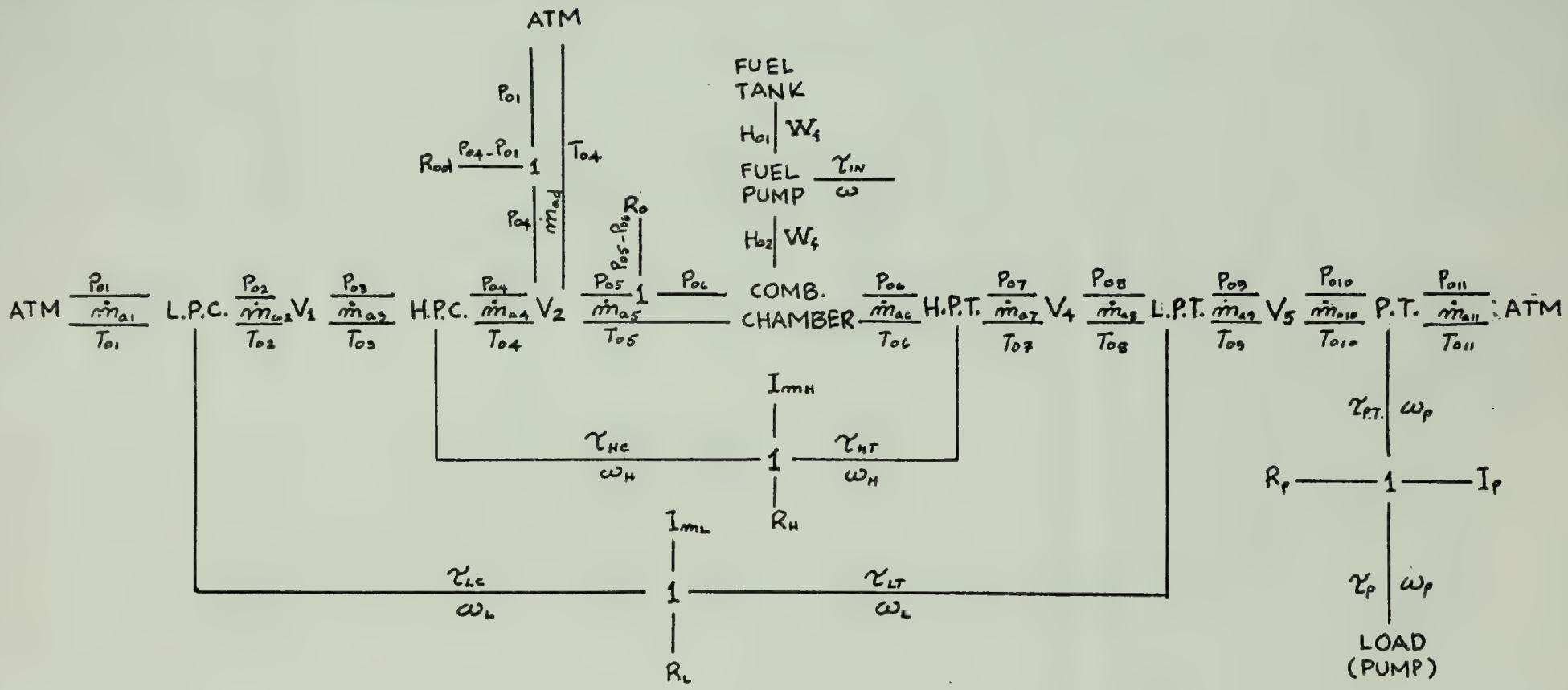

FIGURE 13 BOND GRAPH MODEL OF GAS TURBINE UNIT WITH TWIN SPOOL GAS GENERATOR

From the diagram the following are assumed:

$$\dot{m}_{a1} = \dot{m}_{a2},\ P_{o2} = P_{o3},\ T_{o2} = T_{o3},\ \dot{m}_{a3} = \dot{m}_{a4},\ P_{o4} = P_{o5},$$
$$T_{o4} = T_{o5},\ \dot{m}_{a6} = \dot{m}_{a7},\ P_{o7} = P_{o8},\ T_{o7} = T_{o8},\ \dot{m}_{a8} = \dot{m}_{a9},$$
$$P_{o9} = P_{o10},\ T_{o9} = T_{o10},\ \dot{m}_{a10} = \dot{m}_{a11}$$

Above assumption implies that pressure drops along ducts and diffuser sections of the gas turbines must be included in the overall efficiency of the adjacent compressors and turbines.

From Newton's Law:

$$I_{m_L} \frac{d\omega_L}{dt} = (\tau_{LT} - \tau_{LC} - b_L \omega_L) \qquad (2\text{-}4a)$$

$$I_{m_H} \frac{d\omega_H}{dt} = (\tau_{HT} - \tau_{HC} - b_H \omega_H) \qquad (2\text{-}4b)$$

$$I_P \frac{d\omega_p}{dt} = (\tau_{PT} - \tau_{PP} - b_P \omega_P) \qquad (2\text{-}4c)$$

Assuming air follows ideal gas law:

$$P_o V = m \mathcal{R} T_o \qquad (2\text{-}5)$$

then:

$$V_1 \frac{dP_{o2}}{dt} = (\dot{m}_{a2} - \dot{m}_{a3})\, \mathcal{R} T_{o2} + m_1 \mathcal{R} \dot{T}_{o2} \qquad (2\text{-}5a)$$

$$\frac{d\dot{m}_1}{dt} = \dot{m}_{a2} - \dot{m}_{a3} \qquad (2\text{-}5b)$$

$$V_2 \frac{dP_{o4}}{dt} = (\dot{m}_{4a} - \dot{m}_{ad} - \dot{m}_{a5}) \mathcal{R} T_{o4} + m_2 \mathcal{R} \dot{T}_{o4} \qquad (2\text{-}5c)$$

where:

$$\dot{m}_{ad} = C_d \rho A_{od} \sqrt{2g \ (P_{o4} - P_{o1})} \qquad (2\text{-}5d)$$

$$V_3 \frac{dP_{o6}}{dt} = (\dot{m}_{a5} - \dot{m}_{a6}) \mathcal{R} T_{o6} + m_3 \mathcal{R} \dot{T}_{o6} \qquad (2\text{-}5e)$$

where:

$$\dot{m}_{a5} = C_d \rho A_{od} \sqrt{(P_{o5} - P_{o6}) 2g}$$

$$\frac{dm_3}{dt} = \dot{m}_{a5} - \dot{m}_{a6} \qquad (2\text{-}5f)$$

$$V_4 \frac{dP_{o7}}{dt} = (\dot{m}_{a7} - \dot{m}_{a8}) \mathcal{R} T_{o8} + m_4 \mathcal{R} \dot{T}_{o8} \qquad (2\text{-}5g)$$

$$\frac{dm_4}{dt} = \dot{m}_{a7} - \dot{m}_{a8} \qquad (2\text{-}5h)$$

$$V_6 \frac{dP_{o10}}{dt} = (\dot{m}_{a9} - \dot{m}_{a10}) \mathcal{R} T_{o10} + m_5 \mathcal{R} \dot{T}_{o10} \qquad (2\text{-}5i)$$

$$\frac{dm_5}{dt} = \dot{m}_{a5} - \dot{m}_{a10} \qquad (2\text{-}5j)$$

Equations (2-4) and (2-5) are the equations governing the dynamics of the gas turbine in Fig. 12.

From compressor and turbine maps P_{o2}/P_{o1} versus $(\dot{m}_{a1}\sqrt{T_{o1}})/(A_n P_{o1})$ for different values of $\frac{}{T_{o1}}$ and polytropic

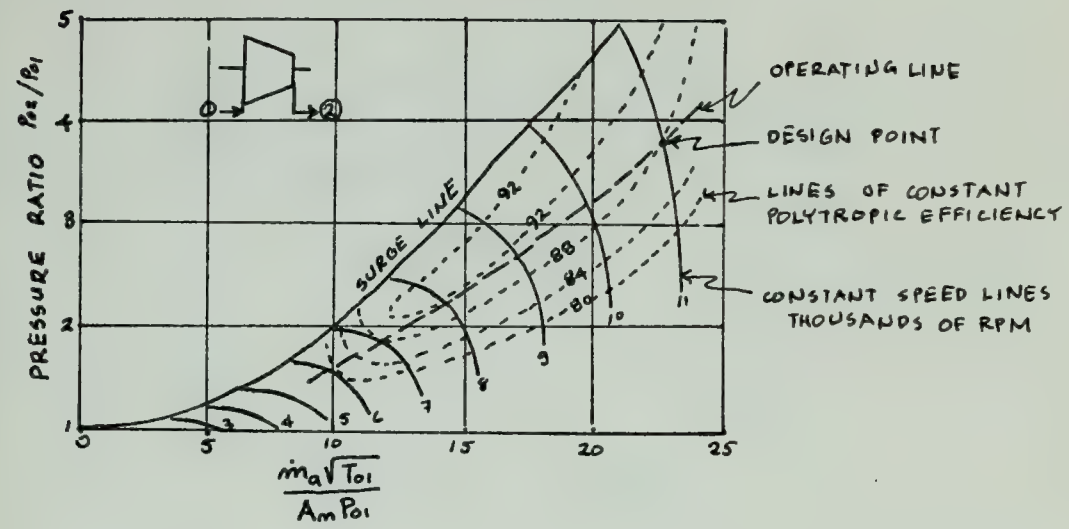

FIGURE 14 OPERATING MAP OF AXIAL COMPRESSORS

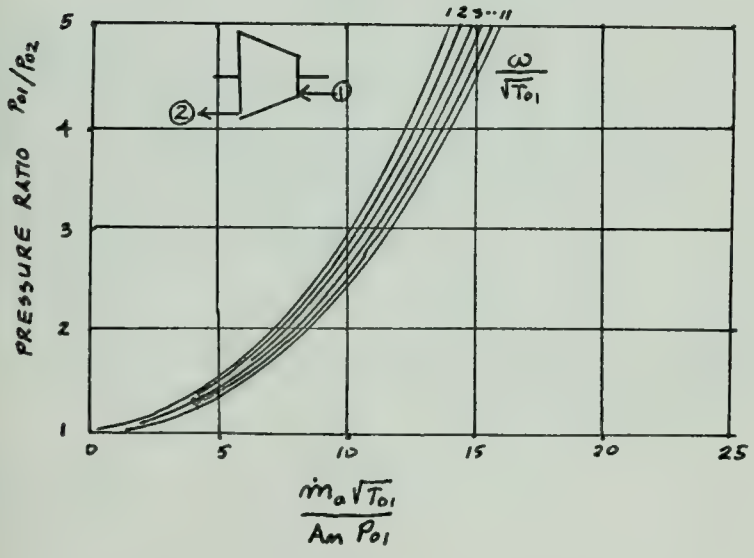

FIGURE 15 OPERATING MAP OF AXIAL TURBINES

efficiency are plotted (Fig. 14 and Fig. 15). Thus $\dot{m}_{a1}$ can be found as functions P_{o2}, P_{o1}, T_{o1} and annulus area (A_n).

From Euler's equation, the torque on the rotor of an ideal lossless compressor or turbine is

$$= \frac{\dot{m}_a r(\Delta C_\theta)}{g}$$

In terms of power:

$$= \dot{m}_a \omega \, r \Delta C_\theta = \dot{m}_a \, \Delta ho$$

Therefore:

$$\tau_{LC} = \frac{\dot{m}_{a1} \, \Delta ho}{\omega_L} \qquad (2\text{-}6)$$

Equation (2-6) will be true for an adiabatic compressor having no storage elements. Thus for a compressor having a polytropic efficiency

$$\eta_{poly_C} = \frac{\frac{(\gamma - 1)}{\gamma}}{\frac{(n - 1)}{n}} = \frac{\frac{R}{C_p}}{\frac{(n - 1)}{n}}$$

therefore:

$$\frac{(n - 1)}{n} = \frac{R}{C_p \eta_{poly_C}}$$

where

$$\frac{P_{o2}}{P_{o1}}^{\frac{(n-1)}{n}} = \frac{T_{o2}}{T_{o1}} \tag{2-7}$$

$$\Delta h_o = C_p \Delta T_o = C_p T_{o1}\left[\frac{T_{o2}}{T_{o1}} - 1\right] = C_p T_{o1}\left[\left(\frac{P_{o2}}{P_{o1}}\right)^{\frac{(n-1)}{n}} - 1\right]$$

$$\Delta h_o = C_p T_{o1}\left[\left(\frac{P_{o2}}{P_{o1}}\right)^{\frac{R}{(C_p \eta_{poly_C})}} - 1\right]$$

From equation (2-6)

$$\tau_{LC} = \dot{m}_a C_p T_{o1}\left[\left(\frac{P_{o2}}{P_{o1}}\right)^{\frac{R}{(C_p \eta_{poly_C})}} - 1\right] \tag{2-8}$$

Likewise for adiabatic turbines having no storage elements and with a given η_{poly_T}:

$$\eta_{poly_T} = \frac{\frac{(n-1)}{n}}{\frac{(\gamma-1)}{\gamma}} \quad \text{or} \quad \frac{(n-1)}{n} = R\eta_{poly_T}$$

therefore

$$-\tau_{LT} = \dot{m}_{a8} C_p T_{o8}\left[\left(\frac{P_{o8}}{P_{o9}}\right)^{\frac{R\eta_{poly_T}}{C_p}} - 1\right] \tag{2-9}$$

Equations similar to (2-8) and (2-9) can likewise be developed for the H.P.C., H.P.T. and P.T., thus defining the differential equations (2-4). Since from equation (2-7) the total temperatures and from performance maps mass flow

rates can be found and the rate of temperature changes can be reconstructed from the solution of the differential equations, equations (2-5) are then defined if the increase in total temperature inside the combustion chamber due to fuel energy is known.

Fig. 16 shows the schematic diagram of the combustion chamber.

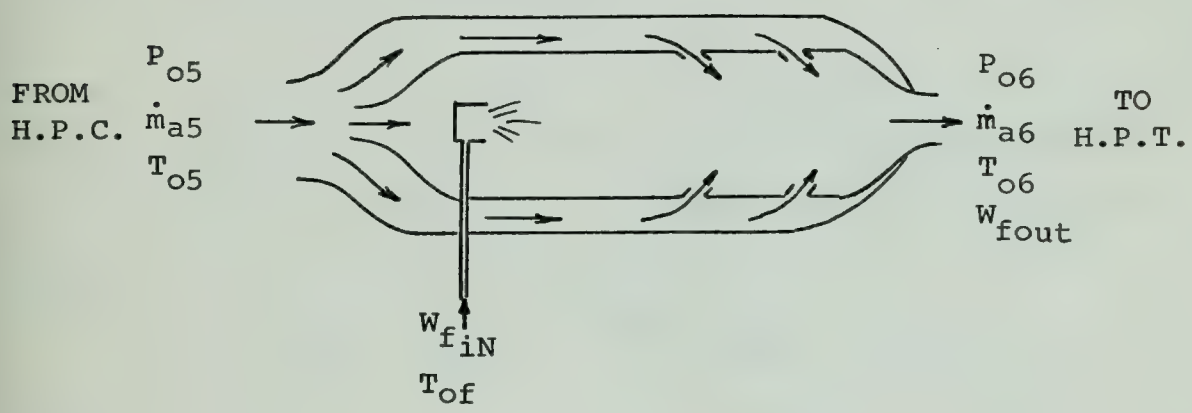

Figure 16. Schematic diagram of the combustion chamber

From the first law of thermodynamics:

$$\dot{m}_{a5} C_{p_a} T_{o5} + W_{fiN}\left[C_{p_{f_1}} T_o + h(t)\right] = \tag{2-10}$$

$$C_p W_{fout} T_{o6} + C_{p_{fg}} (W_{fiN} - W_{fout}) T_{o6} + C_{p_a} (\dot{m}_{a6} - \dot{m}_{a5}) T_{o6}$$

where: C_{p_a} = specific heat of air

$C_{p_{f_1}}$ = specific heat of liquid fuel

$C_{p_{fg}}$ = specific heat of burned fuel

$h(t)$ = instantaneous fuel heating value as defined in equation (2-2)

Since τ_1 and τ_2 in equation (2-2) are very small quantities, it can be assumed that $h(t) = W_f h_f$ where h_f is the heating value of fuel per unit weight, since combustion chambers are usually designed to carry out complete combustion way up before turbine inlet. Thus, equation (2-10) in terms of fuel air ration $W_f/\dot{m}_{a5}$ reduces to:

$$T_{o6} = \frac{C_{p_a} T_{o5} + \frac{W_f}{\dot{m}_{a5}} \left[C_{p_{fl}} T_{of} + h_f \right]}{\frac{W_f}{\dot{m}_{a5}} C_{p_{fg}} + C_{p_a}} \qquad (2\text{-}11)$$

T_{o6} is a significant term since this is the highest temperature which the turbine inlet is subjected to. For control purposes, the measured T_{o6} should account for:

1. transport delay , $e^{-\tau_d s}$, where s is the Laplacian operator and τ_d is the time delay for the burning fuel to reach the turbine inlet, and

2. time delay due to the inertia of thermocouples.

It is worthwhile to mention here that among the quick acting means of temperature protection, fuel-air ratio limiters are widely used which are especially effective at starting and sharp load increase. However, fuel-air ratio limiters have low accuracy since changes in specific heat of fuel or changes in fuel gas ambient temperature and pressure do not make setting corrections. Thus there is

still a need for very quick acting thermocouples since the time constant for heating of the sharp trailing edge of turbine blades is in the order of one to three seconds.

For the case of the LM2500 gas turbine, which has a single spool gas generator, equations (2-5a), (2-5b), (2-5g) and (2-5h) are simply deleted in the mathematical model.

II-5 REDUCTION GEAR:

As mentioned in Chapter I, reduction gear is the impedance matching component to assure that the power turbine rotor of the gas turbine and the pump rotor operate with minimum fuel consumption at a steady state on power levels most often used. Thus it can be represented in bond graph model as in Fig. 17.

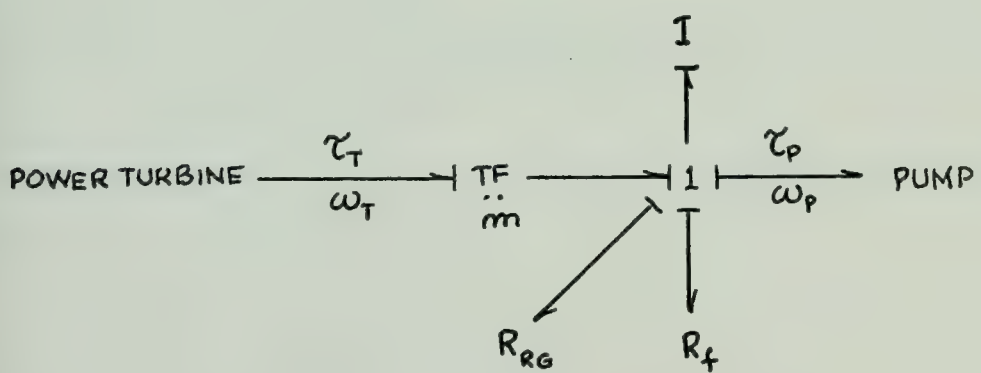

Figure 17. Reduction gear bond graph model

where: τ_T = power turbine torque

ω_T = angular speed of power turbine

τ_p = pump torque

ω_p = angular speed of pump

m = modulo of the transformer TF or the reduction gear ratio

I = combined polar moment of inertia of pump and power turbine referred to the pump shaft

R_f = shaft bearing frictional resistance

R_{RG} = reduction gear frictional resistance associated with reduction gear efficiency

Assuming the reduction gear efficiency and shaft frictional resistance to be of the form:

$$\eta_{RG} = 0.75 + 0.22(1.0 - e^{\frac{-\omega_p}{c_1}}) \qquad (2\text{-}12a)$$

$$R_f = C_2 + C_3 W \qquad (2\text{-}12\text{-}b)$$

and the constants C_1, C_2 and C_3 are to be determined from data, then from Newton's Law:

$$I \frac{d\omega_p}{dt} = m \tau_T \eta_{RG} - R_f - \tau_p \qquad (2\text{-}13a)$$

For the case where the power turbine is developing negative torque at idle, fuel flow rate during transients equation (2-13a) should be:

$$I \frac{d\omega_p}{dt} = \frac{m\tau_T}{\eta_{RG}} - R_f - \tau_p \qquad (2\text{-}13b)$$

II-6 PUMP:

Pumps are energy converters transforming mechanical power to fluid power. In order to understand the basic mechanism of pumps, consider the velocity diagram represented in Fig. 18 for axial and/or centrifugal pumps without guide vanes. The solid lines represent the design point velocity diagram while the dotted lines represent the off design velocity diagram.

U = rotor blade velocity

W_1 = relative velocity of entrant fluid with respect to rotor

C_1 = absolute velocity of entrant fluid to rotor and also exit fluid from stator

C_2 = absolute velocity of exit fluid from rotor or entrant to stator

W_2 = relative velocity of exit fluid from rotor

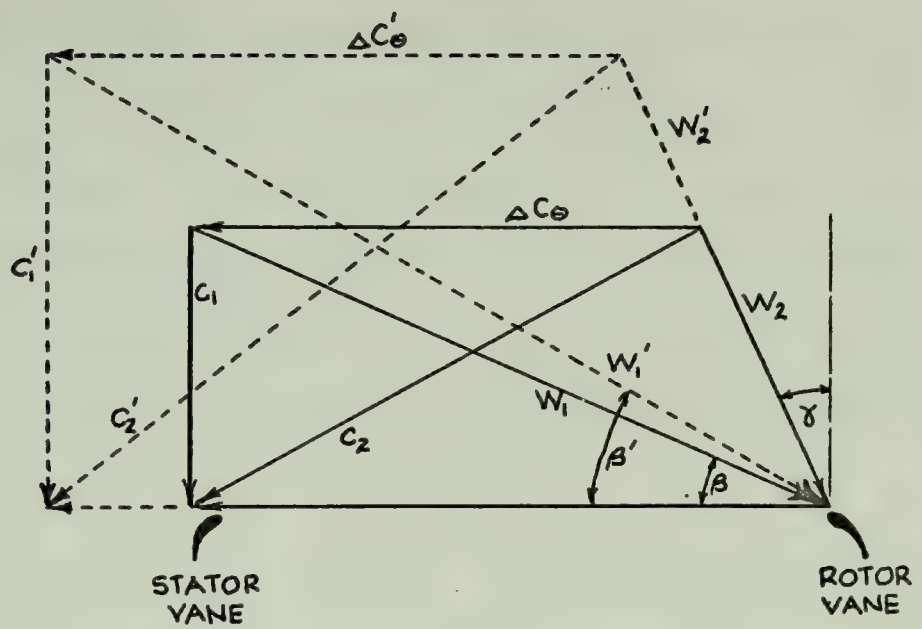

Figure 18. Pump velocity diagram

For a fixed geometry pump, referring to Fig. 18:

$$\Delta C_\theta = W_1(\cos\beta - \sin\beta \tan\gamma) = \phi(\beta) \qquad (2\text{-}14a)$$

$$\Delta C'_\theta = W'_1(\cos\beta' - \sin\beta' \tan\gamma) = \phi(\beta') \qquad (2\text{-}14b)$$

where:

$$W_1 = U^2 + C_1^2 \qquad \sin\beta = \frac{C_1}{\sqrt{U^2 + C_1^2}}$$

$$W'_1 = U'^2 + C'^2_1 \qquad \sin\beta' = \frac{C'_1}{\sqrt{U'^2 + C'^2_1}}$$

From the above equation it can be seen that the change in the tangential velocity component (ΔC_θ) of the fluid at any operating point is a strong function of dynamic similarity "flow coefficient" angle β and a weak

function of angle γ since the deviation angle of the fluid at blade trailing edges is approximately constant. Since $\sin\beta$ and $\cos\beta$ are periodic functions, then pump and/or turbine characteristics must necessarily also be periodic functions of dynamic similarity "flow coefficient" angle β .

From Euler's equation, torque (τ) and pressure (P) are:

$\tau = \rho Q r \Delta C_\theta$ where r is the pump radius

$P = \rho r \Delta C_\theta \omega$ where ω is angular speed

Substituting equation (2-14) results in:

$$\tau = \left[\rho r \phi(\beta)\right] \cdot Q = \mathcal{R}_g(\beta) \cdot Q \qquad (2\text{-}15a)$$

$$P = \left[\rho r \phi(\beta)\right] \cdot \omega = \mathcal{R}_g(\beta) \cdot \omega \qquad (2\text{-}15b)$$

Thus, unlike positive displacement pumps and turbines, which are transformerly coupled, centrifugal and axial pumps and turbines are gyratorly coupled by $R_g(\beta)$.

If appropriate power dissipation terms, $\mathcal{P}_d$, are added to equations (2-15) such that:

$$\mathcal{P}_d = \tau_p \omega - P_p Q > 0 \qquad (2\text{-}16)$$

where: subscript $_p$ = actual pump torque and pressure

$\mathcal{P}_d$ = power dissipation

then for a physical pump we have:

$$\tau_p = R_g \cdot Q + \tau_d = R_g \cdot Q + R_\omega \cdot \omega \qquad (2\text{-}17a)$$

$$P_p = R_g \cdot \omega - P_d = R_g \cdot \omega - R_Q \cdot Q \qquad (2\text{-}17b)$$

where: τ_d = dissipation torque

P_d = dissipation pressure

The bond graph from representation of equation (17) is:

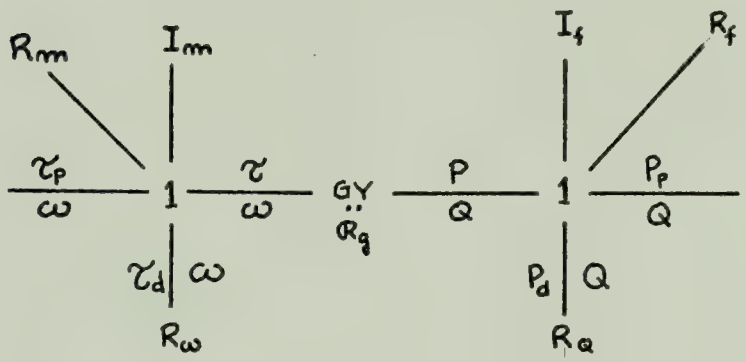

Figure 19. Axial or centrifugal pump bond graph model

where: I_m = polar moment inertia of rotors

I_f = fluid inertance in pipings

R_m = bearing frictional resistance

R_f = pipe frictional resistance

Note that the bearing frictional torque R_m is not the same as the pump torsional resistance R_ω. By referring to

the typical centrifugal pump performance curves of Fig. 20

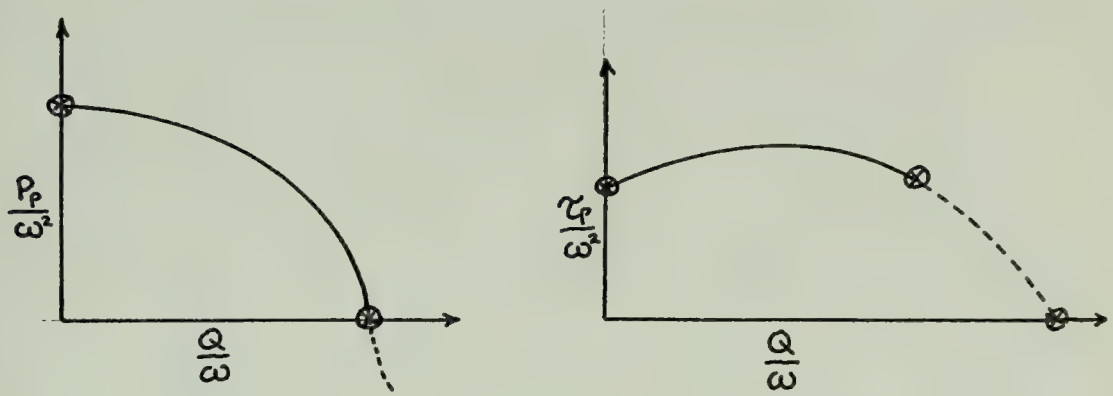

Figure 20. Typical centrifugal pump characteristics

and taking note of the points (x) where the power flow $\tau\omega$ or PQ are zero across the gyrator (GY), it is evident that the dissipation torque $\tau_d = \tau_d(Q, \omega^2)$ and the dissipation pressure $P_d = P_d(Q, \omega^2)$. It can also be shown that R_w and R_q are not independent and can be related by some function $R_d(Q, \omega)$. There the bond graph of Fig. 19 reduces to Fig. 21.

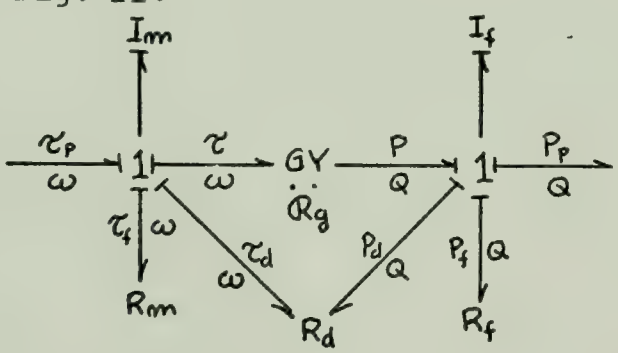

Figure 21. Axial or centrifugal pump model

where: $R_d = R_d(Q,\omega)$ = two port pump resistance

R_m = bearing frictional resistance

R_f = frictional resistance on pipings

From Newton's law and the above diagram:

$$I_m \frac{d\omega}{dt} = \tau_p - \tau_f - (R_g Q + R_w \omega) \qquad (2\text{-}18)$$

$$I_f \frac{dQ}{dt} = (R_g \omega - R_Q Q) - P_f - P_p \qquad (2\text{-}19)$$

where: τ_p = pump input torque

τ_f = shaft bearing frictional torque

P_f = piping resistance friction pressure

P_p = pump pressure load

For S.E.S. waterjet propulsion, the axial pump characteristic used in the system study (Fig. 22) was taken from ref. (6), where the head coefficient $\psi = gHp/U^2$ is expressed as a function of flow coefficient $\phi = C_x/U$. Here the pump pressure P_p of equation (2-17b) is:

$$H_p = \frac{U^2 \psi}{g} \quad \text{or} \quad P_p = \frac{\rho U^2 \psi}{g} = R_g \omega - R_Q Q \qquad (2\text{-}20)$$

where: ρ = density of fluid (lb/ft^3)

g = gravity constant (32.2 ft/sec^2)

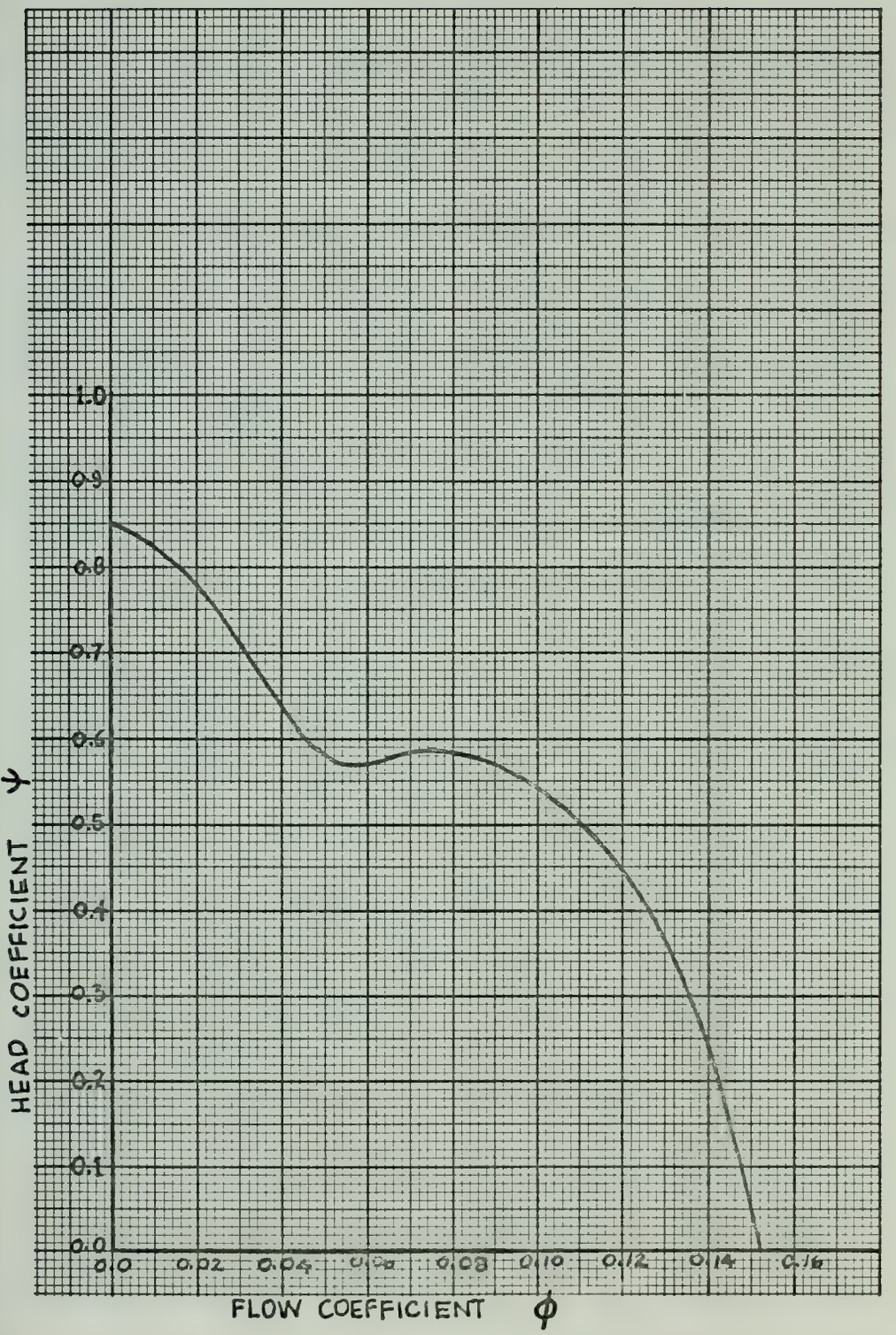

FIGURE 22 PERFORMANCE CHARACTERISTIC OF AXIAL PUMP

The design ϕ and ψ of the above pump are 0.108 and 0.51, respectively. To obtain τ_p of equation (2-17a), a dissipation function coefficient equivalent to equation (2-16) is assumed to be of the form:

$$\mathbb{P}_d = \mathbb{P}_{d_{min}} + C_1(\phi - \phi_d)^2 \qquad (2\text{-}21)$$

where: $\mathbb{P}_d$ = dimensionless power dissipation

$\mathbb{P}_{d_{min}}$ = minimum $\mathbb{P}_d$ (at design point)

ϕ_d = flow coefficient at design point

C_1 = some constant to be determined relating to the efficiency characteristic of the pump

Combining equations (2-21), (2-16) and (2-20), then τ_p and P_p of equations (2-17) in terms of pump dimension reduces to:

$$\tau_p = (\psi\phi + \mathbb{P}_d)\frac{\rho A_n}{2g}\left[\frac{N}{60}\pi\right]^2 D^3 \qquad (2\text{-}22a)$$

$$P_p = \frac{\rho\psi}{g}\left[\frac{N}{60}\pi D\right]^2 \qquad (2\text{-}22b)$$

where: τ_p = pump torque (ft-lb)

ψ = dimensionless head coefficient

ϕ = dimensionless flow coefficient

$\mathbb{P}_d$ = dimensionless power dissipation of equation (2-21)

ρ = water density (64 lb/ft^3)

A_n = pump annulus area (ft^2)

N = pump RPM

D = pump blade tip to tip diameter (ft)

II-7 INLETS:

Flushed and semiflushed inlets shown in Fig. 23 and Fig. 24, respectively are considered to be more practicable to use for S.E.S. than ram inlets.

The geometric parameters affecting the design pressure recovery and drag characteristics of flushed and semiflushed inlets are: entrance width to depth ratio, ramp wall divergence and ramp angle. For fixed geometry inlets, performance at various operating points is best described by efficiency of pressure recovery η_i as a function of velocity ratio V_i/V_o where V_o is the velocity of the craft and V_i is the average axial velocity of the fluid across the inlet throat area A_i. Some typical pressure recovery performances of flushed and semiflushed inlets (ref.(32)) are shown in Fig. 25 and Fig. 26.

Similarly, the drag coefficient

$$C_d = \frac{D}{\frac{1}{2}\frac{\rho}{g}V_o^2 A_i} = \frac{D\ \frac{V_i}{V_o}}{\frac{\rho}{2g}V_o Q}$$

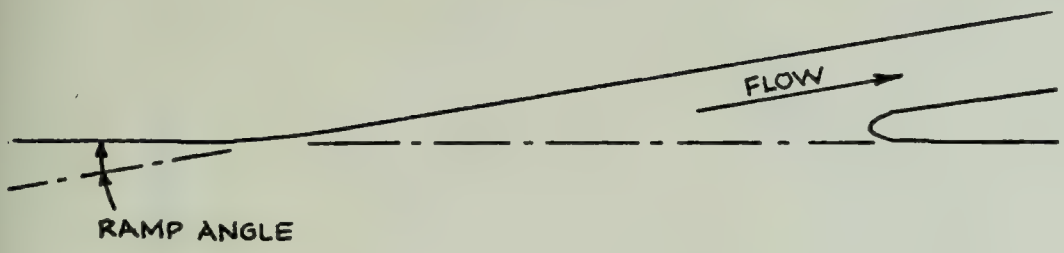

FIGURE 23 FLUSHED INLET

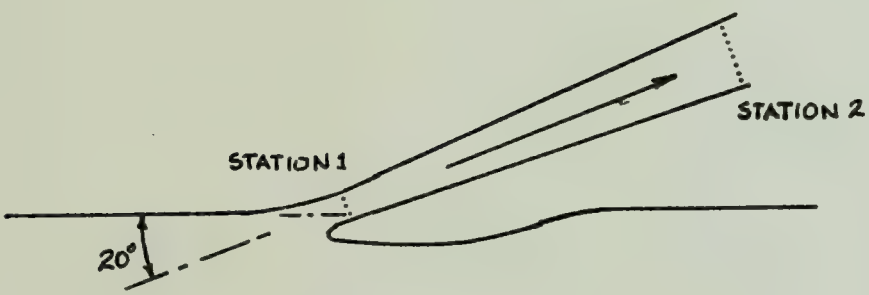

FIGURE 24 SEMIFLUSHED INLET

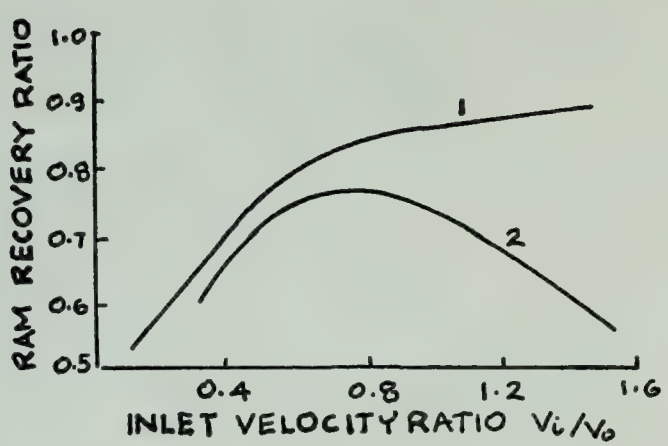

FIGURE 25 FLUSHED INLET RAM RECOVERY RATIO FOR PARALLEL WALLS
1 - MEASURED AFTER INLET SECTION
2 - MEASURED AFTER DIFFUSER SECTION
(WIDTH TO DEPTH RATIO = 2 ; RAMP ANGLE = 15°)

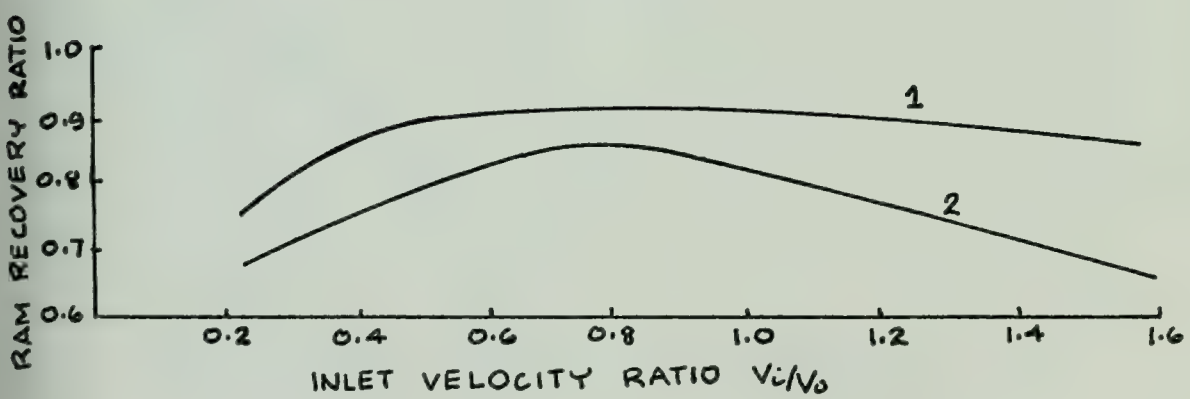

FIGURE 26 SEMIFLUSHED INLET RAM RECOVERY RATIO
1- MEASURED AFTER INLET SECTION
2- MEASURED AFTER DIFFUSER SECTION

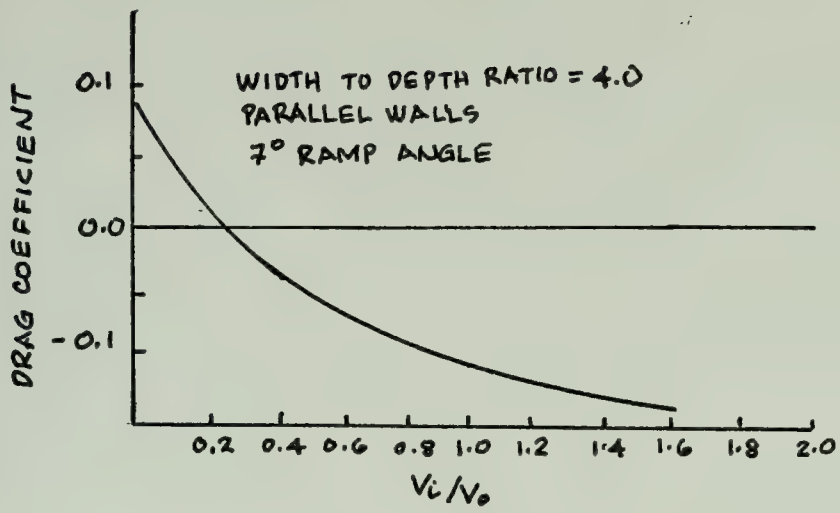

FIGURE 27 FLUSHED INLET DRAG

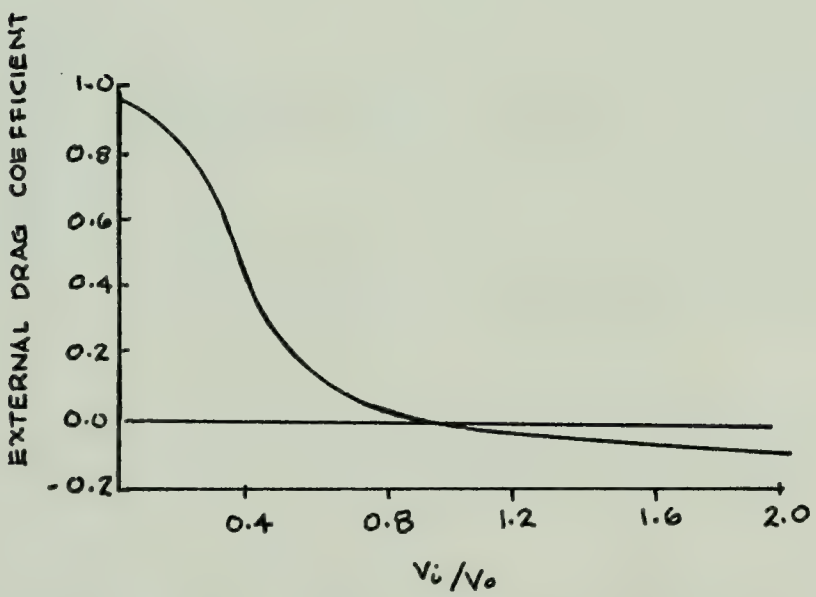

FIGURE 28 DRAG OF SEMIFLUSHED INLET

can also be expressed as a function of the ratio V_i/V_o to describe the drag (D) characteristics of the inlet at various operating conditions. Some typical drag characteristics of flushed and semiflushed inlets (ref.(32)) are shown in Fig. 27 and Fig. 28.

From the above pressure recovery characteristics the bond graph representation of inlet is:

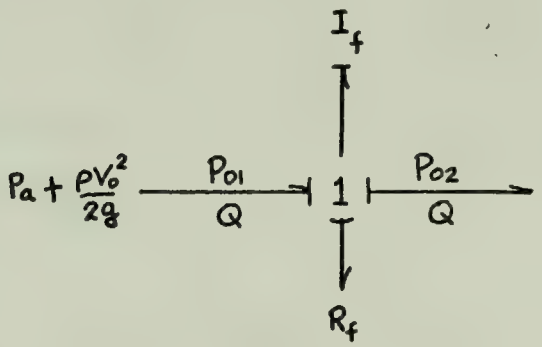

Figure 29. Flushed or semiflushed inlet bond graph model

where: I_f = fluid inertance in the inlet section

P_{o1} = total pressure of the fluid way ahead of the craft

R_f = equivalent resistance of the inlet plus the boundary layer losses at the sidewall of the S.E.S. in front of the inlet

P_{o2} = total pressure at the exit of the inlet or at the entrance of the diffuser section so that at the steady state: $P_{o2} = \eta_i P_{o1}$

II-8 DIFFUSER:

The purpose of the diffuser is to increase the static pressure at pump inlet by converting the kinetic energy to static head. For a given expansion angle and fixed inlet condition, the total pressure loss of a diffuser is proportional to the theoretical value of the total pressure loss for a sudden expansion of the same exit area to inlet area ratio ($A_R = \frac{A_{out}}{A_{in}}$). This proportionality constant is called diffuser loss factor (K_f) and is defined by:

$$K_f = \frac{(P_{o_{in}} - P_{o_{out}})q_1}{\frac{(A_R - 1)}{A_R}} \qquad (2\text{-}23)$$

where: $P_{o_{in}}$ = total pressure at entrance to diffuser

$P_{o_{out}}$ = total pressure at exit to diffuser

q_1 = dynamic pressure at entrance to diffuser

$q_1 = \frac{\rho v^2_{in}}{2g}$

A_R = area ratio

Figure 30 shows the diffuser loss coefficient K_f as a function of area ratio (A_R) and diffusion angle (2θ) for various geometrical shapes of diffusers. The bond graph representation, then, of the diffuser is:

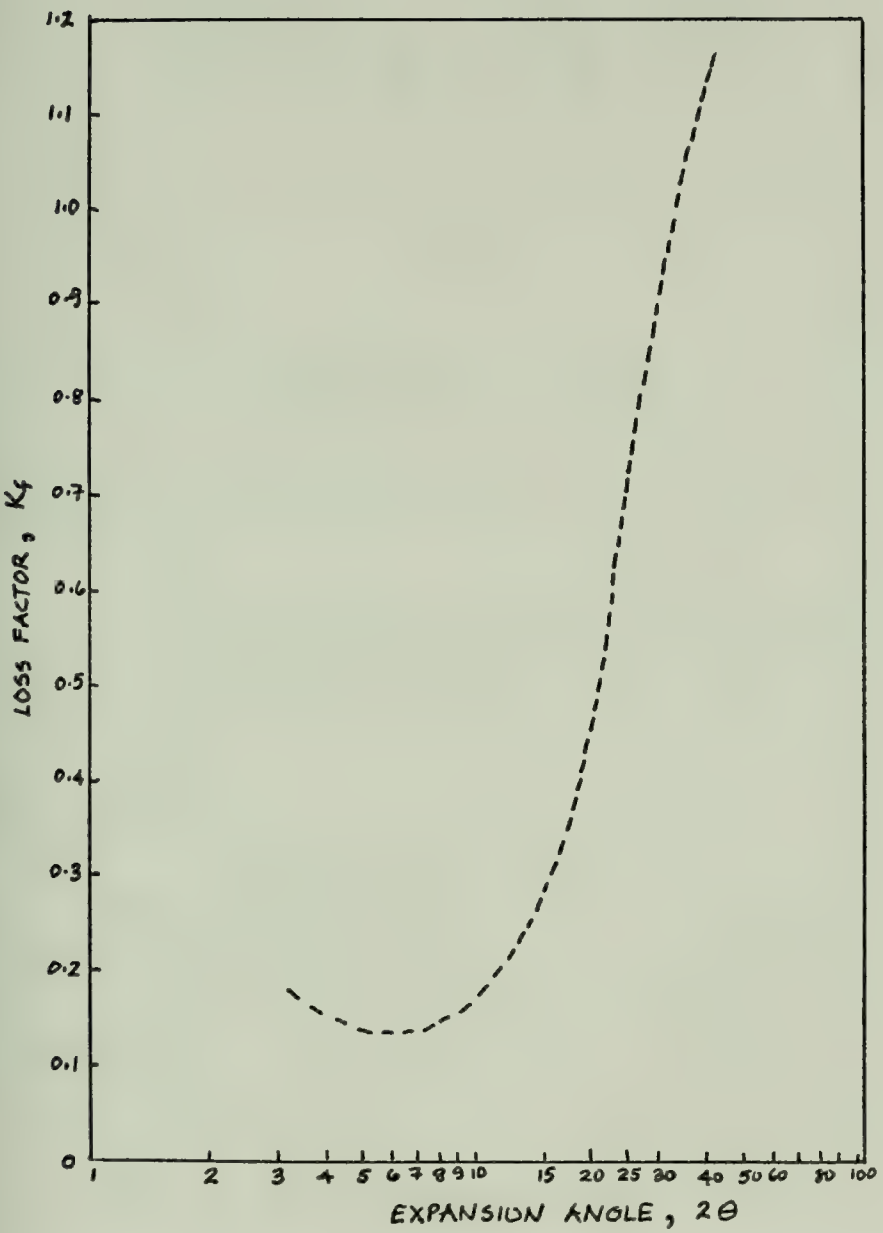

FIGURE 30 RECTANGULAR DIFFUSER LOSS FACTOR

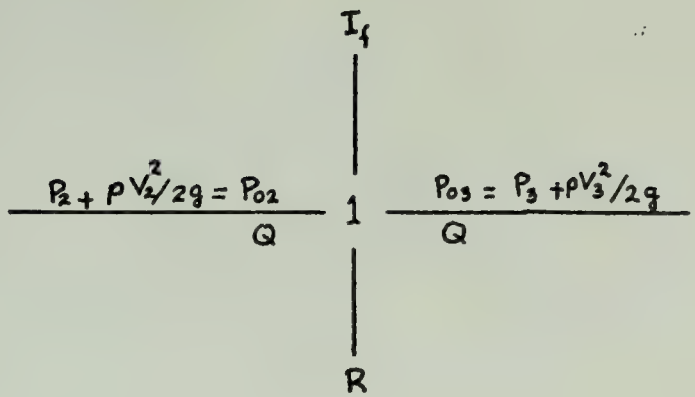

Figure 31. Diffuser bond graph model

so that at the steady state:

$$P_{o3} - P_{o2} = K_f \left[\frac{A_R - 1}{A_R} \right]^2 \rho V_2^2/2g \qquad (2\text{-}24)$$

II-9 NOZZLE:

The purpose of the nozzle is to convert the excess static head of the total head by the pump into kinetic energy head so that thrust can be developed. A well-designed nozzle, unlike diffusers, has negligible loss so that efficiency of 96-99% can be easily attained. The bond graph representation of nozzle is:

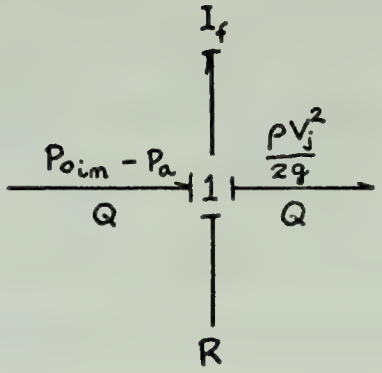

Figure 32. Nozzle bond graph model

so that at the steady state:

$$\frac{\rho V_j^2}{2g} = \eta_n (P_{o_{in}} - P_a) \qquad (2\text{-}25)$$

where $P_{o_{in}}$ = total pressure at the pump exit

P_a = atmospheric pressure

η_n = nozzle efficiency

II-10 S.E.S., MASS, RESISTANCE AND WATERJET PROPULSION THRUST:

The S.E.S. bare hull resistance data used in this study are tabulated in Appendix I. Note that if the boundary layer losses due to S.E.S. sidewall frictional resistance are included in the conputation for the total pressure recovered at the exit of the flushed or semiflushed inlet, then by energy conservation, an equivalent resistance

must be subtracted from the bare hull resistance data above. Otherwise, the propulsion system will be penalized twice. The assumed added mass for the forward motion of the S.E.S. was 10% of the total displacement.

From the conservation of momentum, the instantaneous thrust developed for a fixed reference frame is:

$$\vec{T} = \frac{d}{dt} \iiint_V \left[\frac{\rho}{g} \vec{v} dV \right] + \iint_S \left[\vec{v} (\vec{v} \cdot d\vec{S}) \right] \qquad (2\text{-}26)$$

or in terms of component thrust in x and y direction:

$$T_x = \frac{\rho L_x}{g} \frac{dQ}{dt} + \frac{\rho Q}{g} (V_j \cos\alpha - V_o) \qquad (2\text{-}29a)$$

$$T_y = \frac{\rho L_y}{g} \frac{dQ}{dt} + \frac{\rho Q}{g} (V_j \sin\alpha) \qquad (2\text{-}29b)$$

where: L_x and L_y are the distances between inlet entrance and nozzle exit in x and y directions, respectively.

At the steady state, the "power input" to develop thrust is:

$$\Delta P_{in} Q = \left\{ \frac{\rho V_o^2}{2g} \left[\frac{V_j^2}{V_o^2} - 1 \right] \right\} Q \qquad (2\text{-}28a)$$

and power output is:

$$T_d V_o = \left\{ \frac{\rho Q V_o}{g} \left[\frac{V_j}{V_o} - 1 \right] \right\} V_o \qquad (2\text{-}28b)$$

where:

$$\Delta PQ - T_d V_o \geq 0$$

Since

$$T_d = \frac{\rho V_o}{g}\left[\frac{V_j}{V_o} - 1\right]$$

then it is evident that the power conversion of equations (2-8) is gyratorly coupled with modulo $m_t = \frac{\rho V_o}{g}\left[\frac{V_j}{V_o} - 1\right]$ and the bond graph representation is:

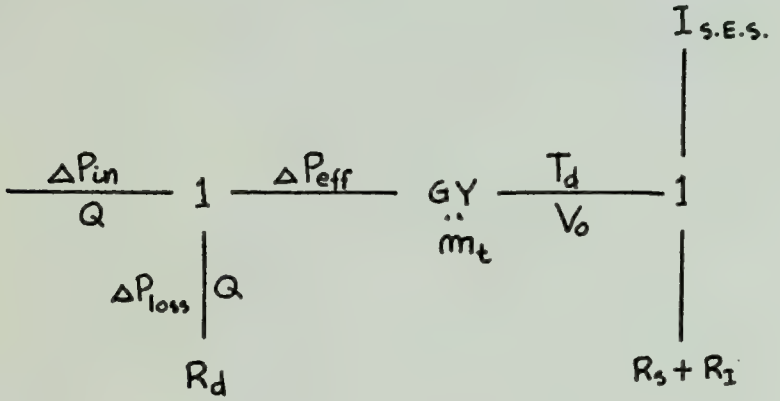

Figure 33. Bond graph model of thrust develop in S.E.S. waterjet system

The equivalent dissipator resistance

$$R_d = \frac{\Delta P_{loss}}{Q} = \frac{\Delta P_{in} - \Delta P_{eff}}{Q}$$

where

$$\Delta P_{eff} = \frac{\rho V_o}{g}\left[\frac{V_j}{V_o} - 1\right] \cdot V_o + m_t \cdot V_o$$

$$P_{in} = \frac{1}{2}\frac{\rho}{g} V_o^2 \left[\frac{V_j^2}{V_o^2} - 1\right]$$

is:

$$R_d = \frac{\rho}{g} |V_o| V_o \left[\frac{1}{2}\frac{|V_j| V_j}{|V_o| V_o} - \frac{V_j}{V_o} - \frac{1}{2}\right] / Q \qquad (2\text{-}29)$$

The overall waterjet system bond graph model which combines all the different components is shown in Fig. 34.

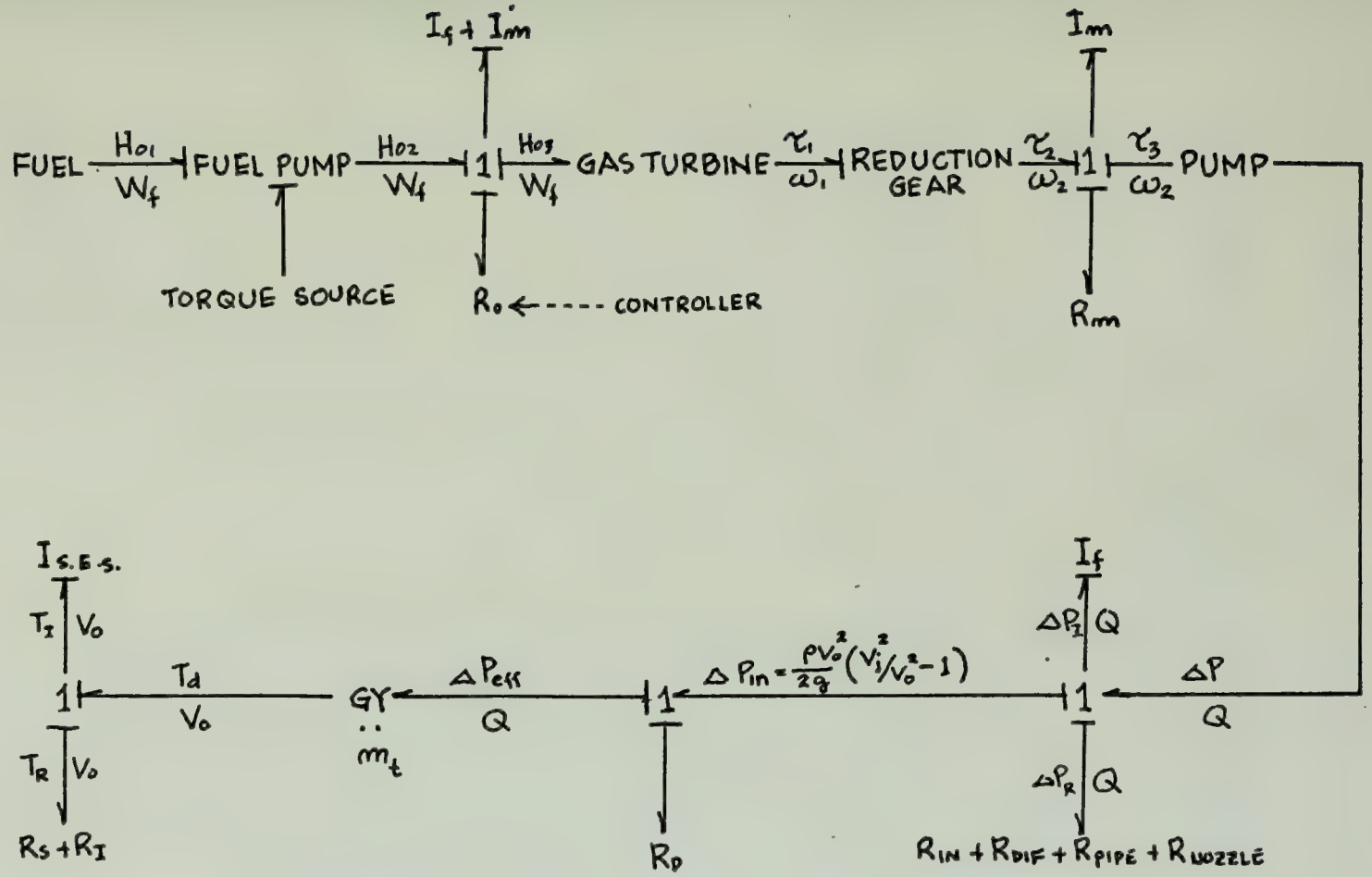

FIGURE 34 BOND GRAPH MODEL OF S.E.S. WATERJET SYSTEM

CHAPTER III

SIMULATION AND CONTROL OF S.E.S. WATERJET PROPULSION PLANT

III-1 GENERAL:

For the purpose of controlling the power turbine speed, the implementation of the detailed model of the gas turbine was found to be unnecessary. This was primarily due to the higher frequency response of the combustion process and pressures in the storage volume of the gas turbine in equations (2-5) compared to the frequency response of power turbine speed. However, for a very low value of polar moment of inertia of the power turbine drive train as referred to the pump shaft, the poles and zeroes of equations (2-4) and (2-5) will be significant in the design of a stable high frequency controller. Likewise, if the primary concern of designing a controller is the avoidance of surge in the compressor and of overtemperature in the turbine inlet of the gas generator then the detailed model will be necessary.

In the case study it was assumed that the LM2500 gas turbine used in the simulation was adequately protected

from overtemperature and surge by its own control package. This gas generator protective control setup was simulated by putting a scheduled limiter on the rate on which fuel flow demand signal can be increased. This rate can be set to have lower value than the built in limiter in LM2500. The purpose of this limiter is to allow time for the gas generator rotor to build up speed and in turn air mass flow rate in order to neutralize the increase in pressure for surge avoidance and the increase in temperature due to sudden fuel flow rate increase.

As for the rest of the gas turbine dynamics, it was noted that the instantaneous torque developed at the power turbine is a function of the instantaneous air mass flow rate and power turbine speed. Air mass flow rate in turn is dependent on the instantaneous temperature and pressure at the storage volume of the duct between power turbine and the last stage of the gas generator. Thus the transfer function of the power turbine torque from equations (2-4), (2-5), (2-7) and (2-9) can be approximated by:

$$\frac{\tau_E}{\tau_{ss}} \approx \left[\frac{1}{\tau_{GG}s+1}\right]\left[\frac{1}{\tau_V s+1}\right] = \frac{1}{\tau_{GG}\tau_V s^2 + (\tau_{GG}+\tau_V)s+1} \qquad (3\text{-}1)$$

where: τ_E = instantaneous power turbine torque

τ_{ss} = steady state power turbine torque which is a function of fuel flow rate (W_f)

and power turbine speed (N_E)

τ_{GG} = time constant for the gas generator

τ_V = time constant for the volume between power turbine and gas generator

s = Laplacian operator

Since τ_{GG} and τ_V are in the order of 10^{-1} second, which is very much lower than the time constant of the power turbine drive train speed, the first term of equation (3-1) can be neglected so that:

$$\frac{\tau_E}{\tau_{ss}} = \frac{1}{(\tau_{GG} + \tau_V)\ s + 1} \qquad (3\text{-}2)$$

The plot of τ_{ss} as function of fuel flow rate W_f and the power turbine RPM is shown in Fig. 8.

III-2 DYNAMIC EQUATIONS OF THE WATERJET PROPULSION PLANT:

With the above approximation, the water propulsion system was reduced to the following non-linear ordinary differential equations:

a. The S.E.S. Velocity Equation

$$\frac{dV_o}{dt} = \frac{g}{W}\left[T_x(V_o,Q) - R_s(V) - R_I(V_o,Q,A_i)\right] \qquad (3\text{-}3a)$$

where: V_o = S.E.S. velocity (ft/sec)

W = S.E.S. mass plus 10% added mass (lbm)

g = gravity (32.2 ft/sec^2)

T_x = waterjet propulsion thrust (lbf)

R_s = S.E.S. bare hull resistance (lbf)

R_I = flushed inlet appendage drag (lbf)

A_i = flushed inlet throat area (ft^2)

The instantaneous thrust (T_x) in the longitudinal direction of the craft from equation (2-27a) is:

$$T_x = \frac{\rho L_x}{g}\left[\frac{dQ}{dt} - A_x\frac{dV_o}{dt}\right] + \frac{\rho Q}{g}(V_j \cos\alpha - V_o) \quad (3\text{-}3a\text{-}1)$$

where: ρ = water density (lbm/ft^3)

L_x = longitudinal distance between the flushed inlet entrance and nozzle area (ft)

A_x = effective cross sectional area in longitudinal direction (ft^2)

V_o = waterjet velocity at the nozzle exit (ft/sec)

α = depression angle of the nozzle

The S.E.S. bare hull resistance (R_s) should be a function of S.E.S. velocity (V_o and S.E.S. operating draft or air cushion pressure. In the simulation, however, it was assumed that the S.E.S. was at designed cushion pressure above hump speed. Below hump speed a resistance (R_s)

proportional to V_o^2 was assumed, so that:

$$R_s = 167.72\ V_o^2 \qquad 0 \leq V_o \leq 50.7 \qquad (3\text{-}3a\text{-}2)$$

$$R_s = 26.726\ V_o^2 - 6935.34\ V_o + 712204.0 \qquad V_o \geq 50.7$$

The flushed inlet drag R from equation (2-23) is:

$$R_I = \frac{1}{2} C_D \frac{\rho}{g} V_o Q \frac{V_i}{V_o} \qquad (3\text{-}3a\text{-}3)$$

For the purpose of controller design the flush inlet drag coefficient C_d was assumed to have a sharper point of minimum value at $V_i/V_o=0.8$. The minimum value of C_d was also assumed to be equal to 0.15 consistent with the published experimental data, so that:

$$C_d = 1.0 \qquad V_i/V_o < 1.0$$

$$C_d = 1.0 - (0.8/0.85)(V_i/V_o) \qquad 1.0 \leq V_i/V_o \leq 0.8$$

$$C_d = 0.2\ V_i/V_o - 0.01 \qquad V_i/V_o > 0.8$$

b. The Pump Speed Equation

$$\frac{dN}{dt} = \frac{60}{2\pi I_m}\left[\tau_s(\tau_E, RGR) - \tau_F(N) - \tau_p(N,Q)\right] \qquad (3\text{-}3b)$$

where: N = pump RPM

I_m = polar moment of inertia of power turbine, reduction gear and pump rotor referred to pump shaft ($ft\text{-}lb/sec^2$)

τ_s = effective engine torque at pump shaft (ft-lbf)

τ_F = shaft bearing friction torque (ft-lbf)

τ_p = pump torque (ft-lbf)

The effective engine torque at pump shaft from equation (2-13) is:

$$\tau_s = (RGR)\,\tau_E\,\eta_{RG} \qquad \tau_E \geq 0 \qquad (3\text{-}3b\text{-}1)$$

$$\tau_s = (RGR)\,\frac{\tau_E}{\eta_{RG}} \qquad \tau_E < 0$$

where: RGR = reduction gear ratio = 5.55

η_{RG} = reduction gear efficiency

$\eta_{RG} = 0.75 + 0.22\,(1 - e^{-N_E/895})$, where

N_E = power turbine speed

The shaft bearing torque (τ_F) is assumed to be:

$$\tau_F = 1000 + 15N \quad \text{(ft-lbf)} \qquad (3\text{-}3b\text{-}2)$$

The pump torque (τ_p) from equation (2-22a) is:

$$\tau_p = (\Psi\phi + \mathbb{P}_d)\,\frac{\rho A_n}{2g}\left[\frac{N}{60}\,\pi\right]^2 D^3 \qquad (3\text{-}3b\text{-}3)$$

where

$$\phi = \frac{\frac{Q}{A_n}}{\frac{N\pi D}{60}}$$

A curve is fitted to the pump characteristics of Fig. 22 for the head coefficient (ψ) as a function of flow coefficient (ϕ) so that:

$$\psi = -83.3\phi^2 - 1.916\phi + 0.85 \qquad \phi \leq 0.04$$

$$\psi = 220\phi^2 - 25.5\phi + 1.308 \qquad 0.0 \leq \phi \leq 0.065$$

$$\psi = -68.217\phi^2 + 10.173\phi + 0.2069 \qquad 0.065 \leq \phi \leq 0.130$$

$$\psi = -318.45\phi^2 + 72.713\phi - 3.6949 \qquad 0.130 \leq \phi \leq 0.152$$

The dimensionless power dissipation $\mathbb{P}_d$ of equation (3-3b-3) was normalized to a pump having an efficiency of 90% at design point so that equation (2-21) yields:

$$\mathbb{P}_d = 0.00623 + 12.4\ (\phi - 0.108)^2$$

c. Waterjet Flow Rate Equation per Pump

$$\frac{dQ}{dt} = \frac{\rho}{I_f}\left[H_p(N,Q) + H_{SV}(V_o, A_i) - H_j(Q) + H_{\dot{V}}\left(\frac{dV_o}{dt}\right)\right] \quad (3\text{-}3c)$$

where:

Q = water flow rate (ft^3/sec)

ρ = water density (lbm/ft^3)

I_f = fluid inertance in pipe ($lb\text{-}sec^2/ft^5$)

H_{SV} = pump net positive suction head (ft)

H_j = waterjet kinetic head at the nozzle (ft)

$H_{\dot{V}}$ = head generated due to S.E.S. acceleration (ft)

The pump head H_p from equation (2-22b) is:

$$H_p = \frac{\psi}{g}\left[\frac{N}{60}\pi D\right]^2 \qquad (3\text{-}3c\text{-}1)$$

The net positive suction head H_{SV} from equation (2-25) and from flushed inlet efficiency characteristics is:

$$H_{SV} = \frac{1}{2}\frac{V_o^2}{g}\eta_i\eta_D - H_{WL} \qquad (3\text{-}3c\text{-}2)$$

where: η_i = flushed inlet efficiency

η_D = diffuser efficiency

H_{WL} = pump height above waterline

$\eta_i = 0.85(1-e^{-0.1Q/A_iV_o})$

$\eta_D = 1-K_f(\frac{A_R-1}{A_R})^2$

The waterjet kinetic head at the nozzle (H_j) is:

$$H_j = \frac{V_j^2}{2g\eta_N} \qquad (3\text{-}3c\text{-}3)$$

where: η_N = nozzle efficiency ≈ 1.0

$V_j = Q/C_cA_{NOZ}$ = waterjet velocity (ft/sec)

C_c = nozzle coefficient of area contraction ≈ 1.0

A_{NOZ} = cross sectional area of nozzle throat (ft^2)

The head generated through S.E.S. acceleration ($H_{\dot{V}}$) is:

$$H_{\dot{V}} = \frac{L_x}{g}\left[\frac{dV_o}{dt} - \frac{1}{A_x}\frac{dQ}{dt}\right] \qquad (3\text{-}3c\text{-}4)$$

where: L_x = distance between entrance to flushed inlet and nozzle exit in the V_o direction (ft)

d. Power Turbine Torque Equation

$$\frac{d\tau_E}{dt} = 0.5\left[\tau_{ss}(W_f, N_E) - \tau_E\right] \qquad (3\text{-}3d)$$

where: τ_E = instantaneous power turbine torque (ft-lbf)

τ_{ss} = steady state power turbine torque as found in the engine performance map

N_E = power turbine RPM

The factor 0.5 is the $(\tau_{GG} + \tau_V)$ term in equation (3-2).

e. Fuel Flow Rate Equation

$$\frac{dW_f}{dt} = 2.0\ (W_{fd} - W_f) \qquad (3\text{-}3e)$$

where: W_f = instantaneous fuel flow rate (lbm/hr)

W_{fd} = fuel flow rate demand signal (lbm/hr)

Equation (3-3e) assumes that LM2500 control package has a built-in servomechanism for the fuel pump with a time constant of 0.5 second and a constant gain of 1.0. The rate limit and hard limit were incorporated in the fuel flow rate demand signal so that

$$\dot{W}_{fd} \leq \dot{W}_{fd_{max}}$$

$$W_{fd_{min}} \leq W_{fd} \leq W_{fd_{max}}$$

The minimum fuel flow rate demand signal $W_{fd_{min}}$ was set to idling fuel flow rate of 800 lbm/hr and the maximum fuel flow rate demand signal $W_{fd_{max}}$ was set to 10,000 lbm/hr. The maximum rate of change of the fuel demand signal $W_{fd_{max}}$ was set to six seconds from $W_{fd_{min}}$ to $W_{fd_{max}}$.

f. The Flushed Inlet Area Servomechanism Equation

$$\frac{dA_i}{dt} = 0.5\ (A_{id} - A_i) \qquad (3\text{-}3f)$$

where: A_i = instantaneous flushed inlet throat area (ft^2)

A_{id} = flushed inlet throat area demand (ft^2)

Equation (3-3f) assumes a hydraulic servoactuator for the flushed inlet throat area with a time constant of two seconds and a constant gain of 1.0. In the simulation, the

hydraulic actuator was set to have a hard limit of 7.0 ft^2 maximum, 1.5 ft^2 minimum, and a rate limit of 0.5 ft^2/sec so that

$$\dot{A}_i \leq 0.5$$

$$1.5 \leq A_i \leq 7.0$$

III-3 PUMP CAVITATION:

To simulate pump cavitation during transient condition at various pump operating points, a dimensionless suction head criteron was assumed to be:

$$\Psi_{SVC} = \frac{g\ H_{SVC}}{U^2} = \Psi_{SVC}(\phi)$$

where: H_{SVC} = critical net positive pump suction head (ft)

U = pump blade tip velocity (ft/sec)

A curve is fitted into the pump cavitation data (Fig. 22) so that Ψ_{SVC} is defined as a function ϕ. The pump is assumed to cavitate if the actual dimensionless suction head $\Psi_{SVA} = \frac{g\ H_{SV}}{U^2}$ fell below Ψ_{SVC}. The degree of degradation in pump performance was assumed to be of the form:

$$\Psi_C = \Psi\left[1 - C_1\left[\frac{\Psi_{SVC}-\Psi_{SVA}}{\Psi_{SVC}}\right]^2\right] \quad \Psi_{SVA} < \Psi_{SVC} \qquad (3\text{-}5)$$

where: ψ_c = dimensionless head with cavitation

ψ = dimensionless head without cavitation

C_1 = some constant to fit the pump cavitation data

Substituting equation (3-5) to equation (3-3c-1), the pump head generated with cavitation is:

$$H_p = \frac{\psi}{g}\left[1 - C_1\left[\frac{\psi_{SVC} - \psi_{SVA}}{\psi_{SVC}}\right]^2\right]\left[\frac{N}{60}\pi D\right]^2 \quad \psi_{SVA} < \psi_{SVC} \tag{3-6}$$

The dimensionless power dissipated when there is cavitation $\mathbb{P}_{dc}$ is also assumed to be of the form:

$$\mathbb{P}_{dc} = \mathbb{P}_d\left[1.0 + C_2\left[\frac{\psi_{SVC} - \psi_{SVA}}{\psi_{SVC}}\right]\right] \quad \psi_{SVA} < \psi_{SVC} \tag{3-7}$$

where: $\mathbb{P}_d$ = dimensionless power dissipated without cavitation as defined in equation (2-21)

C_2 = some constant to be determined from pump data

Substituting ψ_c and P_{dc} in equation (3-3b-3), pump torque with cavitation is:

$$\tau_p = \left[\phi\psi_c + P_{dc}\right]\frac{\rho A_n}{g}\left[\frac{N}{60}\pi\right]^2 D^2 \quad \psi_{SVA} < \psi_{SVC}$$

III-4 LINEARIZED DYNAMIC EQUATION OF THE WATERJET PROPULSION:

The linear expansion of equation (3-3a) about a steady state operating point yields:

$$\dot{V}_o = \dot{V}_{oo} + \frac{g}{W}\left[\frac{\partial T_x}{\partial V}(V_o - V_{oo}) + \frac{\partial T_x}{\partial Q}(Q - Q_o) - \frac{\partial R_s}{\partial V}(V_o - V_{oo})\right.$$

$$\left. - \frac{\partial R_i}{\partial V}(V_o - V_{oo}) - \frac{\partial R_i}{\partial Q}(Q - Q_o) - \frac{\partial R_i}{\partial A_i}(A_i - A_{io})\right]$$

The subscript $_o$ represents the steady state operating point values of the state variables and the partial derivatives are evaluated at the corresponding steady state operating point values. Similar expressions can be derived for the rest of the equations of (3-3). At steady state:

$$\dot{V}_{oo} = \dot{N}_o = \dot{Q}_o = \dot{\tau}_{E_o} = \dot{W}_{f_o} = \dot{A}_{i_o} = 0$$

Defining:

$$V_o - V_{oo} = V_{o*} \qquad \text{and} \qquad \dot{V}_o - \dot{V}_{oo} = \dot{V}_o = \dot{V}_{o*}$$

$$Q - Q_o = Q_* \qquad \text{and} \qquad \dot{Q} - \dot{Q}_o = \dot{Q} = \dot{Q}_*$$

etc. yields the linear form of equations (3-3).

$$\begin{bmatrix} \dot{V}_{o*} \\ \dot{N}_{*} \\ \dot{Q}_{*} \\ \dot{\tau}_{E*} \\ \dot{W}_{f*} \\ \dot{A}_{i*} \end{bmatrix} = \begin{bmatrix} A_{11} & 0 & A_{13} & 0 & 0 & A_{16} \\ 0 & A_{22} & A_{23} & A_{24} & 0 & 0 \\ A_{31} & A_{32} & A_{33} & 0 & 0 & A_{36} \\ 0 & A_{42} & 0 & A_{44} & A_{45} & 0 \\ 0 & 0 & 0 & 0 & A_{55} & 0 \\ 0 & 0 & 0 & 0 & 0 & A_{66} \end{bmatrix} \begin{bmatrix} V_{o*} \\ N_{*} \\ Q_{*} \\ \tau_{E*} \\ W_{f*} \\ A_{i*} \end{bmatrix} + \begin{bmatrix} 0 & 0 \\ 0 & 0 \\ 0 & 0 \\ 0 & 0 \\ B_{51} & 0 \\ 0 & B_{62} \end{bmatrix} \begin{bmatrix} \overset{*}{W}_{fd} \\ \overset{*}{A}_{id} \end{bmatrix} \qquad (3\text{-}8)$$

where:

$$A_{11} = \frac{g}{W}\left[\frac{\partial T_x}{\partial V_o} - \frac{\partial R_s}{\partial V_o} - \frac{\partial R_I}{\partial V_o}\right]$$

$$A_{13} = \frac{g}{W}\left[\frac{\partial T_x}{\partial Q}\right]$$

$$A_{16} = \frac{g}{W}\left[-\frac{\partial R_I}{\partial A_i}\right]$$

$$A_{22} = \frac{60}{2\ I_m}\left[-\frac{\partial \tau_F}{\partial N} - \frac{\partial \tau_p}{\partial N}\right]$$

$$A_{23} = \frac{60}{2\ I_m}\left[-\frac{\partial \tau_p}{\partial Q}\right]$$

$$A_{24} = \frac{60}{2\ I_m}\left[\frac{\partial \tau_s}{\partial \tau_E}\right] = \frac{60}{2\pi I_m}\ \eta_{RG}\,RGR$$

$$A_{31} = \frac{64.2}{I_f}\left[\frac{\partial H_{SV}}{\partial V_o}\right]$$

$$A_{32} = \frac{64.2}{I_f}\left[\frac{\partial H_p}{\partial N}\right]$$

$$A_{33} = \frac{64.2}{I_f}\left[\frac{\partial H_p}{\partial Q} - \frac{\partial H_i}{\partial Q}\right]$$

$$A_{36} = \frac{64.2}{I}\left[\frac{\partial H_{SV}}{\partial A_i}\right] \approx 0.0$$

$$A_{42} = 0.5\left[\frac{\partial \tau_{ss}}{\partial N_E} \cdot \frac{\partial N_E}{\partial N}\right] = 0.5\ RGR\left[\frac{\partial \tau_{ss}}{\partial N_E}\right]$$

$$A_{44} = 0.5\left[-\frac{\partial \tau_E}{\partial \tau_E}\right] = -0.5$$

$$A_{45} = 0.5\left[\frac{\partial \tau_{ss}}{\partial W_f}\right]$$

$$A_{55} = 2.0\left[-\frac{\partial W_f}{\partial W_f}\right] = -2.0$$

$$A_{66} = 0.5\left[-\frac{\partial A_i}{\partial A_i}\right] = -0.5$$

$$B_{51} = 2.0\left[\frac{\partial W_{fd}}{\partial W_{fd}}\right] = 2.0$$

$$B_{62} = 0.5\left[\frac{\partial A_{id}}{\partial A_{id}}\right] = 0.5$$

The block diagram of equation (3-8) is shown as solid lines in Fig. 35. The broken lines represent the controller. The cuts in the diagram at points x , y , and z will be discussed in the succeeding sections.

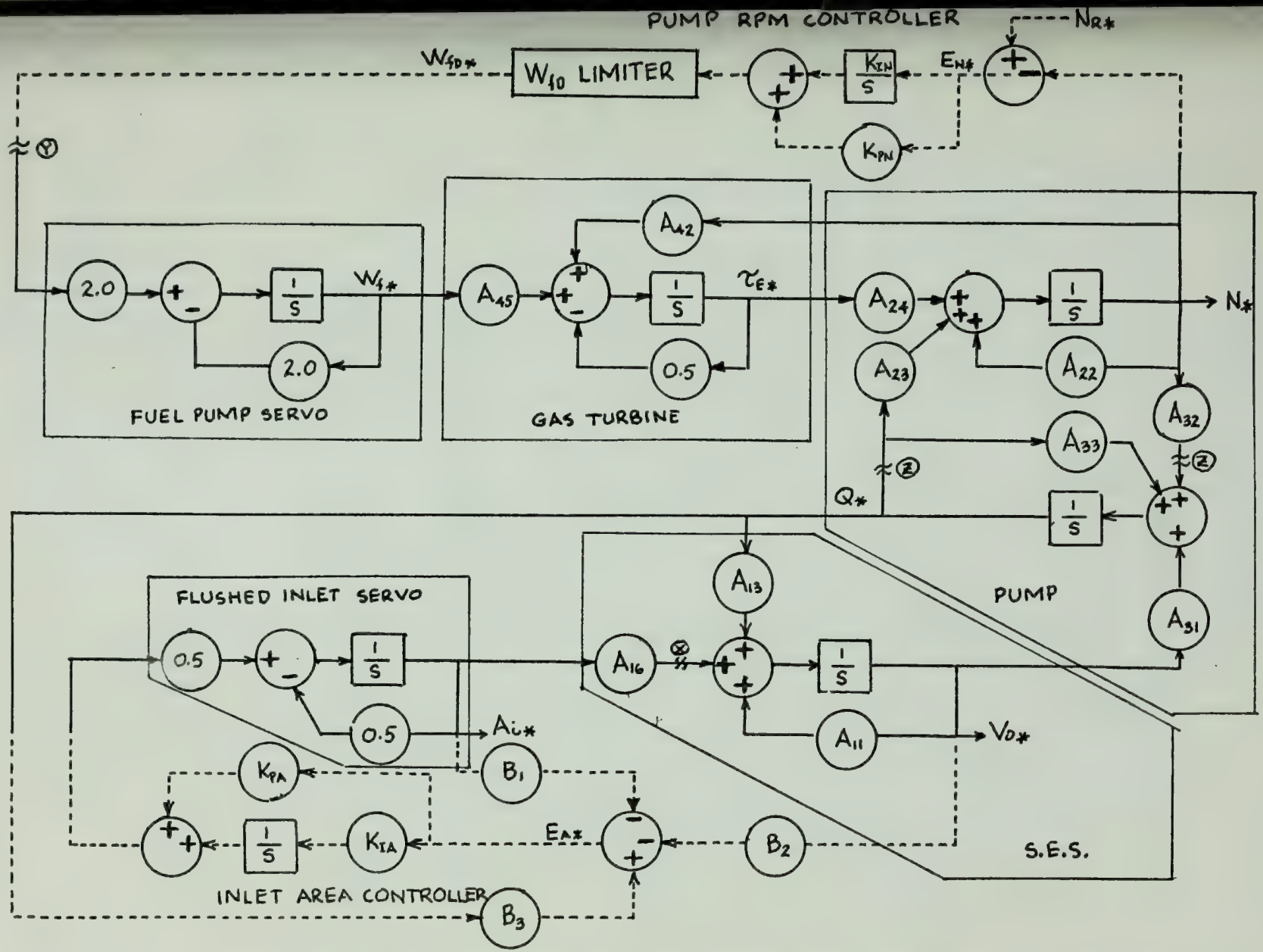

FIGURE 35 BLOCK DIAGRAM OF THE LINEARIZED S.E.S. WATEJET SYSTEM

III-5 FLUSHED INLET THROAT AREA CONTROL:

For the performance of semiflushed or flushed inlet to be optimum 1) pressure recovery must be maximum and 2) drag must be minimum. Fortunately, these two criteria were not contradictory, as can be seen in the performance curves of Fig. 25, 26, 27, 28 of Chapter II. At the inlet to ship velocity ratio of $V_i/V_o \approx 0.8$, the above two conditions are satisfied. A control algorithm then can be set up in such a way that V_i/V_o (or equivalently $Q/A_iV_o = 0.8$) at steady state and at least close to 0.8 during transients. A preliminary proportional and integral control for the flushed inlet actuator was set up in the form of:

$$A_{id_P} = K_{P_A} \left(\frac{Q}{A_iV_o} - 0.8\right) \tag{3-9a}$$

$$\dot{A}_{id_I} = K_{I_A} \left(\frac{Q}{A_iV_o} - 0.8\right) \tag{3-9b}$$

so that:

$$A_{id} = A_{id_P} + A_{id_I} \tag{3-9c}$$

Substituting (3-9) to (3-3f) yields:

$$\dot{A}_i = -0.5A_i + 0.5A_{id_I} + 0.5K_{P_A} \left(\frac{Q}{A_iV_o} - 0.8\right) \tag{3-10}$$

Taking the linear form of equations (3-9b) and (3-10) and including them in equations (3-8) yields:

$$\begin{bmatrix} \dot{V}_* \\ \dot{N}_* \\ \dot{Q}_* \\ \dot{\tau}_{E*} \\ \dot{W}_{f*} \\ \dot{A}_{i*} \\ \dot{A}_{id_{I*}} \end{bmatrix} = \begin{bmatrix} A_{11} & 0 & A_{13} & 0 & 0 & A_{16} & 0 \\ 0 & A_{22} & A_{23} & A_{24} & 0 & 0 & 0 \\ A_{31} & A_{32} & A_{33} & 0 & 0 & 0 & 0 \\ 0 & A_{42} & 0 & A_{44} & A_{45} & 0 & 0 \\ 0 & 0 & 0 & 0 & A_{55} & 0 & 0 \\ \bar{A}_{61} & 0 & \bar{A}_{63} & 0 & 0 & \bar{A}_{66} & \bar{A}_{67} \\ \bar{A}_{71} & 0 & \bar{A}_{73} & 0 & 0 & \bar{A}_{76} & 0 \end{bmatrix} \begin{bmatrix} V_* \\ N_* \\ Q_* \\ \tau_{E*} \\ W_{f*} \\ A_{i*} \\ A_{id_{I*}} \end{bmatrix} + \begin{bmatrix} 0 \\ 0 \\ 0 \\ 0 \\ B_{51} \\ 0 \\ 0 \end{bmatrix} \begin{bmatrix} W_{fd} \end{bmatrix} \qquad (3\text{-}11)$$

where:

$$\bar{A}_{61} = 0.5\, K_{PA} \frac{\partial\left[\frac{Q}{A_i V_o}\right]}{\partial V_o} = -0.5\, K_{PA}\left[\frac{Q}{A_i V_o^2}\right]$$

$$\bar{A}_{63} = 0.5\, K_{PA} \frac{\partial\left[\frac{Q}{A_i V_o}\right]}{\partial Q} = 0.5\, K_{PA}\left[\frac{1}{A_i V_o}\right]$$

$$\bar{A}_{66} = A_{66} + 0.5 K_{PA} \frac{\partial\left[\frac{Q}{A_i V_o}\right]}{\partial A_i} = -0.5\, K_{PA}\left[\frac{Q}{A_i^2 V_o}\right] + A_{66}$$

$$\bar{A}_{67} = 0.5$$

$$\bar{A}_{71} = -K_{IA}\left[\frac{Q}{A_i V_o^2}\right]$$

$$\bar{A}_{73} = K_{IA}\left[\frac{1}{A_{io}V_{o}}\right]$$

$$\bar{A}_{76} = -K_{IA}\left[\frac{Q}{A_{i}^{2}V_{o}}\right]$$

This PI control is shown in Fig. 35, in which:

$$B_1 = \frac{Q}{A_i V_o^2}$$

$$B_2 = \frac{1}{A_i V_o}$$

$$B_3 = \frac{Q}{A_i^2 V_o}$$

To obtain the steady state values of V_{oo}, N_o, Q_o, τ_{E_o}, W_{f_o} and A_{i_o} an open loop response to different levels of W_{fd} using conservative values of K_{IA} and K_{PA} were obtained. Some typical responses are shown in Fig. 36.

To obtain an optimum K_{IA} and K_{PA}, an open loop transfer function A_{i*}/V_{o*} by cutting the loop at point x in Fig. 35 was obtained using MBODE program. Such open loop transfer functions can be represented in matrix form:

$$\begin{bmatrix} \dot{V}_* \\ \dot{N}_* \\ \dot{Q}_* \\ \dot{\tau}_{E_*} \\ \dot{W}_{f_*} \\ \dot{A}_{i_*} \\ \dot{A}_{id_{I_*}} \end{bmatrix} = \begin{bmatrix} A_{11} & 0 & A_{13} & 0 & 0 & 0 & 0 \\ 0 & A_{22} & A_{23} & A_{24} & 0 & 0 & 0 \\ A_{31} & A_{32} & A_{33} & 0 & 0 & 0 & 0 \\ 0 & A_{42} & 0 & A_{44} & A_{45} & 0 & 0 \\ 0 & 0 & 0 & 0 & A_{55} & 0 & 0 \\ \bar{A}_{61} & 0 & \bar{A}_{63} & 0 & 0 & \bar{A}_{66} & \bar{A}_{67} \\ \bar{A}_{71} & 0 & \bar{A}_{73} & 0 & 0 & \bar{A}_{76} & 0 \end{bmatrix} \begin{bmatrix} V_* \\ N_* \\ Q_* \\ \tau_{E_*} \\ W_{f_*} \\ A_{i_*} \\ A_{id_{I_*}} \end{bmatrix} + \begin{bmatrix} 1 \\ 0 \\ 0 \\ 0 \\ 0 \\ 0 \\ 0 \end{bmatrix} \begin{bmatrix} V_* \end{bmatrix}$$

$$\begin{bmatrix} Y \end{bmatrix} = \begin{bmatrix} 0 & 0 & 0 & 0 & 0 & 1 & 0 \end{bmatrix} \begin{bmatrix} V_* \\ N_* \\ Q_* \\ \tau_{E*} \\ W_{f*} \\ A_{i*} \\ A_{id_{I_*}} \end{bmatrix}$$

where A_{16} of equation (3-11) is set to zero.

The zero location can be adjusted by the ratio of K_{IA}/K_{PA} depending on the location of poles and zeroes of the hydraulic servoactuator for the flushed inlet at various operating points. The hard limit and rate limit of the actuator, on the other hand, sets a constraint on the maximum value of K_{IA} that can be used, otherwise excessive

overshoot occurs. For the case study presented, the hard limit and rate limit on the actuator was overcome by setting $K_{IA} = 0.5$ and $K_p = 5.0$ and putting a hard limit on the integrator portion of the controller equal to the hard limit of the actuator, so that the maximum and minimum values of A_{id_I} were 7.0 and 1.5, respectively.

Thus for the control of the flushed inlet geometry some means to measure Q, V, A_i must be provided in order to keep track of V_i/V_o. The time delays associated with these measurements must also be included for the proper location of the zero of the PI controller.

III-6 OPEN LOOP SIMULATION TO FUEL DEMAND SIGNAL:

The fuel demand scheduled limiter used in open loop simulation was set to have a maximum rate of change from idling W_{fd} to maximum W_{fd} in six seconds and a hard limit of idling W_{fd} = 800 lbm/hr and maximum W_{fd} = 10,000 lbm/hr. The $H_{V_o}^{\cdot}$ term in the flow equation (3-3c) and the $\frac{\rho L_x}{g}\left[\frac{dQ}{dt} - A_x \frac{dV_o}{dt}\right]$ term in the thrust equation (3-3a-1) were neglected since they were negligibly small compared to the other terms. Since S.E.S. under study uses six engines, the thrust equation (3-3a-1) and the inlet appendage drag equation (3-3a-3) were multiplied by six for the simulation of the

straight line motion of the craft. Computer runs were made using a stepped fuel demand signal (W_{fd}) from each engine idling fuel flow rate of 800 lbm/hr to various levels of W_{fd} up to maximum W_{fd} of 10,000 lbm/hr per engine. The stepped W_{fd} signal was filtered by the maximum rate change of the Scheduled W_{fd} limiter with the setting discussed above. For a realistic open loop simulation, the flushed inlet area control loop discussed in the preceeding section was closed. Pump cavitation was observed at the stepped W_{fd} of 5,000 lbm/hr/engine and above. Some responses of pump RPM, pump flow rate (ft^3/sec), S.E.S. velocity (ft/sec) and flushed inlet area (ft^2) to the stepped W_{fd} made are plotted in Fig. 36.

Fig. 36 responses, however, were obtained using a higher value of fluid inertance (I_f) in the pipings than the computed value for a faster YSYS solution (i.e., using higher value of time step). Comparison of the response with the actual value of I (i.e., using very small value of time step) yields a similar result. The higher value of I_f used served as a filter to the oscillatory solution of YSYS to pump flow rate during transient and especially in the cavitation regime when the time step is greater than 0.1 second.

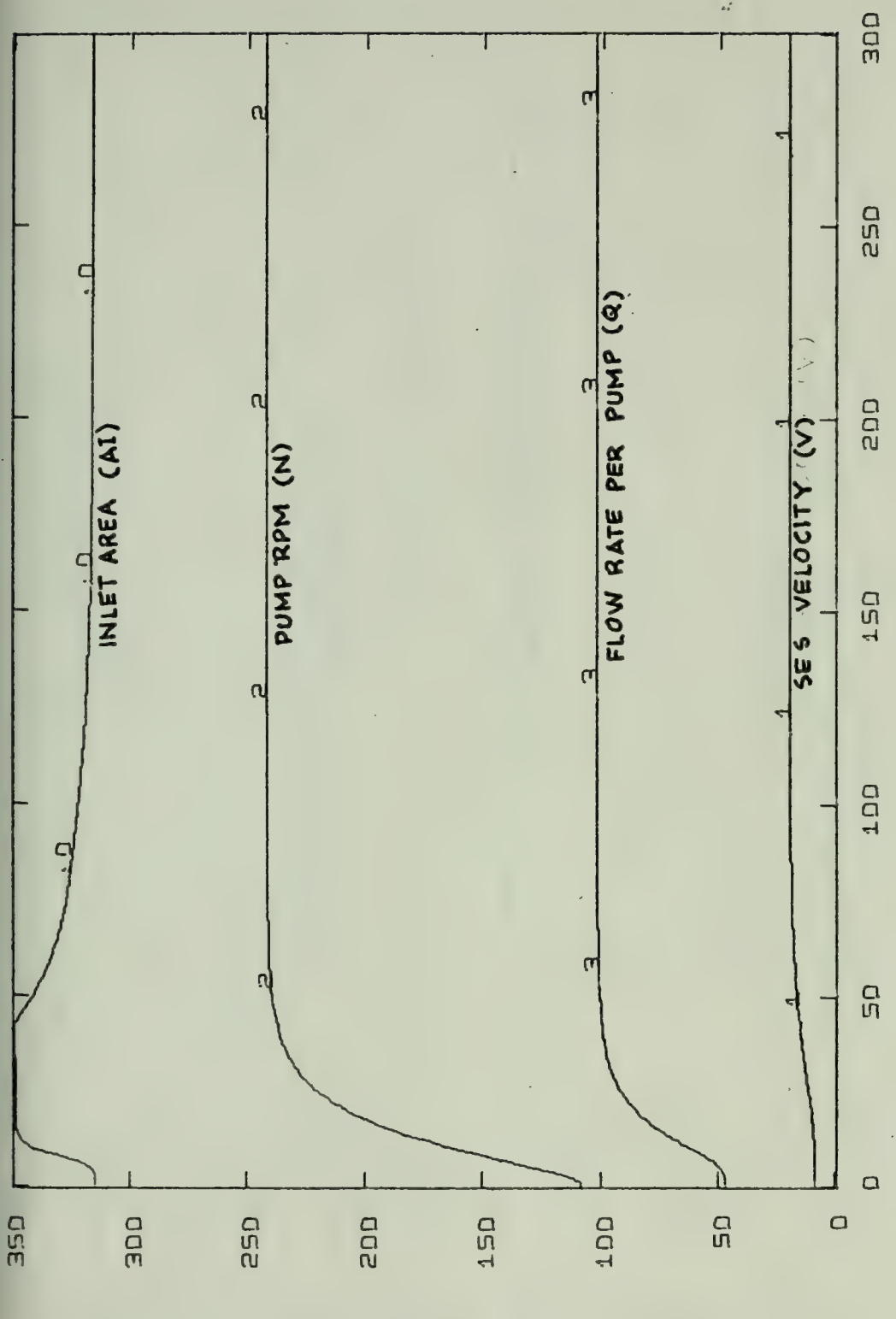

FIGURE 36-1 ACCELERATION FROM 800 TO 2000 LBM/HR FUEL DEMAND SETTING

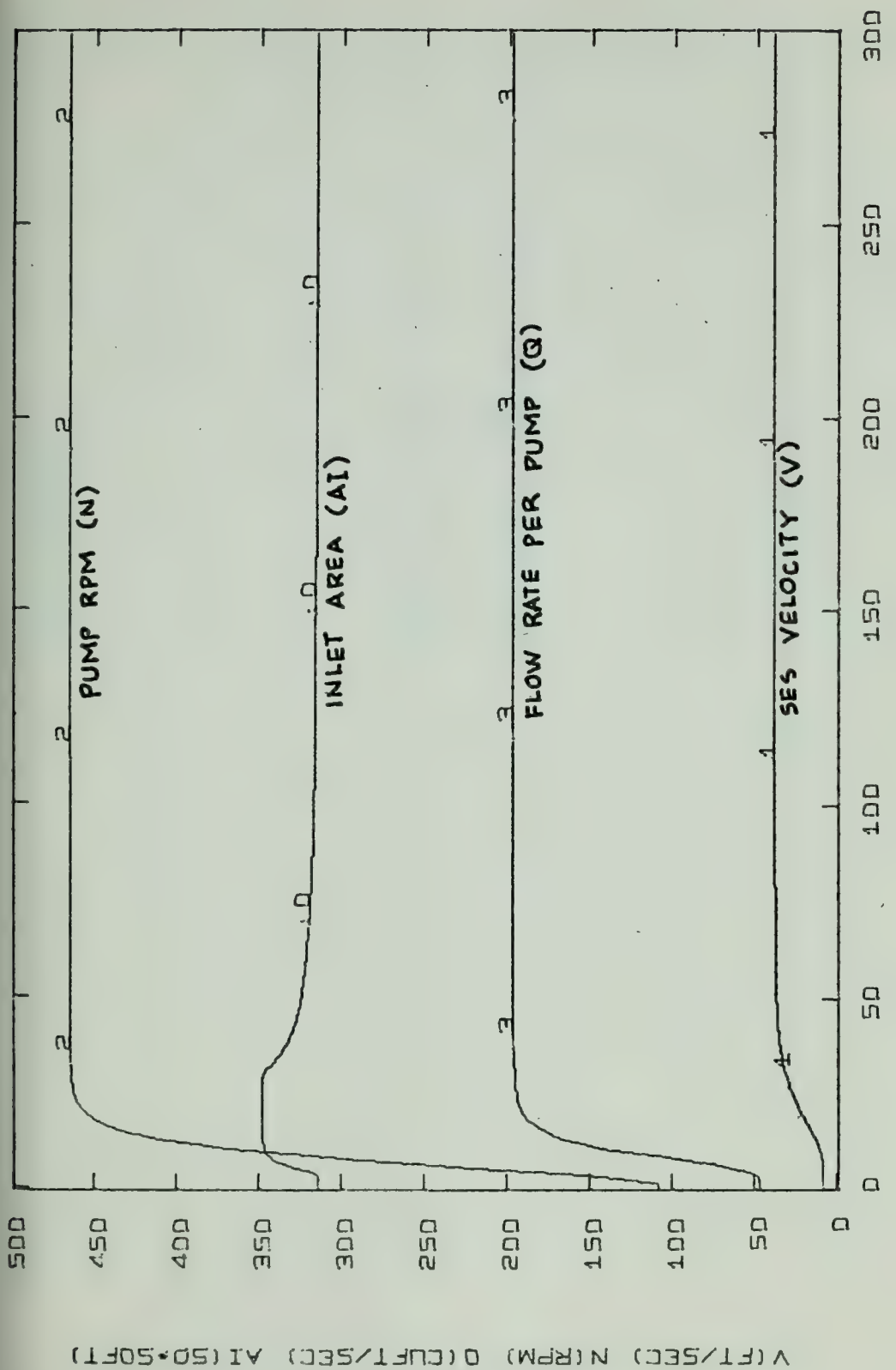

FIGURE 36-2 ACCELERATION FROM 800 TO 5000 LBM/HR FUEL DEMAND SETTING

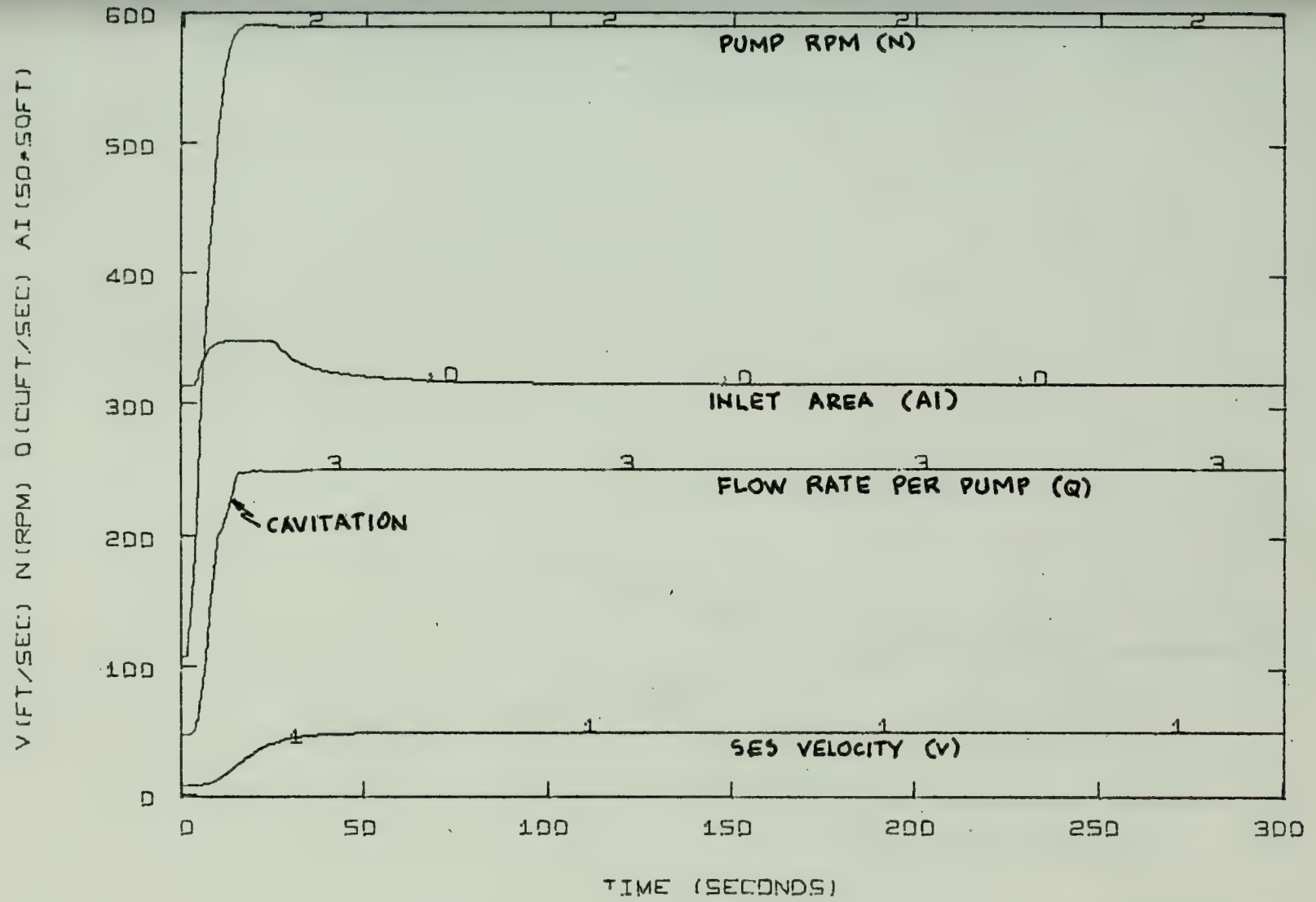

FIGURE 36-3 ACCELERATION FROM 800 TO 8000 LBM/HR FUEL DEMAND SETTING

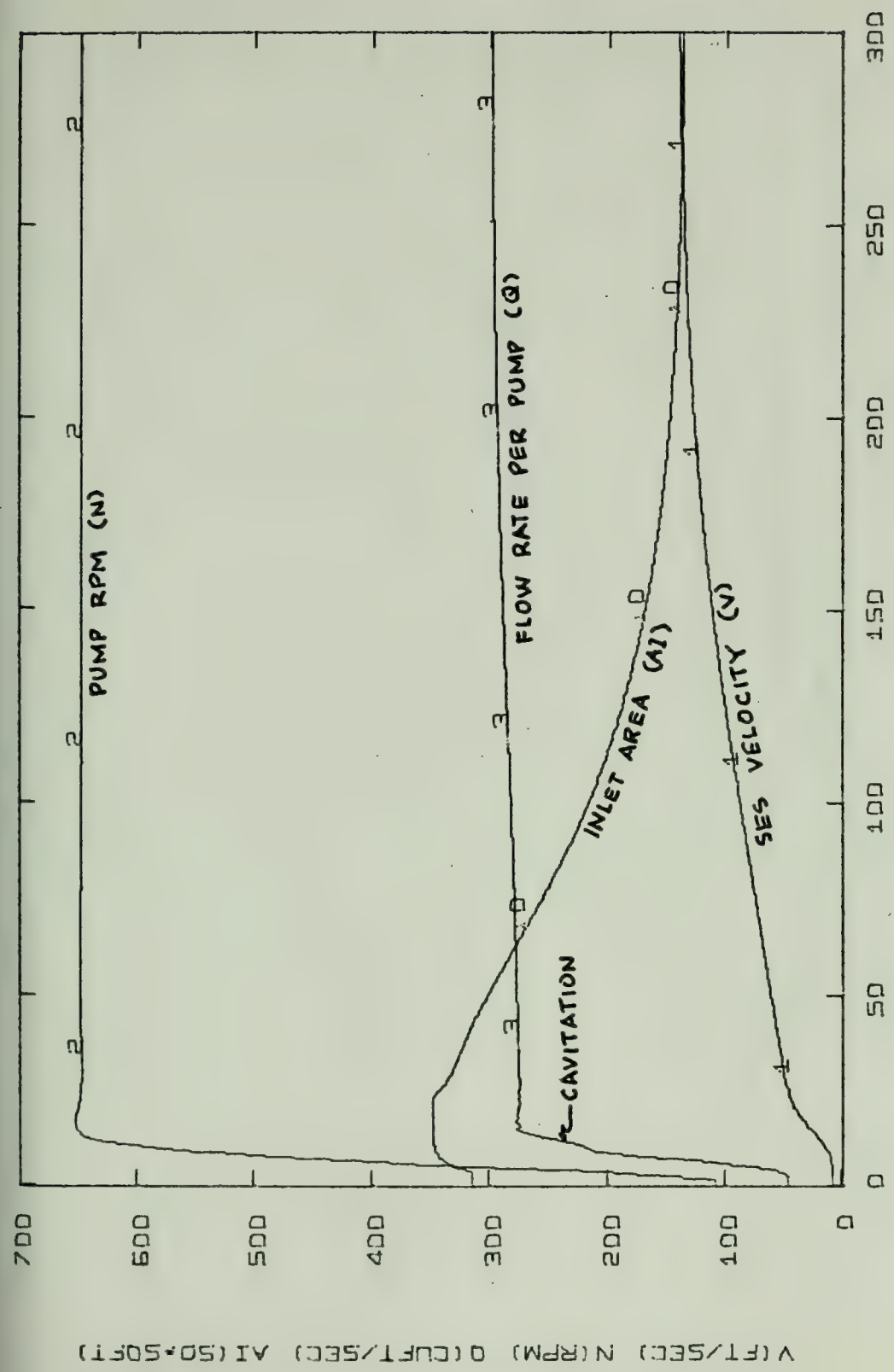

FIGURE 3.6-4 ACCELERATION FROM 800 TO 10000 LBM/HR FUEL DEMAND SETTING

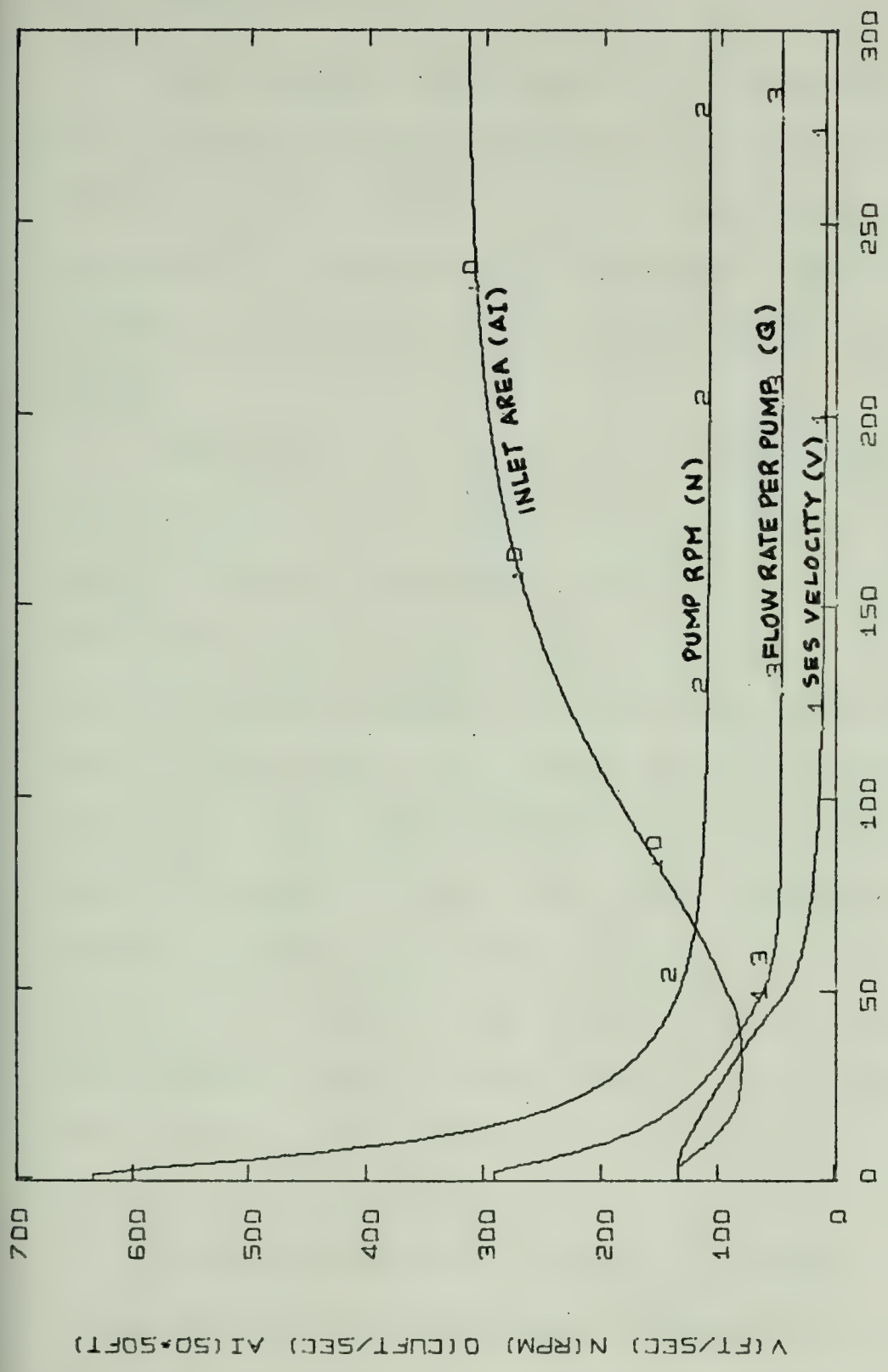

FIGURE 36-5 DECELERATION FROM 9500 TO 800 LBM/HR FUEL DEMAND SETTING

III-7 PUMP RPM CONTROL:

Since pump shaft RPM appears to be the easiest to measure accurately and appears to be the most effective indicator of power turbine stress overload, it was decided to base the fuel demand signal on the error (E_N) between the throttle RPM setting (N_R) and the actual pump shaft RPM (N).

By inspection of Fig. 35, the open loop transfer function N_*/W_{fd*} yields a type 0 system. Such open loop transfer function, represented in matrix form of equation (3-11) with the output matrix $[C] = [0\ 1\ 0\ 0\ 0\ 0\ 0]$, was verified using MBODE program and the result yields no pole at the origin in the s plane. Thus, to reduce the error ($E_{N*} = N_{R*} - N_*$) to zero at steady state, an integral control is needed. A proportional control is also needed to bring N_* close to N_{R*} faster for large error (E_N). In order to obtain the gains K_{PN}, K_{IN} for above PI control, MBODE program was used to locate the open loop poles and zeroes of N_*/W_{fd*} for various levels of W_{fd}, i.e., 800 lbm/hr to 10,000 lbm/hr.

In the MBODE solution, however, of equation (3-11) the A_{33} term was so big compared to the A_{11}, A_{22}, A_{44}, A_{55} and A_{66} terms that a big numerical error resulted. It

was therefore necessary to reduce the order of the system to six by setting:

$$Q_* = 0 = A_{31} V_* + A_{32} N_* + A_{33} Q_*$$

This is equivalent to setting the fluid inertance to zero or shifting the pole due A_{33} to $-\infty$ in the s-plane. Such a procedure will yield a solution very close to the true solution since the pole due to A_{33}, being so far away to the left of the other system poles and zeroes, is effectively at $-\infty$. Solving for Q_* yields:

$$Q_* = \frac{A_{31}}{A_{33}} V_* - \frac{A_{32}}{A_{33}} N_* \qquad (3\text{-}13)$$

Substituting equation (3-13) into $\dot{V}_*$, $\dot{E}_*$, $\dot{A}_{i_*}$ and $\dot{A}_{id_{I_*}}$ of equation (3-11) results in:

$$\begin{bmatrix} \dot{V}_* \\ \dot{N}_* \\ \dot{\tau}_{E_*} \\ \dot{W}_{f_*} \\ \dot{A}_{i_*} \\ \dot{A}_{id_{I_*}} \end{bmatrix} = \begin{bmatrix} a_{11} & a_{22} & 0 & 0 & a_{15} & 0 \\ a_{21} & a_{22} & a_{23} & 0 & 0 & 0 \\ 0 & a_{32} & a_{33} & a_{34} & 0 & 0 \\ 0 & 0 & 0 & a_{44} & 0 & 0 \\ a_{51} & a_{52} & 0 & 0 & a_{55} & a_{56} \\ a_{61} & a_{62} & 0 & 0 & a_{65} & 0 \end{bmatrix} \begin{bmatrix} V_* \\ N_* \\ \tau_{E_*} \\ W_{f_*} \\ A_{i_*} \\ A_{id_{I_*}} \end{bmatrix} + \begin{bmatrix} 0 \\ 0 \\ 0 \\ b_4 \\ 0 \\ 0 \end{bmatrix} \begin{bmatrix} W_{fd} \end{bmatrix}$$

where:

$$a_{11} = A_{11} - \frac{A_{13}\ A_{31}}{A_{33}}$$

$$a_{22} = - \frac{A_{13}\ A_{32}}{A_{33}}$$

$$a_{15} = A_{16}$$

$$a_{21} = - \frac{A_{23}\ A_{31}}{A_{33}}$$

$$a_{22} = A_{22} - \frac{A_{23}\ A_{32}}{A_{33}}$$

$$a_{23} = A_{24}$$

$$a_{32} = A_{42}$$

$$a_{33} = A_{44}$$

$$a_{34} = A_{45}$$

$$a_{51} = \bar{A}_{61} - \frac{\bar{A}_{63}\ \bar{A}_{31}}{A_{33}}$$

$$a_{52} = \frac{\bar{A}_{63}\ \bar{A}_{32}}{A_{33}}$$

With the above PI control, since $W_f = 2.0(W_{fd}-W_f)$ and $W_{fd} = (K_{PN} + \frac{K_{IN}}{s})(N_R-N)$, then the closed loop transfer function N_*/N_{R*} is represented by:

$$\begin{bmatrix} \dot{V}_* \\ \dot{N}_* \\ \dot{\tau}_{E_*} \\ \dot{W}_{f_*} \\ \dot{A}_{i*} \\ \dot{A}_{id_{I_*}} \\ \dot{W}_{fd_{I*}} \end{bmatrix} = \begin{bmatrix} a_{11} & a_{12} & 0 & 0 & a_{15} & 0 & 0 \\ a_{21} & a_{22} & a_{23} & 0 & 0 & 0 & 0 \\ 0 & a_{32} & a_{33} & a_{34} & 0 & 0 & 0 \\ 0 & a_{42} & 0 & a_{44} & 0 & 0 & a_{47} \\ a_{51} & a_{52} & 0 & 0 & a_{55} & a_{56} & 0 \\ a_{61} & a_{62} & 0 & 0 & a_{65} & 0 & 0 \\ 0 & a_{72} & 0 & 0 & 0 & 0 & 0 \end{bmatrix} \begin{bmatrix} V_* \\ N_* \\ \tau_{E_*} \\ W_{f_*} \\ A_{i_*} \\ A_{id_{I_*}} \\ W_{fd_{I_*}} \end{bmatrix} + \begin{bmatrix} 0 \\ 0 \\ 0 \\ b_4 \\ 0 \\ 0 \\ b_7 \end{bmatrix} \begin{bmatrix} N_{R_*} \end{bmatrix} \qquad (3\text{-}15)$$

with the output matrix $[C] = [0\ 1\ 0\ 0\ 0\ 0\ 0]$

where:

$$a_{42} = -2.0\ K_{PN}$$

$$a_{47} = +2.0$$

$$a_{72} = -K_{IN}$$

$$b_4 = +2.0\ K_{PN}$$

$$b_7 = +K_{IN}$$

$$a_{55} = A_{66}$$

$$a_{61} = \bar{A}_{71} - \frac{\bar{A}_{73}\,\bar{A}_{31}}{A_{33}}$$

$$a_{62} = \frac{\bar{A}_{73}\,\bar{A}_{32}}{A_{33}}\,N_*$$

$$a_{65} = \bar{A}_{76}$$

$$b_4 = B_{15}$$

An MBODE result for the value of matrix A of equation (3-14) at W_{fd} = 5,000 lbm/hr with output matrix [C] = [0 1 0 0 0 0] indicates that three of the zeroes cancel out three of the poles of the open loop transfer $N_*(s)/W_{fd_*}(s)$ and is plotted in Fig. 37.

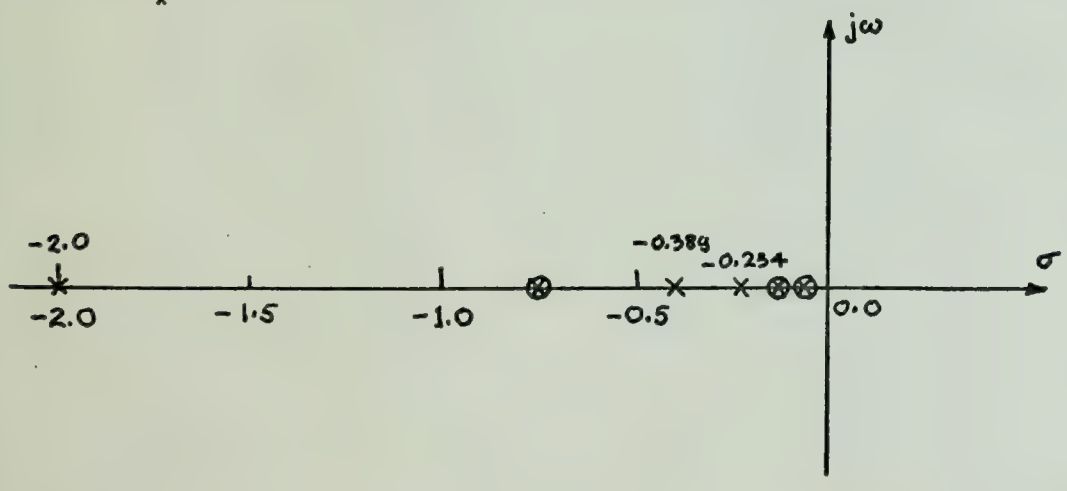

Figure 37. Open loop poles and zeroes of N_*/W_{fd_*}

Thus in the PI controller of the form:

$$K_{PN} + \frac{K_{IN}}{s} = \frac{K_{PN}}{s}\left[\frac{K_{IN}}{K_{PN}} + s\right]$$

K_{IN}/K_{PN} can be adjusted so that the zero of the controller is in the vicinity of -0.234 and the gain K_{PN} also adjusted so that closed loop pole is within the 45° line indicated in Fig. 38 for a fast response with less than 5% overshoot.

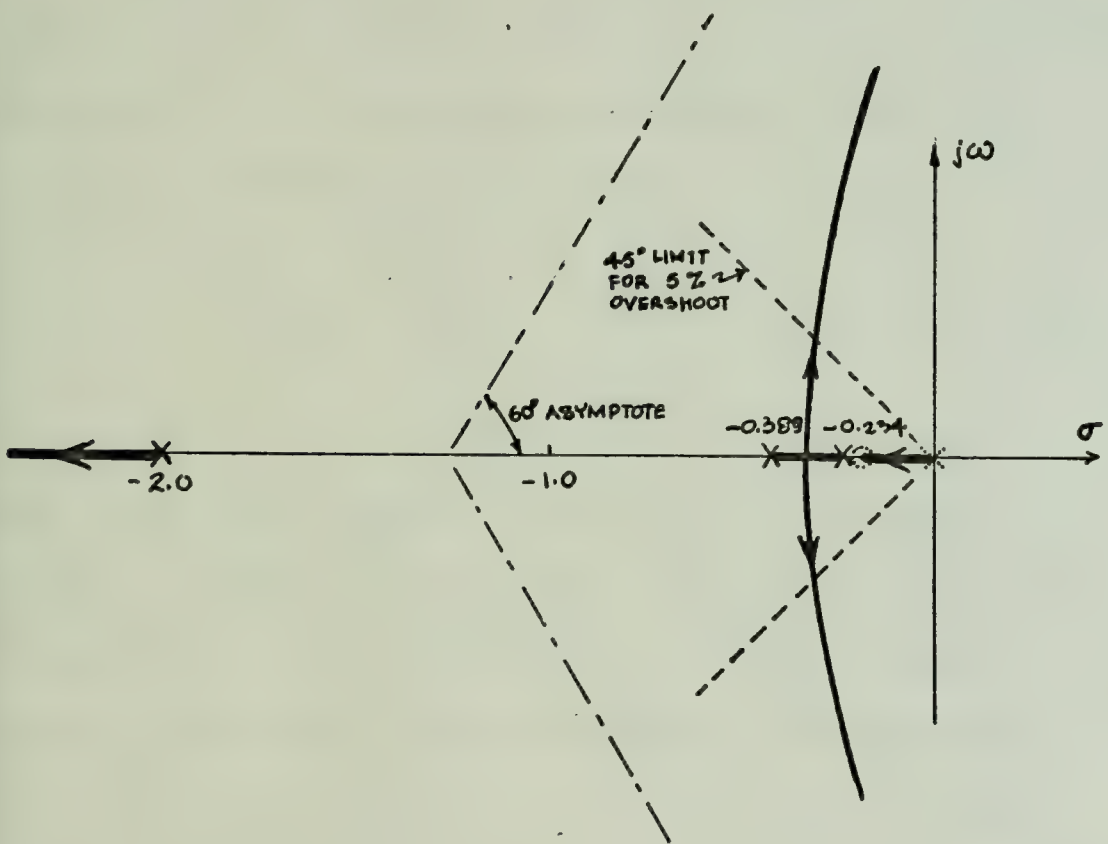

Figure 38. Root locus plot for $K_{IN}/K_{PN} \approx 0.234$

III-8 ANTIWINDUP LOGIC FOR PUMP RPM CONTROL:

In order to compensate for 1) the excessive overshoot and oscillation during transient caused by the hard limit and rate limit on W_{fd} signal and 2) the shifting of the two rightmost uncancelled poles of equation (3-14) towards the origin at low power level, the K_{PN} and K_{IN} were adjusted accordingly in the form as shown in Fig. 39.

The idea behind such a scheduled K_{IN} and K_{PN} is to set the gains of the PI control for small error signals to be equal to the optimum values as found in the linear analysis of section III-7, so that:

$$R_{P_{max}} = f_1(N_R)$$

$$K_{I_{max}} = f_2(N_R)$$

The $f_1(N_R)$ and $f_2(N_R)$ are the plots of the optimum K_{PN} and K_{IN} as function of N_R which will yield a fast stable response with less than 5% overshoot about an operating point N_R for small error disturbance. For large error disturbance, however, the value of $K_{I_{max}}$ is too large to be compatible with the rate and hard limit of the scheduled fuel demand limiter. Large overshoot occurs because by the time the integral part of the fuel demand signal (W_{fd_I}) has

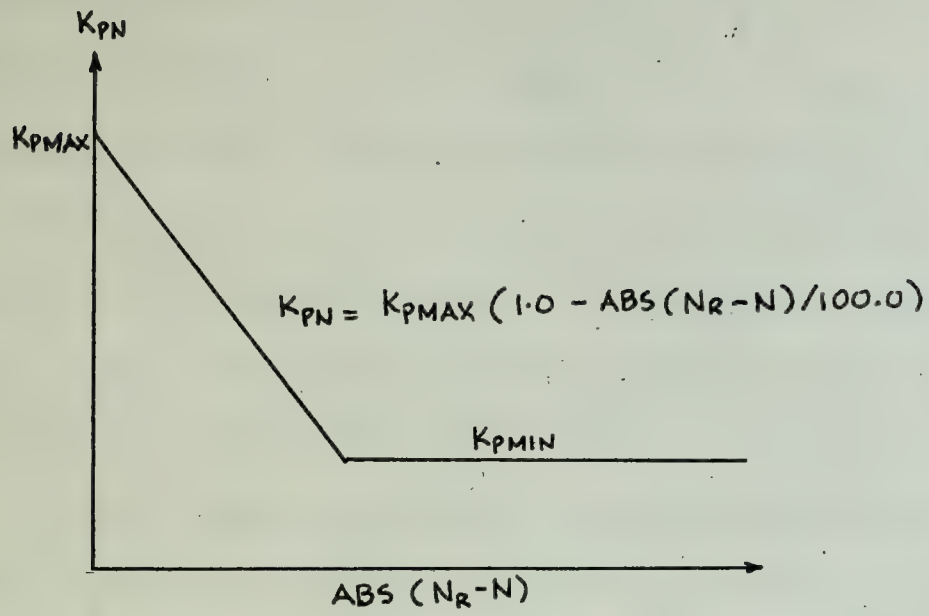

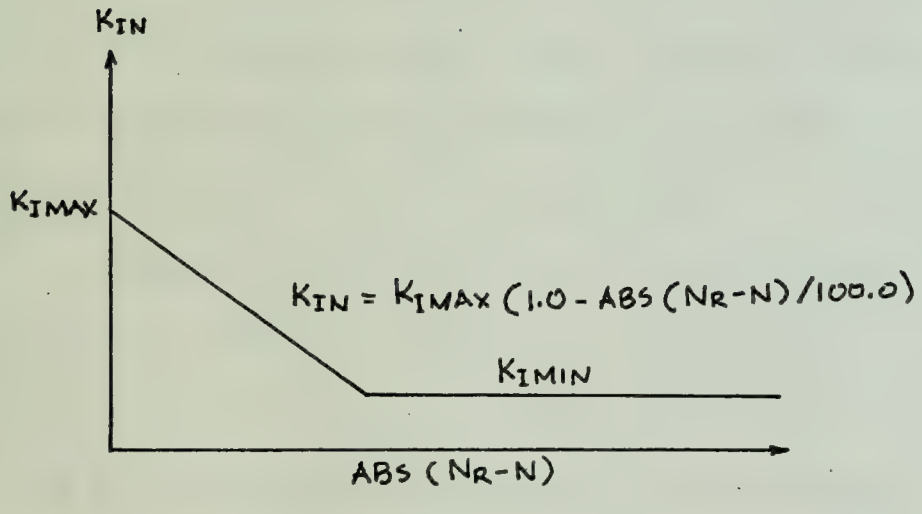

FIGURE 39 PUMP RPM PROPORTIONAL AND INTEGRAL SCHEDULED GAINS

reached the correct value of W_f for a steady state N_R, the error signal is still lagging too far behind. This is due to the fact that the correcting signal W_{fd} acting on the fuel pump servo is considerably less than the combined integral and proportional fuel demand signal ($W_{fd_I} + W_{fd_P}$) due to the filtering action of the scheduled W_{fd} limiter. Since for large error the proportional part of the fuel demand signal (W_{fd_P}) by itself is large enough to be filtered by the W_{fd} limiter, K_{IN} therefore can be set at a lower value and still get the same speed of response in pump RPM (N). Thus $K_{I_{min}}$ can be set so that by the time the error signal goes to zero, the integral part of fuel demand signal (W_{fd_I}) is equal to the actual fuel flow rate (W_f) for reference pump RPM (N_R). Overshoot through this setup is eliminated.

However, for K_P = constant = $K_{P_{max}}$, it was observed that some secondary oscillation occurs during the acceleration transient (Fig. 33b). This is due to the hard limit on the W_{fd} signal for large error. When the error signal was decreased to a value such that W_{fd} was no longer hard limited, the W_{fd} signal decreased rapidly, which caused the actual fuel flow rate W_f to decrease slightly. To

overcome this effect, a negative sloping function of K_{PN} with respect to absolute value of error was set so as to maintain always an increasing fuel flow rate (W_f) during acceleration transient. $K_{P_{min}}$ was also set so that for large errors W_{fd_P} will still be hard limited.

III-9 CONTROL ALGORITHMS TEST RESULT:

The following hard maneuvers were simulated to test the control algorithms for pump RPM and for the flushed inlet throat area:

(a) Acceleration from 109 to 635 RPM Throttle Setting

This simulation was conducted by putting a step change in RPM throttle setting. The 109 RPM corresponds to idling power setting and the 635 RPM corresponds to 95% of the maximum intermittent power rating of the engine. The results are plotted in real time (seconds) in Fig. 40. The labels and scales are:

V = S.E.S. velocity (ft/sec)

N = pump RPM

Q = water flow rate per pump (ft^3/sec)

Number of pumps = 6

WF = actual fuel flow rate per engine (lbm/hr)X100.0

Number of engines = 6

AI = actual flushed inlet throat area per inlet (ft^2)X50.0

Number of inlets = 6

TRST = total thrust of the six (6) waterjet system (lbf)

TE = engine torque (ft-lbf)

TP = pump torque (ft-lbf)

Notice that the gas turbine is dually protected from surge, overtemperature and transient mechanical overstresses by 1) the fuel demand rate limiter, and 2) by the PI controller gains scheduler of Fig. 39. Thus for large errors the fuel demand signal received by the engine will at most be a six second ramp signal. This is verified by the WF plots in Fig. 40.

The response in pump RPM shows that the controller setup of Fig. 39 is fast and stable. In addition, it has no overshoot. There is also no secondary oscillation due to the rate and hard limits of the W_{fd} scheduler during transient as this was taken care of by the negative sloping function of K_{PN} with respect to the absolute value of error. Thus as the error decreases the fuel pump still receives an increasing W_{fd} signal.

The flushed inlet throat area (A_i) increased in the initial transient to accommodate more flow at low S.E.S.

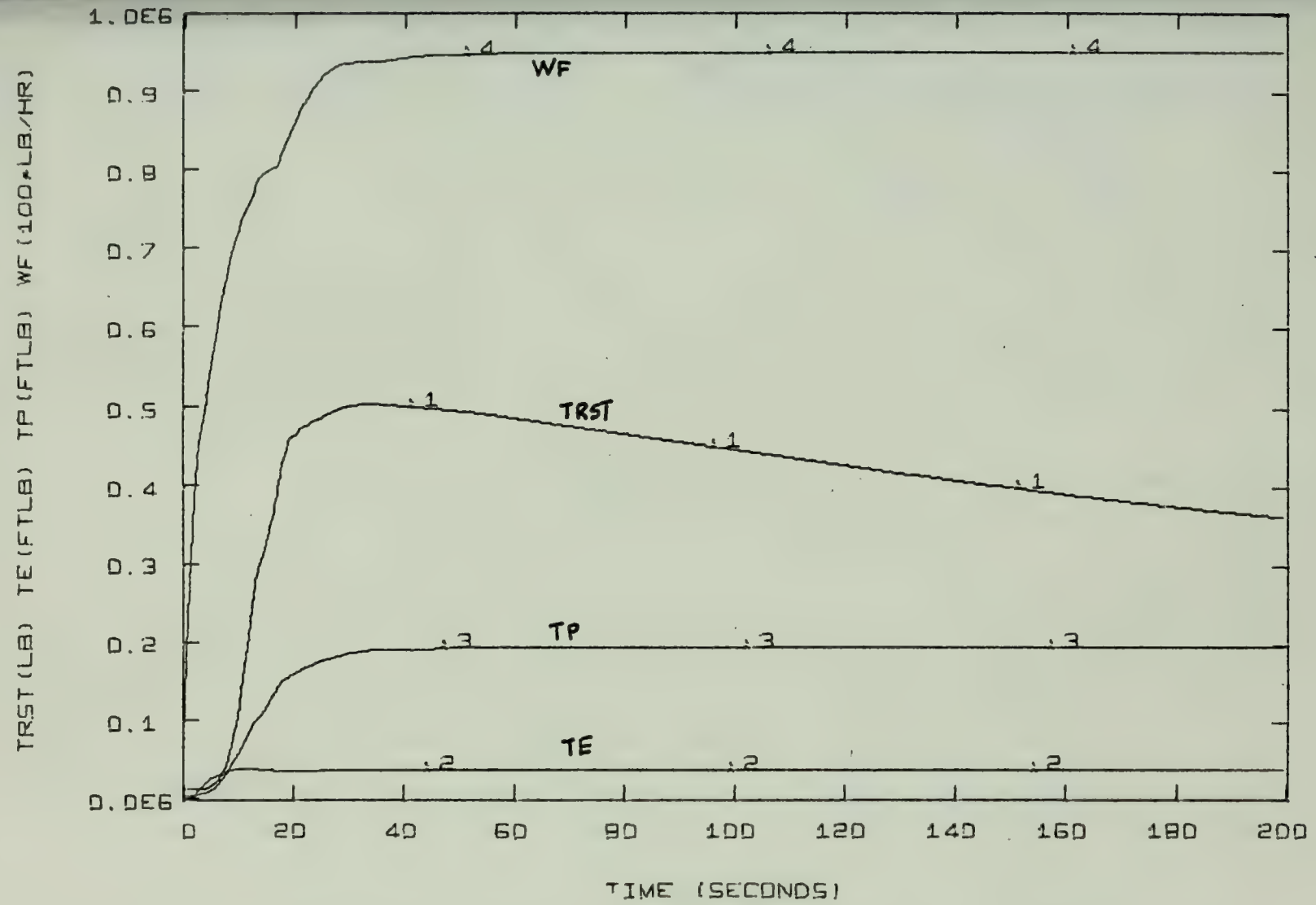

FIGURE: 40 ACCELERATION FROM 109 TO 635 RPM THROTTLE SETTING

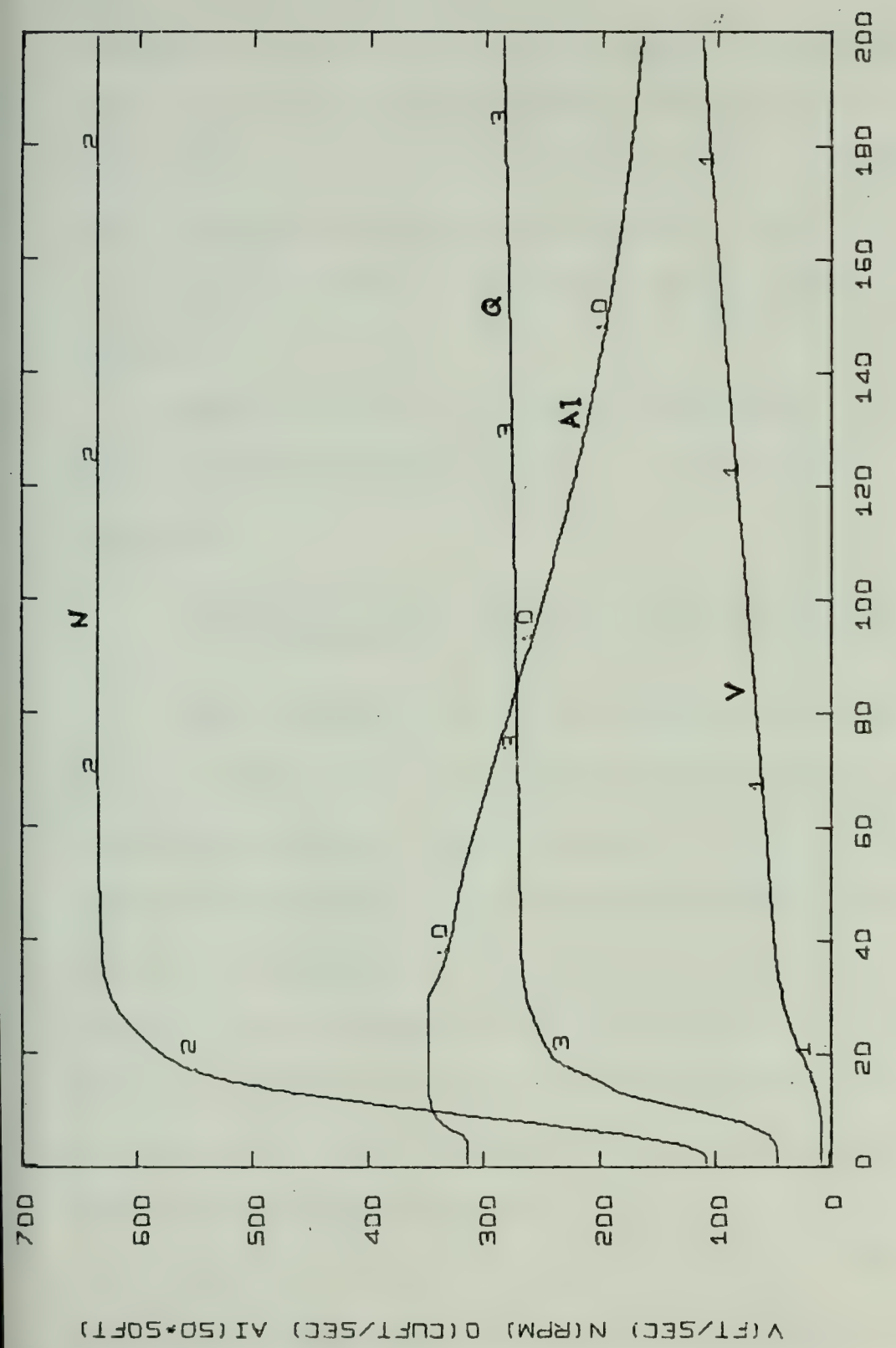

FIGURE 40 ACCELERATION FROM 109 TO 635 RPM THROTTLE SETTING

speed to generate the acceleration force. It finally decreases as the S.E.S. builds up speed, maintaining V_i/V_o close to 0.8 value during transient and exactly 0.8 at steady state. Thus, setting a hard limit alone on the integral part of the PI controller for the flushed inlet is enough to overcome the rate and hard limit of the flushed inlet actuator.

The pump torque (τ_p) and engine torque (τ_E) are plotted to check mechanical stress overloads during transients.

(b) Deceleration from 635 to 150 RPM Throttle Setting

This simulation was also conducted by putting a step change in RPM setting. In order to protect the gas turbine gas generator turbine inlet from sudden change in temperature the fuel demand rate limiter for decreasing fuel flow rate was set arbitrarily to six second ramp. The PI controller gains scheduler of Fig. 39 likewise contributes to this protection as an added precaution. The results are plotted in Fig. 41. The labels and scales are the same as those of the acceleration test.

From the plots it can be seen that the response of pump RPM was slower than in acceleration and has slight overshoot. This was expected since the damping term in

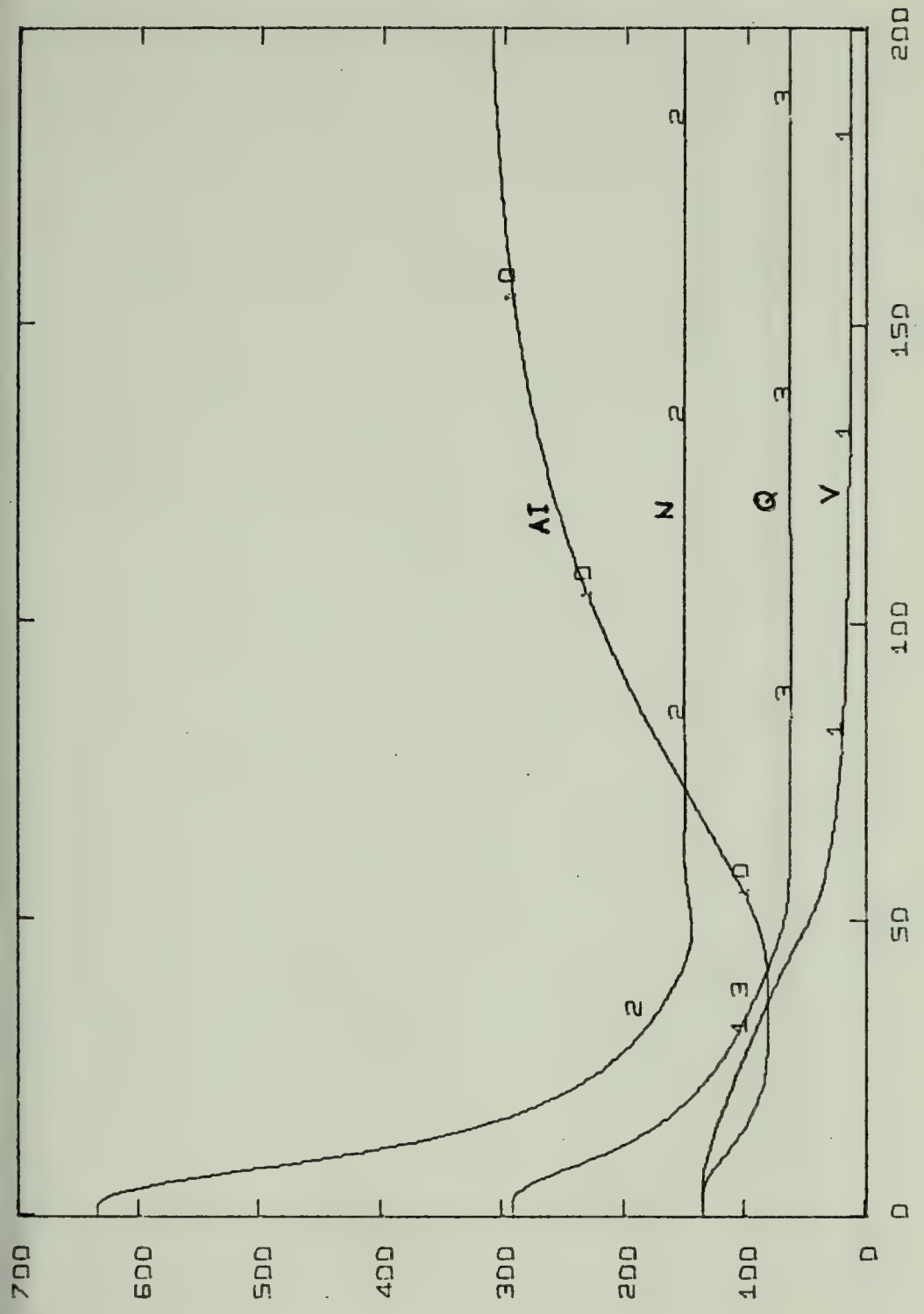

FIGURE 41 DECELERATION FROM 635 TO 150 RPM THROTTLE SETTING

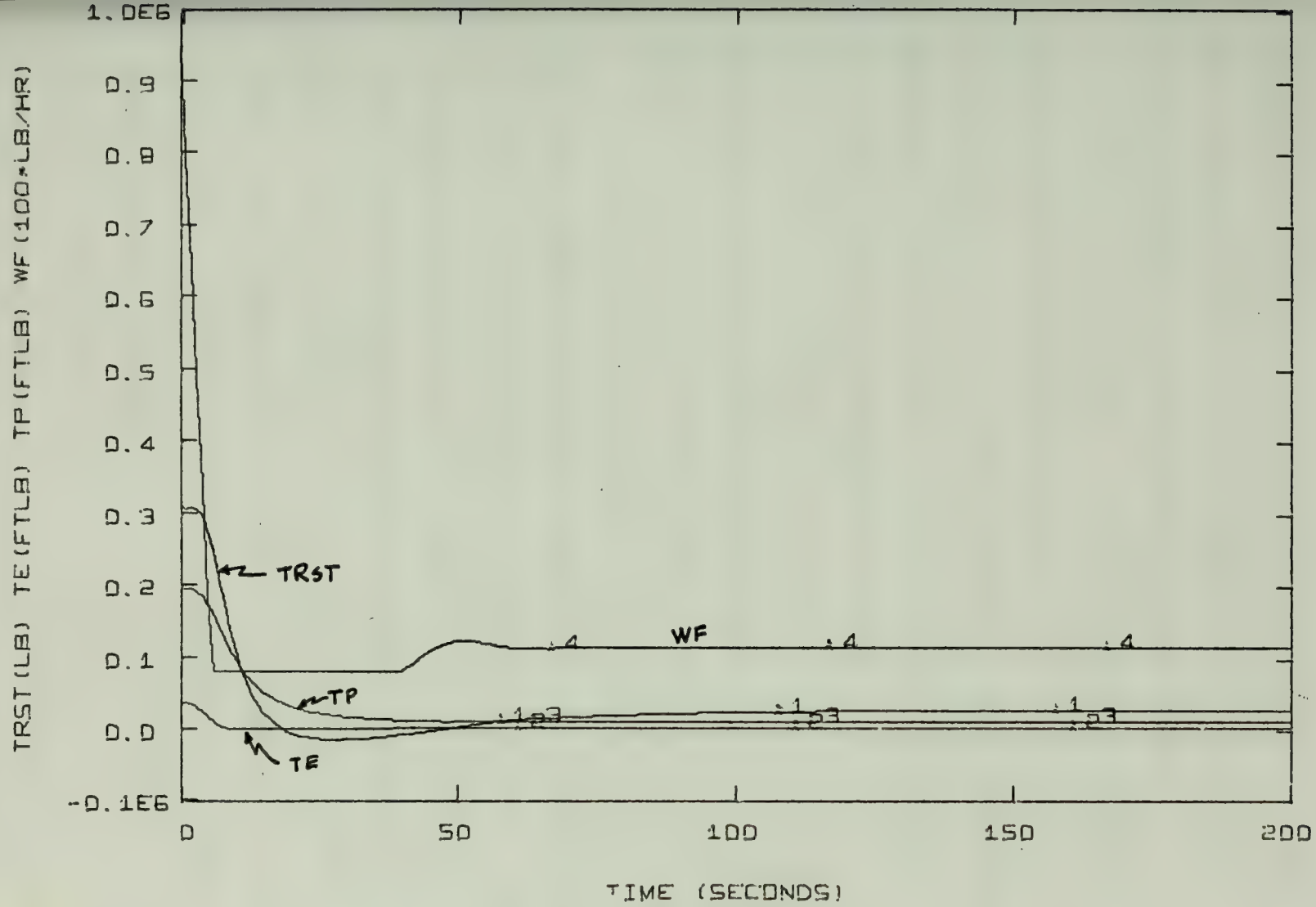

FIGURE 41 DECELERATION FROM 635 TO 150 RPM THROTTLE SETTING

pump RPM varies approximately to the square of pump RPM. Such an overshoot, however, is within acceptable limits and in addition it occurs at approximately 10% of the maximum intermittent power rating of the engine.

Thus, it is evident from the pump RPM responses that the PI controller gain of Fig. 39 works optimally throughout the whole operating range of the waterjet system, that is, 1) fast response, 2) less than 5% overshoot, 3) stable and 4) no steady state error.

From the plot of W_f it can be seen that the actual fuel flow is rate and hard limited even without the actuator itself being rate and hard limited.

The plot of the flushed inlet throat area (A_i) showed an initial decrease to its minimum hard limit for several seconds in an attempt to bring V_i/V_o equal to 0.8. This did not present a problem on the integral part of the PI controller for the flushed inlet since the integrator was also set to have a minimum hard limit equal to the minimum hard limit of the flushed inlet actuator. As the water flow rate Q and S.E.S. velocity V_o came to a steady state, the inlet throat area (A_i) increased to its steady state value so that V_i/V_o is exactly equal to 0.8.

The pump torque (τ_p) and engine torque (τ_E) were plotted to check back flow of power during deceleration.

CONCLUSIONS

From the result of the open loop simulation to a step fuel flow rate for the waterjet propulsion for S.E.S. several conclusions can be made. The first conclusion is that despite the pump being designed not to cavitate at hump speed with a thrust to resistance ratio of 1.2, cavitation can still occur during transients since designed pump head and designed pump flow rates for the hump speed can be reached way earlier before the S.E.S. goes to hump speed during acceleration. However, such cavitation only occurs for a few seconds.

The second conclusion is that for a fixed designed area nozzle the pump is operating very close to the designed ϕ and ψ at steady state for all power levels; likewise, the gas turbine is operating very close to the point of maximum efficiency for all power levels at steady state.

The third conclusion is that in the criteria for designing the speed at which the inlet area can change, there are two variables involved, namely the flow rate Q and the S.E.S. velocity V_o. During transients it was noted that Q changes faster than V_o. Thus, if local cavitation is to

be avoided in the inlet during transient, the rate of change of the term $Q/A_i V_o$ should be considered.

As already discussed in the MBODE analysis of poles and zeroes locations of the system the prime mover and the pump dynamics can be decoupled from the S.E.S. motion dynamics so that the design of a stable control for pump RPM can be simplified. A similar finding was found to be true also between the inlet area dynamics and the S.E.S. motion dynamics.

In the fuel demand scheduled rate limiter incorporated in the RPM control of pump, cavitation can be avoided during transient by setting the rate limiter to some lower value for the normal operation of the S.E.S. For the hard acceleration maneuvers the fuel demand scheduled rate limiter can be set according to what the gas turbine characteristic may allow for surge and overtemperature.

The control algorithm of Fig. 39 works for a rate limited and hard limited actuator and is recommendable since analog or digital implementation is relatively simple. It also works throughout the whole nonlinear operating range of the waterjet system.

RECOMMENDATIONS

The paper presented as it is, is like a textbook approach to the basic principles involved in the system. Several engineering approximations were made for a simplified digital simulation and control of the pump RPM and flushed inlet area. The following recommendations are then made for future work in this area of study.

1. In the control of the flushed inlet, only the throat area was considered in this work. This was intended to serve as a reference in the actual reshaping of the whole flushed inlet geometry consistent with maintaining maximum possible pressure recovery, avoidance of cavitation and minimum drag. The mechanical implementation of this scheme deserves some further study.

2. The fuel demand scheduled rate limiter still needs some refinement to avoid cavitation during acceleration for S.E.S. normal operation. Such a limiter should be consistent with the operating height of the pump above the waterline, and S.E.S. motion, prime mover and pump dynamics.

3. In order for the S.E.S. to maintain a straight line motion there is a need for another set of controls to

regulate the thrusts of all the waterjet systems. Similarly, turning maneuvers with and without the use of thrust deflectors deserve some further study.

4. Backing maneuvers with thrust reversers were not included in the study due to the absence of data on flushed inlet performance in the backward motion. This problem should also be investigated.

5. It will be recommendable to implement a hybrid simulation of the system so that the complete gas turbine model as presented in Chapter II can also be included.

REFERENCES

1. D.C. Karnopp and R.C. Rosenberg, Analysis and Simulation of Multiport System - the Bond Graph Approach to Physical System Dynamics, M.I.T. Press.

2. H.M. Paynter and D.C. Karnoff, "Design and Control of Multiport Engineering Systems," Proceedings of IFAC Tokyo Symposium, pp 443-454.

3. R.C. Percival, "Optimization of Waterjet Propulsion Pumps for Hydrofoil Application," M.I.T. Thesis, Ocean Engineering, May, 1972.

4. B.T. Conner, "A Study of Ram Type Intake Parameters," M.I.T. Thesis, Ocean Engineering, May, 1972.

5. Waterjet Propulsion System Study, Report NR 2, Pump Selection and Design, Lockheed contract NObs-88605, September, 1965.

6. J.E. Crouse, et al., "Design and Overall Performance of an Axial Flow Pump Rotor with a Blade Tip Diffusion Factor of 0.43," NASA TND-2295, May, 1964.

7. J.E. Crouse, et al., "Investigation of Performance of an Axial Flow Pump Stage Designed by Blade Element Theory - Design and Overall Performance," NASA TND-591, 1961.

8. R.P. Gill, "Design Optimization of Waterjet Propulsion System for Hydrofoils," M.I.T. Thesis, Ocean Engineering, May, 1972.

9. M. Rosenblatt and Son, Inc., Conceptual Design Handbook for Surface Effect Ships, February, 1973.

10. A.J. Stepanoff, Centrifigal and Axial Flow Pumps, Second Edition, John Willey and Sons, Inc., New York.

11. C.E. Bentz, "Controlling Future Jet Engines," Mechanical Engineering Journal, February, 1969.

12. L.C. Kramer, D.W. Jenkins, "A New Technique for Preventing Direct Digital Control Windup," Presented at 1971 Joint Automatic Controls Conference of American Automatic Control Councel, Washington University, St. Louis, Missouri, August, 1971.

13. C.J. Rubis, "Acceleration and Steady-State Propulsion Dynamics of a Gas Turbine Ship with Controllable Pitch Propeller," Presented at the Annual Meeting of the Society of Naval Architects and Marine Engineers, New York, November, 1972.

14. H.I.H. Suvaranamuttoo, "The Use of a Hybrid Computer in the Optimization of Gas Turbine Control Parameters," Transactions of ASME Journal of Engineering for Power, May, 1973.

15. C. Muller and C. Stasiowski, "Automation of Jet Engines and Gas Turbines for the Propulsion of High-Speed Vessels," The American Society of Mechanical Engineers, United Engineering Center, February, 1970.

16. L.B. Sarantsev, "Analysis of the Dynamics of Gas Turbines and Their Control Systems," Transactions of ASME Journal of Engineering for Power, July, 1971.

17. C.E. Bentz, "Controlling Future Jet Engines," Mechanical Engineering, February, 1971.

18. E.A. Mossman and L.M. Randall, "An Experimental Investigation of the Design Variables for NACA Submerged Duet Entrances," NACA RM A7130, January, 1948.

19. P.K. Pierpont and R.R. Howell, "Low-Speed Investigation of a Semisubmerged Air Scoop With and Without Boundary Layer Suction," NACA RM LH515, February, 1951.

20. J.R. Henry, C.C. Wood and S.W. Wilbur, "Summary of Subsonic Diffuser Data," NACA RM L56 F05, 1956.

21. E.G. Reid, "Performance Characteristics of Plane-Wall Two-Dimensional Diffusers," NACA Tech Note 2888, 1953.

22. Katsuhiko Ogata, Modern Control Engineering, ed. William Everitt and William W. Seifert, Prentice Hall, Inc., Englewood Cliffs, New Jersey, 1970.

23. J.T. Tozzi, "Direct Digital Control of a Marine Gas Turbine Propulsion Plant with Controllable-Reversible Pitch Propeller," M.I.T. Thesis, Ocean Engineering, May, 1973.

24. E. Freeman, "Digital Simulation of Ship Propulsion Trains Utilizing Gas Turbine and Diesel Prime Movers," M.I.T. Thesis, Ocean Engineering, May, 1973.

25. A.L. Markunas, "Modeling, Simulation and Control of Gas Turbine," M.I.T. Thesis, Mechanical Engineering, May, 1972.

26. J.W. Donnelly, "Mathematical Description of a Marine Gas Turbine System," NAVSECPHILADIV RDT&E Project C-53-II, 27 October, 1972.

27. E.J. Johnson, "Development of Fluidic Controls for Advanced Integrated Propulsion Systems," ASME Journal, March, 1968.

28. A. Bodnaruk and C.J. Rubis, "Acceleration Performance Analysis of Gas Turbine Destroyer Escort," ASME Journal, May, 1970.

29. W.I. Rowen, "Controlling the Gas Turbine in a Shipboard Environment - A Study in Propulsion Dynamics," ASME Journal, May, 1970.

30. C.E. Bentz, "Propulsion System Controls Capabilities and Future Requirements," ASME Journal, March, 1968.

31. D. Wilson, "Patterning Stage Characteristics for Wide Range Axial Compressors," ASME Journal, November, 1960.

32. Water Propulsion System Study Report No. 5 System Design and Analysis, LR-17885-5, Lockheed Contract No. NO65-88605.

APPENDIX I

The following are the particulars of the S.E.S. under study:

Length to beam ratio = 2.37

Cushion pressure to length ratio = 2.5

Cushion pressure = 412 lbf/ft^2

Displacement = 2109 tons

Number of lift engines = 2

Number of propulsion engines = 6

Designed cruise speed = 80 knots

Maximum intermittent engine rating = 22,500 HP

Maximum continuous engine rating = 20,500 HP

Range = 2,000 miles

Hump speed = 30 knots

Bare hull resistance (smooth sea, cushion borne):

Velocity (Knots)	Resistance (lbf)	Velocity (Knots)	Resistance (lbf)
28.45	422918	45	299578
30	429438	50	282030
35	367391	55	271360
40	326606	60	265899

Velocity (Knots)	Resistance (lbf)	Velocity (Knots)	Resistance (lbf)
65	261984	85	269772
70	258695	90	278874
75	259040	95	290098
80	263038	100	303252

APPENDIX II

The steady operating point values of S.E.S. velocity (V_{oo}), pump RPM (N_o), water flow rate per pump (Q_{oo}), throat area per inlet (A_{i_o}) and reduction gear efficiency (η_{RG_o}) for different values of fuel flow rate per engine (W_{f_o}) are:

W_{f_o} (lbm/hr)	V_{oo} (ft/sec)	N_o (RPM)	Q_o (ft^3/sec)	Ai_o (ft^2)	η_{RG_o}
800	9.3	109	47,38	6.307	0.858
2,000	20.1	241.8	101.6	6.318	0.92
3,000	28.96	346.8	146.4	6.319	0.944
4,000	34.37	410.3	173.7	6.317	0.952
5,000	43.22	465.6	197.5	6.317	0.957
6,000	46.62	514	218.0	6.317	0.961
7,000	49.67	553.9	235.6	6.317	0.962
8,000	103.0	589.9	251.2	6.317	0.963
8,500	124.0	605.8	263.9	3.202	0.964
9,000	124.0	620.9	280.4	2.822	0.965
9,500	135.2	635.6	292.0	2.701	0.966
10,000	142	647.9	298.6	2.628	0.966

From the above operating point values, power turbine torque (τ_{E_o}), pump flow coefficient (ϕ_o) and head coefficient (ψ_o) can be determined. Thus the matrix A of the linearized waterjet system equation (3-8) can be evaluated so that:

for $W_{fd} = 800$

$$A = \begin{bmatrix} -0.0264 & 0.0 & 0.00514 & 0.0 & 0.0 & -0.00055 \\ 0.0 & -0.0293 & -0.00757 & 0.001302 & 0.0 & 0.0 \\ 0.5172 & 1.25 & -3.024 & 0.0 & 0.0 & 0.0 \\ 0.0 & -4.459 & 0.0 & -0.5 & 4.0 & 0.0 \\ 0.0 & 0.0 & 0.0 & 0.0 & -2.0 & 0.0 \\ 0.0 & 0.0 & 0.0 & 0.0 & 0.0 & -0.5 \end{bmatrix}$$

for $W_{fd} = 5{,}000$

$$A = \begin{bmatrix} -0.1088 & 0.0 & 0.02139 & 0.0 & 0.0 & -0.0094 \\ 0.0 & -0.0106 & -0.04479 & 0.001449 & 0.0 & 0.0 \\ 2.119 & 5.2 & -12.337 & 0.0 & 0.0 & 0.0 \\ 0.0 & -20.179 & 0.0 & -0.5 & 3.4 & 0.0 \\ 0.0 & 0.0 & 0.0 & 0.0 & -2.0 & 0.0 \\ 0.0 & 0.0 & 0.0 & 0.0 & 0.0 & -0.5 \end{bmatrix}$$

for W_{fd} = 10,000

$$\begin{bmatrix} -0.03283 & 0.0 & 0.02556 & 0.0 & 0.0 & -0.1242 \\ 0.0 & -0.1754 & 0.0019 & 0.0014 & 0.0 & 0.0 \\ 7.7 & 7.704 & -19.706 & 0.0 & 0.0 & 0.0 \\ 0.0 & -32.506 & 0.0 & -0.5 & 2.65 & 0.0 \\ 0.0 & 0.0 & 0.0 & 0.0 & -2.0 & 0.0 \\ 0.0 & 0.0 & 0.0 & 0.0 & 0.0 & -0.5 \end{bmatrix}$$

The above constants were used in designing controller gains for small disturbance.

APPENDIX III

Subroutine EQSIM is required by DYSYS for the solution of the dynamic equation of the system. The DYSYS program is available at M.I.T. mechanical and civil engineering computer facilities.

Subroutine LM250 represents the LM2500 performance map of Fig. 8. The inputs to the subroutines are power turbine RPM and fuel flow rate and the output is power turbine torque.

```
      SUBROUTINE EQSIM
      COMMON T,DT,Y(20),DY(20),STIME,FTIME,NEWDT,IFWRT,N
C     DATA FOR: DISPLACEMENT (TONS)
C               POLAR MOMENT OF INERTIA  (FTLB/SECSQ)
C               FLUID INERTANCE (SLUGS/FT)
C               REDUCTION GEAR RATIO
      DATA DISP,XJ,XI,RGR/2109.0,35000.0,25.0,5.55/
C     DATA FOR: DIFFUSER LENGHT (FT)
C               DIFFUSER EXIT AREA (SQFT)
C               AREA WATER JET NOZZLE (SQFT)
C               NUMBER OF ENGINES
C               PUMP DIAMETER (SQFT)
      DATA DL,A2,AJ,XNE,D/18.0,13.52,1.30,6.0,5.98/
C     Y(1)=SES SPEED (FT/SEC)
C     Y(2)=PUMP SPEED (RPM)
C     Y(3)=WATER FLOW RATE (CUFT/SEC)
C     Y(4)=ACTUAL ENGINE TORQUE (FTLBS)
C     Y(5)=ACTUAL FUEL FLOW RATE (LBS/HOUR)
C     Y(6)=ACTUAL INLET AREA (SQFT)
C     Y(7)=INLET AREA DEMAND (SQFT)
C     Y(8)=INTEGRAL PART OF FUEL FLOW RATE DEMAND (LBS/HR)
C     Y(9)=PROPORTIONAL PART FUEL FLOW RATE DEMAND (LBS/HR)
      IF(NEWDT) 1,3,2
    1 KI=8
      KO=5
      XI=250.0
C     REFERENCE PUMP RPM (RPM)
      READ(KI,100) XRPM
  100 FORMAT(F10.0)
      AID=Y(7)
      WFD=Y(5)
C     FUEL FLOW RATE CHANGE LIMITER
      TFMIN=6.0
      FRATE=9200.0/TFMIN
C     SES MASS (SLUGS)
      W=DISP*2240.0*1.08/32.2
```

```
C     PUMP ANNULUS AREA (SQFT)
      ANLUS=3.1416*D**2/4.0*(1.0-0.72**2)
C     CONSTANT FOR CALCULATING PUMP TORQUE
      C2=1.99*ANLUS/2.0*(3.1416/60.0)**2*D**3
C     WATER JET PROPULSION THRUST (LBS)
      BETA=5.0/57.29
    2 TRST=1.99*Y(3)*(Y(3)*CCS(BETA)/AJ-Y(1))*XNE
      IF(T.GE.0.0) DT=1.0
C     SES RESISTANCE (LBS)
      IF(Y(1).LE.50.67) RS=167.72*Y(1)**2
      IF(Y(1).GT.50.67) RS=26.726*Y(1)**2-6935.34*Y(1)+712204.0
C     INLET TO SES VELOCITY RATIO
      VIVO=Y(3)/Y(6)/AMAX1(Y(1),0.001)
      IF(VIVO.LE.0.8) CDI=1.0-VIVO*0.85/0.8
      IF(VIVO.GT.0.8) CDI=VIVO*0.2-0.01
      CDI=AMIN1(1.0,CDI)
C     INLET APPENDAGE DRAG (LBS)
      RI=CDI*0.5*1.99*Y(1)**2*Y(6)*XNE
C     SES TOTAL RESISTANCE (LBS)
      RT=RS+RI
C     LM 2500 CHARACTERISTICS
      WF=Y(5)
      RPM=Y(2)*RGR
      CALL LM250(WF,RPM,TORQ)
C     ACTUAL ENGINE TORQUE (FTLB)
      TORQE=Y(4)
      ARATE=0.5
C     ACTUAL SHAFT TORQUE (FTLB)
      ETARG=0.75+0.22*(1.0-EXP(-RPM/895.0))
      IF(TORQE.LT.0.0)TORQS=TORQE*RGR/ETARG
      IF(TORQE.GE.0.0)TORQS=TORQE*RGR*ETARG
C     SHAFT FRICTION TORQUE
      TORQF=1000.0+15.0*Y(2)
C     DIFFUSER ASPECT RATIO
      AR=A2/Y(6)
C     DIFFUSER ANGLE (DEGREES)
```

```
      TT=(SQRT(AR)-1.0)*Y(6)/DL
      THETA=ATAN(TT)*28.645
C     DIFFUSER LOSS COEFFICIENT
      DKF=0.006*(ABS(2.0*THETA-10.0))**1.8+0.2
C     INLET EFFICIENCY
      ETAI=0.85*(1.0-EXP(-VIVO/0.25))
C     TOTAL HEAD AFTER INLET (FT)
      THAI=Y(1)**2/64.2*ETAI
C     HEIGHT OF PUMP ABOVE WATERLINE (FT)
      HW=18.0*(1.0-EXP(-Y(1)/40.0))-4.0
      HN=HW
C     KINETIC HEAD OF WATERJET ACROSS THE NOZZLE (FT)
      HJ=(Y(3)/AJ)**2/64.4
      THBP=THAI*(1.0-DKF)-HW
C     PUMP WATER AXIAL VELOCITY (FT/SEC)
      CX=Y(3)/ANLUS
C     PUMP BLADE TIP VELCCITY (FT/SEC)
      VB=3.1416*D*Y(2)/60.0
C     PUMP CHARACTERISTICS W/O CAVITATION
      PHI=CX/VB
      IF(PHI.LE.0.04) PSI=-83.3*PHI**2-1.916*PHI+0.85
      IF(0.04.LT.PHI.AND.PHI.LE.0.065) PSI=220.0*PHI**2-25.5*PHI+1.308
      IF(0.065.LT.PHI.AND.PHI.LE.0.130) PSI=-68.217*PHI**2+10.173*PHI+0.
     12069
      IF(0.130.LT.PHI.AND.PHI.LE.0.152) PSI=-318.45*PHI**2+72.713*PHI-3.
     16949
      IF(0.152.LT.PHI) PSI=188.0*(PHI-0.152)**2-21.6*(PHI-0.152)
C     DIMENSIONLESS PUMP POWER DISSIPATION W/O CAVITATION
      PD=12.40*(PHI-0.108)**2+0.00623
C     DIMENSIONLESS SUCTION HEAD CRITERIA
      IF(PHI.LE.0.11) PSIC=0.16826*PHI**2
      IF(0.11.LT.PHI) PSIC=1.772*PHI**2-0.223*PHI+0.005126
C     DIMENSIONLESS SUCTION HEAD ACTUAL
      PSIS=THBP*32.2/VB**2
C     TEST FOR CAVITATION
      TESTC=PSIC-PSIS
```

```
      IF(TESTC.LT.0.0) GO TO 4
      DT=0.2
C     PUMP CHARACTERISTICS WITH CAVITATION
      PD=PD+0.2*PHI*PSI*(TESTC/PSIC)**2
      PSI=PSI*(1.0-(TESTC/PSIC)**2)
      IF(PSI.LT.0.0) PSI=0.0
      HP=PSI*VB**2/32.2
      TORQP=(PHI*PSI+PD)*Y(2)**2*C2
      GO TO 5
C     PUMP HEAD W/O CAVITATION
    4 HP=PSI*VB**2/32.2
C     PUMP TORQUE W/O CAVITATION
      TORQP=(PHI*PSI+PD)*Y(2)**2*C2
    5 ERROR=XRPM-Y(2)
C     PROPORTIONAL AND INTEGRAL GAIN
      XKPMX=30.0
      XKPMN=20.5-0.025*XRPM
      XKP=XKPMX*(1.00-ABS(ERROR)/100.0)
      XKP=AMIN1(XKPMX,AMAX1(XKP,XKPMN))
      XKIMX=1.0+0.007*XRPM
      XKIMN=110000.0/(XJ+10000.0*TFMIN)
      XKI=XKIMX*(1.00-ABS(ERROR)/100.0)
      XKI=AMIN1(XKIMX,AMAX1(XKI,XKIMN))
      Y(10)=Y(6)*50.0
      Y(11)=TRST
      Y(12)=TORQS
      Y(13)=TORQP
      Y(14)=Y(5)*100.0
      Y(15)=PHI
      Y(16)=TESTC
      Y(17)=HP
      Y(18)=THBP
      Y(19)=HJ
      Y(20)=HN
      ABLIM=Y(6)-DT*ARATE
      AULIM=Y(6)+DT*ARATE
```

```
      FULIM=WFD+DT*FRATE
      FBLIM=WFD-DT*FRATE
    3 DY(1)=(TRST-RT)/W
      DY(2)=(TORQS-TORQF-TORQP)/XJ*9.549
      DY(3)=(HP+THBP-HJ-HN)/XI*64.2
      DY(4)=0.5*(TORQ-Y(4))
      DY(5)=2.0*(WFD-Y(5))
      DY(6)=0.5*(AID-Y(6))
      Y(6)=AMIN1(7.00,AULIM,AMAX1(Y(6),ABLIM,1.50))
      DY(7)=0.5*(VIVO-0.8)
      Y(7)=AMIN1(6.50,AMAX1(Y(7),2.00))
      AID=5.0*(VIVO-0.8)+Y(7)
      AID=AMIN1(7.00,AMAX1(AID,1.50))
      Y(8)=AMIN1(10000.0,AMAX1(Y(8),800.0))
      DY(8)=ERROR*XKI
      Y(9)=ERROR*XKP
      WFD=Y(8)+Y(9)
      WFD=AMIN1(10000.0,FULIM,AMAX1(800.0,FBLIM,WFD))
      RETURN
      END
```

```
      SUBROUTINE LM250 (WF,RPM,TORQ)
      REAL SLOPE(11),BIAS(11)
      DATA SLOPE/1.607,1.750,2.847,5.057,6.482,7.272,8.389,9.280,10.307,
     111.111,11.714/
      DATA BIAS/0.0,3500.0,10250.0,22000.0,31500.0,40000.0,49500.0,58000
     1.0,67000.0,75000.0,82000.0/
      I=WF/1000.0
      T1=BIAS(I+1)-RPM*SLOPE(I+1)
      T2=BIAS(I+2)-RPM*SLOPE(I+2)
      WI=I
      TORQ=T1+(T2-T1)*(WF/1000.0-WI)
      RETURN
      END
```

153004

Thesis
B825 Bruce
Dynamics, simulation
and control of waterjet
propulsion for S. E. S.